

# Test av Peltonturbin i Vannkraftlaboratoriet

**Martine Cecilie S Wessel**

Master i energi og miljø

Innlevert: juni 2014

Hovedveileder: Ole Gunnar Dahlhaug, EPT

Medveileder: Torbjørn K. Nielsen, EPT  
Bjørn Winther Solemslie, EPT

Norges teknisk-naturvitenskapelige universitet  
Institutt for energi- og prosesseteknikk



EPT-M-2014- 129

**MASTEROPPGAVE**

for

Martine Wessel

Våren 2014

**Test av en Pelton turbin i Vannkraftlaboratoriet***Laboratory test of a Pelton turbine***Bakgrunn**

Blant Norges 1050 kraftverk så er det ca. 30% som har Pelton turbiner installert. Mange av disse turbinene er mer enn 40 år gamle og det er tid for oppgraderinger og eventuelt utskifting av disse. Selv om Pelton turbinen er over 100 år gammel er det fremdeles områder hvor kunnskap mangler, da spesielt innen strømmingen i skovlene.

Ved Vannkraftlaboratoriet er det blitt designet en modellturbin som skal testes i laboratoriet for å bedre kunnskapen rundt strømmingen i skovlene. All informasjon om denne turbinen skal publiseres slik at alle som ønsker å gjennomføre analyser kan gjøre dette uten noen form for restriksjoner av resultater.

**Mål**

Gjennomføre hydrauliske målinger og høyhastighetsfilming av strømmingen i skovlen til en referanse modellturbin designet ved Vannkraftlaboratoriet.

**Oppgaven bearbeides ut fra følgende punkter:**

1. Gjennomføre modelltest av to Pelton løpehjul ved Vannkraftlaboratoriet
2. Gjennomføre filming med høyhastighetskamera på 2 modellturbiner
3. Analysere resultatene med hensyn på virkningsgrad og strømming i skovlene.
4. Utarbeide detaljert prosedyre for testing av Pelton turbiner i Vannkraftlaboratoriet. Prosedyrene skal skrives på engelsk og norsk.
5. Dersom det er tid, så skal studenten legge til rette for og gjennomføre trykk målinger i en skovl på løpehjulet.



Senest 14 dager etter utlevering av oppgaven skal kandidaten levere/sende instituttet en detaljert fremdrift- og eventuelt forsøksplan for oppgaven til evaluering og eventuelt diskusjon med faglig ansvarlig/veiledere. Detaljer ved eventuell utførelse av dataprogrammer skal avtales nærmere i samråd med faglig ansvarlig.

Besvarelsen redigeres mest mulig som en forskningsrapport med et sammendrag både på norsk og engelsk, konklusjon, litteraturliste, innholdsfortegnelse etc. Ved utarbeidelsen av teksten skal kandidaten legge vekt på å gjøre teksten oversiktlig og velskrevet. Med henblikk på lesning av besvarelsen er det viktig at de nødvendige henvisninger for korresponderende steder i tekst, tabeller og figurer anføres på begge steder. Ved bedømmelsen legges det stor vekt på at resultatene er grundig bearbeidet, at de oppstilles tabellarisk og/eller grafisk på en oversiktlig måte, og at de er diskutert utførlig.

Alle benyttede kilder, også muntlige opplysninger, skal oppgis på fullstendig måte. For tidsskrifter og bøker oppgis forfatter, tittel, årgang, sidetall og eventuelt figurnummer.

Det forutsettes at kandidaten tar initiativ til og holder nødvendig kontakt med faglærer og veileder(e). Kandidaten skal rette seg etter de reglementer og retningslinjer som gjelder ved alle (andre) fagmiljøer som kandidaten har kontakt med gjennom sin utførelse av oppgaven, samt etter eventuelle pålegg fra Institutt for energi- og prosesssteknikk.

Risikovurdering av kandidatens arbeid skal gjennomføres i henhold til instituttets prosedyrer. Risikovurderingen skal dokumenteres og inngå som del av besvarelsen. Hendelser relatert til kandidatens arbeid med uheldig innvirkning på helse, miljø eller sikkerhet, skal dokumenteres og inngå som en del av besvarelsen. Hvis dokumentasjonen på risikovurderingen utgjør veldig mange sider, leveres den fulle versjonen elektronisk til veileder og et utdrag inkluderes i besvarelsen.

I henhold til ”Utfyllende regler til studieforskriften for teknologistudiet/sivilingeniørstudiet” ved NTNU § 20, forbeholder instituttet seg retten til å benytte alle resultater og data til undervisnings- og forskningsformål, samt til fremtidige publikasjoner.

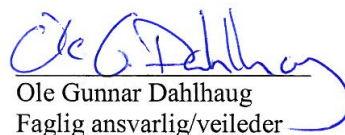
Besvarelsen leveres digitalt i DAIM. Et faglig sammendrag med oppgavens tittel, kandidatens navn, veileders navn, årstall, institutt navn, og NTNUs logo og navn, leveres til instituttet som en separat pdf-fil. Etter avtale leveres besvarelse og evt. annet materiale til veileder i digitalt format.

- Arbeid i Vannkraftlaboratoriet  
 Feltarbeid

NTNU, Institutt for energi- og prosesssteknikk, 14. januar 2014



Olav Bolland  
Instituttleder



Ole Gunnar Dahlhaug  
Faglig ansvarlig/veileder

Medveiledere:      Torbjørn K. Nielsen      Professor  
                         Bjørn Winther Solemslie      PhD-student



# Preface

During this past year at NTNU I have learnt alot about the Water Power Laboratory as well as all the challenges about laboratory work. This master thesis has been demanding, but at the same time interesting and alot of fun. My knowledge within planning, execution and analyzing model tests has increased substantially during the semester and it has been a great experience.

I want to especially thank PhD candidate Bjørn Winther Solemslie for essential help and assistance throughout the semester. Ole Gunnar Dahlhaugs positive nature and guidance have been much appreciated. During the work of this master thesis a lot of help was provided by the laboratory staff. I want to thank Trygve Opland, Bård Brandåstrø and Joar Grilstad for good advice and help with installations and adjustment of laboratory equipment. A special thanks goes to DynaVec AS and Kari Haugan for providing information and help in the laboratory.

Last but not least I want to thank my fellow students and all the employees at the Water Power Laboratory for this wonderful year.

Martine C. S. Wessel

Martine C. S. Wessel  
Trondheim , June 9, 2014





# Sammendrag

I denne oppgaven har det blitt gjennomført modelltester av Peltonturbiner ved Vannkraftlaboratoriet på NTNU. Modellriggen er presentert og gjennomføringen av virkningsgradsmålingene er beskrevet. Målet med denne oppgaven var opprinnelig å gjennomføre modelltest og observasjon av strømming i skovlen på to forskjellige modellturbiner tilgjengelig i laboratoriet. Likevel fikk jeg muligheten til å sammenligne 21 og 22 skovler for et skovldesign, sammenligne det første skovldesignet med et annet, itillegg til en tredje modellturbin. Målet med oppgaven ble dermed mer omfattende enn først antatt.

Observasjoner av strømmingen i skovlene, ved bruk av et høyhastighetskamera tilgjengelig i laboratoriet, ble gjennomført på tre forskjellige skovldesign, hvor av ett design ble kjørt med både 21 og 22 skovler. Modelltester av tre forskjellige løpehjul ble gjennomført hvorav ett skovldesign ble testet for både 21 og 22 skovler mens et annet skovldesign ble testet for 23 skovler. De tre skovldesignene undersøkt blir presentert som det første, det andre og det tredje designet. Det først og andre skovldesignet er designet av ingeniører fra DyneVec AS, en leverandør av vannturbiner. Det tredje skovldesign er designet av PhD kandidat Bjørn Winther Solemslie.

Resultatene fra modelltestene korresponderte med de forskjellige observasjonene fra filming med høyhastighetskamera. Modelltesten gjennomført for det første av de tre skovldesignene resulterte i høyeste virkningsgrad på 90.32% for 21 skovler og 90.62% for 22 skovler. Dette resultatet sammenfaller med en lavere grad av bakvask observert for 22 skovler. Observasjoner av strømming i skovlen for det andre designet, som var litt forskjellig fra det første,

avdekket en høyere grad av bakvask. Høyeste virkningsgrad oppnådd for det tredje designet var 83.42%.

Forskjellige bidrag til energitap i løpehjul er presentert og sannsynlige tegn på coriolis og coandaeffekten er diskutert. Forskjellig grad av bakvask og vanntap gjennom skovlens utskjæring samt interaksjon mellom skovl og vannstråle er undersøkt.

Muligheter for gjennomføring av trykkmålinger i skovl ved bruk av piezo-resistive trykktansdusere er undersøkt. På grunn av tidbegrensninger ble anvendelsen av dette utstyret ved Vannkraftlaboratoriet ikke undersøkt og implementert.

# Abstract

In this thesis model tests of Pelton turbines has been conducted in Water Power Laboratory at Norwegian University of Science and Technology. The turbine test rig is presented and the procedure of the efficiency is described. Originally the object of this master thesis was to conduct a model test and flow observations for two model turbines available in the laboratory. However, I had the opportunity to compare 21 and 22 buckets for one design, compare the first bucket design with another slightly different from the first, as well as a third model. The object of this report is therefore more comprehensive than first assumed.

Flow observations, using a high-speed camera available in the laboratory, was carried out for three different bucket designs, of which one of them was run for 21 and 22 buckets. Model tests of three different runners was conducted of which one design was run with 23 buckets and another was run with both 21 and 22. The three bucket designs investigated in this thesis will be presented as the first, the second and the third design. The first and the second sets of buckets are designed by engineers from DynaVec AS, a supplier of hydro turbines. The third set of buckets investigated is designed by PhD candidate Bjørn Winther Solemslie.

The results from the model tests conducted corresponded with the different observations from filming with high-speed camera. From the model test conducted for the first design in question the highest efficiency obtained was 90.32% for 21 buckets and 90.62% for 22 buckets. This result coincide with less back wash observed for 22 buckets. Flow observations from the second design, that was slightly different from the first, revealed a higher degree of

back wash. The highest efficiency obtained for the third design was 83.42%

Different contributions to energy loss is presented and probable signs of the Coriolis and Coanda effect is discussed. The evidence of back wash and water loss through the bucket cut-out are discussed for the different bucket designs in question as well as the interaction between the bucket and the water jet.

The possibility of conducting onboard pressure measurements in the Pelton turbine buckets using piezo-resistive pressure transducers is investigated. Due to time limitations was the application of this equipment in the Water Power Laboratory not investigated and implemented.

# Contents

<b>1</b>	<b>Introduction</b>	<b>1</b>
<b>2</b>	<b>Theory</b>	<b>3</b>
2.1	Pelton turbine design . . . . .	4
2.1.1	Number of buckets . . . . .	4
2.1.2	Bucket angle of setting . . . . .	4
2.1.3	Bucket surface shape . . . . .	5
2.2	Optimal rotational speed . . . . .	5
2.2.1	Outlet velocity diagrams . . . . .	7
2.3	Reduced Values . . . . .	8
2.4	Testing Turbine Models . . . . .	9
2.5	Hydraulic efficiency . . . . .	9
2.5.1	Influence of head and speed variations . . . . .	10
2.6	Flow observations . . . . .	10
2.6.1	Requirements . . . . .	12
2.7	Onboard pressure measurement . . . . .	13
2.7.1	Piezo-resistive pressure transducers . . . . .	13
<b>3</b>	<b>Equipment and Method</b>	<b>17</b>
3.1	Instrumentation . . . . .	18
3.2	Calibration . . . . .	19
3.2.1	Volume flow meter . . . . .	20
3.2.2	Torque transducer . . . . .	20
3.2.3	Friction torque transducer . . . . .	23
3.2.4	Differential pressure transmitter . . . . .	24
3.2.5	Temperature measurement . . . . .	25

3.3	The Test Matrix . . . . .	25
3.4	Analysis procedure for experimental data . . . . .	26
<b>4</b>	<b>Filming With High-Speed Camera</b>	<b>29</b>
4.1	Camera settings and properties . . . . .	29
4.2	Rig improvements . . . . .	30
4.2.1	Trigger . . . . .	30
<b>5</b>	<b>Uncertainty Analysis</b>	<b>33</b>
5.1	Uncertainty in Calibration . . . . .	35
5.1.1	Uncertainty in the calibration of the differential pressure transmitter . . . . .	35
5.1.2	Uncertainty in the calibration of the volume flow meter	36
5.1.3	Uncertainty in the calibration of the torque transducer	37
5.1.4	Uncertainty in the calibration of the friction torque transducer . . . . .	37
5.2	Uncertainty of the tests . . . . .	38
5.2.1	Total uncertainty of the hydraulic efficiency . . . . .	39
5.2.2	Uncertainty in the efficiency . . . . .	40
<b>6</b>	<b>Results</b>	<b>41</b>
6.1	Model tests . . . . .	41
6.1.1	First design - 21 buckets . . . . .	41
6.1.2	First design - 22 buckets . . . . .	41
6.1.3	Third design - 23 buckets . . . . .	42
6.2	Filming with high speed camera . . . . .	44
6.2.1	First design - 21 buckets . . . . .	47
6.2.2	First design - 22 buckets . . . . .	49
6.2.3	Second design . . . . .	50
6.2.4	Third design . . . . .	52
<b>7</b>	<b>Discussion</b>	<b>55</b>
7.1	Misplaced nozzle . . . . .	55
7.2	Problems encountered during the experiments . . . . .	56
7.3	First design - 21 buckets . . . . .	56
7.4	First design - 22 buckets . . . . .	56
7.5	Second design . . . . .	57

7.6	Third design - 23 buckets . . . . .	57
7.6.1	Loss . . . . .	58
7.6.2	Misplaced nozzle . . . . .	58
7.6.3	Multiple efficiency peaks . . . . .	59
7.6.4	Effect of lowered effective head . . . . .	60
7.7	General observations . . . . .	61
7.7.1	Irregular water film . . . . .	62
7.7.2	Forces acting on the water flow . . . . .	62
7.8	Onboard pressure measurements . . . . .	64
7.8.1	Location and distribution of sensors . . . . .	64
7.8.2	Instrumented shaft . . . . .	64
<b>8</b>	<b>Conclusion</b>	<b>65</b>
<b>9</b>	<b>Further Work</b>	<b>67</b>
9.1	Pressure measurement in the buckets . . . . .	67
9.2	Onboard borescope . . . . .	67
9.3	Future work . . . . .	67
<b>A</b>	<b>Calibration data</b>	<b>III</b>
<b>B</b>	<b>Test Procedure</b>	<b>XV</b>
A	Start Up . . . . .	XV
B	Taking Measurements for a Hill Diagram . . . . .	XVI
C	Shut Down . . . . .	XVIII
<b>C</b>	<b>Prosedyre for modelltest - Norwegian</b>	<b>XIX</b>
A	Igangsetting av Pelton-sløyfen . . . . .	XIX
B	Gjennomføring av tester . . . . .	XX
C	Nedkjøring av Pelton-sløyfen . . . . .	XXI
<b>D</b>	<b>Results</b>	<b>XXV</b>
<b>E</b>	<b>Filming with high-speed camera</b>	<b>XXIX</b>
A	First design - 21 buckets . . . . .	XXX
B	First design - 22 buckets . . . . .	XXXIV
C	Second design . . . . .	XXXV
D	Pelton buckets designed by Bjørn Winther Solemslie . . . . .	XXXVII

<b>F</b>	<b>Uncertainty Analysis</b>	<b>XLVII</b>
A	Uncertainty in the calibration . . . . .	XLVII
A.1	Uncertainty in the calibration of the differential pressure transmitter . . . . .	XLVII
A.2	Uncertainty in the calibration of the volume flow meter	XLVIII
A.3	Uncertainty in the calibration of the torque transducer	XLVIII
A.4	Uncertainty in the calibration of the friction torque transducer . . . . .	XLIX
B	Uncertainty of the Test . . . . .	XLIX
B.1	Rotational Speed . . . . .	XLIX
B.2	Hydraulic energy . . . . .	L
<b>G</b>	<b>Matlab source code</b>	<b>LIII</b>
A	Import raw data . . . . .	LIII
B	Calculate mean data from raw data . . . . .	LV
C	Add systematic uncertainty to mean data matrix . . . . .	LIX
D	Efficiency curve fitting . . . . .	LXI
E	Plot efficiency Hill chart . . . . .	LXII



# List of Figures

2.1	The main dimensions [2] . . . . .	3
2.2	Width of the bucket [2] . . . . .	3
2.3	Relative path of the water jet [7] . . . . .	4
2.4	Definitions related to the bucket, ref Bjørn Winther Solemslie	5
2.5	Velocity diagram for a Pelton turbine [1] . . . . .	6
2.6	Velocity diagram for the outlet of a Pelton bucket . . . . .	7
2.7	Sketch of Pelton turbine buckets without and with backwash, respectively [12] . . . . .	8
2.8	Bucket angle definition [7] . . . . .	12
2.9	Onboard endoscope location and assembly [7] . . . . .	14
2.10	Field of observation [7] . . . . .	14
2.11	Wheatstone bridge of a piezo-resistive sensor [7] . . . . .	15
2.12	Wheatstone bridge . . . . .	15
3.1	The Pelton turbine model . . . . .	17
3.2	The Pelton turbine test rig [8] . . . . .	17
3.3	Schematic overview of instrument setup . . . . .	19
3.4	Calibration curve for the volume flow meter . . . . .	20
3.5	Calibrating the torque transducer . . . . .	21
3.6	Calibration curve for the torque transducer . . . . .	22
3.7	Uncertainty band for the torque transducer calibration . . . .	22
3.8	Setup for the friction torque calibration . . . . .	23
3.9	Calibration curve for the friction torque transducer . . . . .	24
3.10	Calibration curve for the differential pressure transmitter . . .	25
3.11	The difference between the first and the second design, ref Dynavec AS . . . . .	27
3.12	The third bucket design, ref Bjørn Winther Solemslie . . . . .	27

3.13	Operating points investigated for the first bucket design . . .	28
3.14	Operating points investigated for the third bucket design . . .	28
4.1	Placement of camera and light source . . . . .	30
6.1	Hill-diagram, first design, 21 buckets . . . . .	42
6.2	Hill-diagram, first design, 22 buckets . . . . .	43
6.3	Hill-diagram, first model test . . . . .	44
6.4	Hill-diagram, second model test . . . . .	45
6.5	First design, 21 buckets, 70m head, $n_{11} = 41$ . . . . .	47
6.6	First design, 21 buckets, 70m head, $Q_{11} = 0.020$ , $n_{11} = 41$ . .	48
6.7	First design, 22 buckets, 70m head, $Q_{11} = 0.020$ , $n_{11} = 41$ . .	49
6.8	$Q_{11} = 0.020$ , $n_{11} = 41$ . . . . .	50
6.9	$Q_{11} = 0.022$ , $n_{11} = 41$ . . . . .	51
6.10	Third design, 25m head, $Q_{11} = 0.012$ , $n_{11} = 44$ . . . . .	53
6.11	Third design, 25m head, $Q_{11} = 0.012$ , $n_{11} = 38.5$ . . . . .	53
6.12	Third design, 70m head, $Q_{11} = 0.012$ , $n_{11} = 44$ . . . . .	54
7.1	Misplaced nozzle . . . . .	55
7.2	Adjusted nozzle . . . . .	55
7.3	The difference between the first and the second design, ref Dynavec AS . . . . .	58
7.4	Second design . . . . .	59
7.5	Third design, $n_{11} = 41$ , $Q_{11} = 0.0101$ . . . . .	60
7.6	Third design, $n_{11} = 44$ , $Q_{11} = 0.0176$ . . . . .	61
7.7	Water loss through bucket lip . . . . .	62
7.8	Development of water jet . . . . .	63
C.1	Valve number 1 for controlling the water adjusting the nozzle	XXII
C.2	Valve number 2 for controlling the water adjusting the nozzle	XXII
C.3	Valves for venting out air ahead of pressure sensor . . . . .	XXIII
E.1	70m head, Nozzle opening=14mm, $n_{11} = 41$ . . . . .	XXX
E.2	70m head, Nozzle opening=18mm, $n_{11} = 41$ . . . . .	XXX
E.3	70m head, Nozzle opening=18mm, $n_{11} = 41$ . . . . .	XXXI
E.4	70m head, Nozzle opening=18mm, $n_{11} = 41$ . . . . .	XXXI
E.5	70m head, Nozzle opening=22mm, $n_{11} = 41$ . . . . .	XXXII
E.6	70m head, Nozzle opening=24mm, $n_{11} = 41$ . . . . .	XXXII

E.7	70m head, Nozzle opening=24mm, $n_{11} = 41$	XXXIII
E.8	70m head, Nozzle opening=18mm, $n_{11} = 41$	XXXIV
E.9	70m head, Nozzle opening=14mm, $n_{11} = 41$	XXXV
E.10	70m head, Nozzle opening=18mm, $n_{11} = 41$	XXXV
E.11	70m head, Nozzle opening=22mm, $n_{11} = 41$	XXXVI
E.12	70m head, Nozzle opening=24mm, $n_{11} = 41$	XXXVI
E.13	70m head, Nozzle opening=24mm, $n_{11} = 41$	XXXVI
E.14	70m head, $Q_{11} = 0,022$ , $n_{11} = 41$	XXXVI
E.15	25m head, Nozzle opening=6mm, $n_{11} = 38,5$	XXXVII
E.16	25m head, Nozzle opening=8mm, $n_{11} = 38,5$	XXXVII
E.17	25m head, Nozzle opening=10mm, $n_{11} = 38,5$	XXXVIII
E.18	25m head, Nozzle opening=12mm, $n_{11} = 38,5$	XXXVIII
E.19	25m head, Nozzle opening=14mm, $n_{11} = 38,5$	XXXIX
E.20	25m head, Nozzle opening=16mm, $n_{11} = 38,5$	XXXIX
E.21	25m head, Nozzle opening=18mm, $n_{11} = 38,5$	XXXIX
E.22	25m head, Nozzle opening=6mm, $n_{11} = 41$	XXXIX
E.23	25m head, Nozzle opening=8mm, $n_{11} = 41$	XL
E.24	25m head, Nozzle opening=10mm, $n_{11} = 41$	XL
E.25	25m head, Nozzle opening=12mm, $n_{11} = 41$	XL
E.26	25m head, Nozzle opening=14mm, $n_{11} = 41$	XL
E.27	25m head, Nozzle opening=16mm, $n_{11} = 41$	XLI
E.28	25m head, Nozzle opening=18mm, $n_{11} = 41$	XLI
E.29	25m head, Nozzle opening=6mm, $n_{11} = 44$	XLI
E.30	25m head, Nozzle opening=8mm, $n_{11} = 44$	XLI
E.31	25m head, Nozzle opening=10mm, $n_{11} = 44$	XLII
E.32	25m head, Nozzle opening=12mm, $n_{11} = 44$	XLII
E.33	25m head, Nozzle opening=14mm, $n_{11} = 44$	XLII
E.34	25m head, Nozzle opening=16mm, $n_{11} = 44$	XLII
E.35	25m head, Nozzle opening=18mm, $n_{11} = 44$	XLIII
E.36	70m head, Nozzle opening=6mm, $n_{11} = 44$	XLIII
E.37	70m head, Nozzle opening=8mm, $n_{11} = 44$	XLIII
E.38	70m head, Nozzle opening=10mm, $n_{11} = 44$	XLIII
E.39	70m head, Nozzle opening=12mm, $n_{11} = 44$	XLIV
E.40	70m head, Nozzle opening=14mm, $n_{11} = 44$	XLIV
E.41	70m head, Nozzle opening=16mm, $n_{11} = 44$	XLIV
E.42	70m head, Nozzle opening=18mm, $n_{11} = 44$	XLIV

E.43	70m head, Nozzle opening=6mm, $n_{11} = 41$	. . . . .	XLV
E.44	70m head, Nozzle opening=8mm, $n_{11} = 41$	. . . . .	XLV
E.45	70m head, Nozzle opening=10mm, $n_{11} = 41$	. . . . .	XLV
E.46	70m head, Nozzle opening=12mm, $n_{11} = 41$	. . . . .	XLV
E.47	70m head, Nozzle opening=14mm, $n_{11} = 41$	. . . . .	XLVI
E.48	70m head, Nozzle opening=16mm, $n_{11} = 41$	. . . . .	XLVI
E.49	70m head, Nozzle opening=18mm, $n_{11} = 41$	. . . . .	XLVI

# List of Tables

3.1	Instruments . . . . .	18
3.2	The different turbines investigated . . . . .	26
5.1	Component errors in the calibration of an instrument . . . . .	35
5.2	Component errors in the test . . . . .	38
6.1	Calculation of the location of BEP . . . . .	46



# Nomenclature

Symbol	Description	Unit
$arm$	Torque arm	$m$
$B$	Bucket width	$m$
$c$	Absolute water velocity	$m/s$
$D$	Diameter	$m$
$E$	Specific hydraulic energy	$J/kg$
$e_X$	Total absolute error in quantity X	
$F$	Force	$N$
$f$	Friction factor	
$f_{X_{cal}}$	Total relative uncertainty of calibration of the instrument measuring the quantity X	
$f_X$	Total relative error in quantity X	
$g$	Acceleration of gravity	$m/s^2$
$\Delta h$	Height difference	$m$
$H_e$	Effective head	$m$
$H_{dyn}$	Dynamic head	$m$
$H_{stat}$	Static head	$m$
$m$	Mass	$kg$
$N$	Number of measurements	
$n$	Rotational speed	$rpm$
$n_{11}$	Modified speed factor	$rpm\sqrt{m}$
$n_{ED}$	Speed factor	
$P$	Power	$W$
$P_m$	Mechanical power	$W$
$P_h$	Hydraulic power	$W$

$P_{Lm}$	Power dissipated in bearings and shaft seals	$W$
$p_{amp}$	Atmospheric pressure	$Pa$
$p_M$	Measured atmospheric pressure	$Pa$
$\Delta p$	Differential pressure	$Pa$
$Q$	Volumetric flow rate	$m^3/s$
$Q_{11}$	Modified discharge factor	$l/sm^{5/2}$
$Q_{ED}$	Discharge factor	
$Re$	Reynolds number	
$S_X$	Standard deviation of the output of the measurements	
$S_{XX}$	Experimental error variation of input around the linear approximation	
$S_{XY}$	Experimental error co-variation of output and input around the linear approximation	
$S_{YY}$	Experimental error variation of output around the linear approximation	
$T$	Temperature	$^{\circ}C$
$t_{\alpha/2}$	t-value for confidence level $1 - \alpha$	
$u$	Peripheral velocity	$m/s$
$\bar{X}$	Arithmetic mean of measurements	
$Z$	Number of nozzles	

### Greek letters

<b>Symbol</b>	<b>Description</b>	<b>Unit</b>
$\alpha$	Confidence level, $1 - \alpha$	
$\beta$	Jet angle of attack on the bucket	deg
$\eta_h$	Hydraulic efficiency	
$\omega$	Rotational speed	$m/s$
$\bar{\rho}$	Mean water density	$kg/m^3$
$\rho$	Water density	$kg/m^3$
$\sigma$	Loss coefficient	
$\tau$	Torque	$Nm$



## Abbreviation

<b>Symbol</b>	<b>Description</b>	<b>Unit</b>
<i>BEP</i>	Best Efficiency Point	
<i>CFD</i>	Computational Fluid Dynamics	
<i>IEC</i>	International Electrotechnical Commission	
<i>NTNU</i>	Norwegian University of Science and Technology	



# Chapter 1

## Introduction

Hydro power is an important source of renewable energy and Norway is a country blessed with a topology and climate suited for the production of electricity by hydro power. As climate change has led to an increased focus on renewable energy, an increase in the efficiency of energy transfer from renewable resources is of key interest.

Even though the Pelton turbine is 100 years old there are still areas lacking knowledge. The Pelton turbine only utilizes the velocity to extract energy from the water as it passes through the turbine. It is therefore defined as an impulse turbine, and it is best suitable for high head and relatively low flow rate.

For Pelton turbines, research and development are mainly performed by experimental or analytical studies. The turbine design is a result of long and fastidious laboratory tests to determine and predict the performances of the machine and estimate the rupture threshold, due to fatigue or corrosion, and the service life. Experimental investigations of the flow in Pelton turbines that are presented in the literature can be divided in three classes. These classes are (i) flow observations, (ii) pressure measurements, and (iii) water film thickness. During the fall of 2013 experiments on one Pelton turbine was conducted in relation to the authors project thesis [13]. Anna Louise Martinsen conducted experiments with pressure measurements in the Pelton turbine buckets at NTNU in 2000 [5]. Stine Trefall investigated the flow in

Pelton turbines and conducted model tests of several Pelton turbine models in the Water Power Laboratory at NTNU in 2011 [12]. Alexandre Perrig conducted experiments on a Pelton turbine model including model tests, pressure measurements in the turbine bucket and flow observations [7]. This master thesis will focus on flow observations by filming with a high-speed camera available in the Water power laboratory at NTNU as well as model tests of Pelton turbines. Flow observations together with corresponding model tests can provide a better understanding and knowledge around the behavior of the water flow in a Pelton turbine.

# Chapter 2

## Theory

The Pelton turbine is an impulse turbine, also known as a partial turbine or an action turbine. It is suitable for high head and a relatively low flow rate. The Pelton turbine differs from reaction turbines such as Francis and Kaplan by the fact that the energy extracted from the water is associated with velocity. Through one or multiple nozzles, the pressure energy in the water is transformed to dynamic pressure, or velocity. The Pelton turbine has a wide operating range and is therefore suitable for power plants with large variations in the water discharge and pressure. [1]

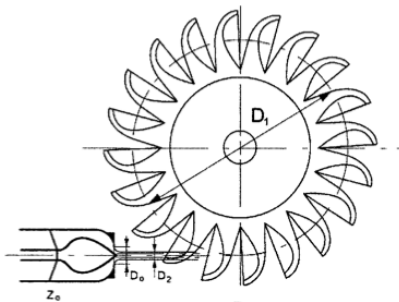


Figure 2.1: The main dimensions [2]

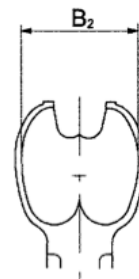


Figure 2.2: Width of the bucket [2]

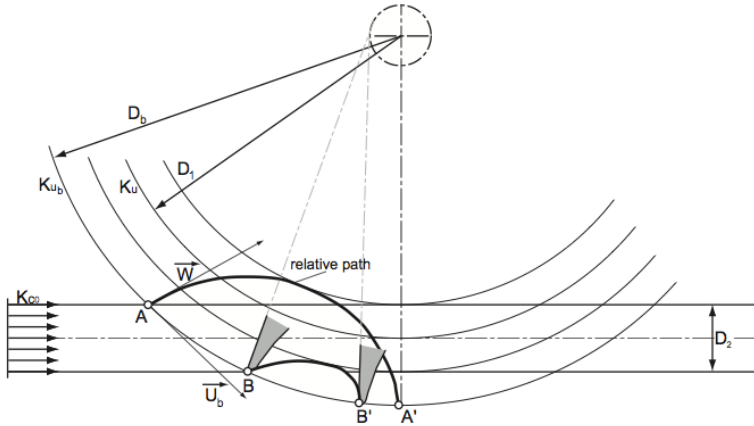


Figure 2.3: Relative path of the water jet [7]

## 2.1 Pelton turbine design

The main dimensions of the Pelton turbine is illustrated in Figure 2.1 and 2.2 and the definitions related to the bucket is illustrated in Figure 2.4.

### 2.1.1 Number of buckets

The number of buckets for a runner must be determined so that no water is lost and at the same time minimize the risks of interactions between the outflowing water and the oncoming buckets.

### 2.1.2 Bucket angle of setting

The bucket angle is set so that the splitter in the bucket is perpendicular to the jet axis when the center of gravity of the jet reaches the bucket. The runner pitch is determined by the paths of the bucket tip, diameter  $D_p$ , the Pelton diameter,  $D_1$ , and the relative paths of the water from the upper and lower part of the jet, respectively AA' and BB' in Figure 2.3. The bucket pitch must be determined so that no water from the lower part of the jet can escape the runner without encountering any bucket, *i.e* it must be smaller than the arc BB' [7].

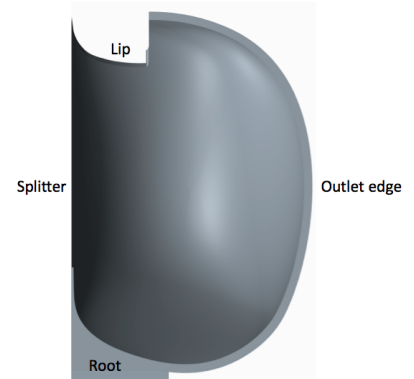


Figure 2.4: Definitions related to the bucket, ref Bjørn Winther Solemslie

### 2.1.3 Bucket surface shape

The design process of the buckets consist of defining elevation curves of the inner surface. The cut-out area at the backside of the bucket and the bucket backside shapes are to be designed so that the jet does not impinge on the cut-out too early. The dimension of the bucket are proportional to the jet diameter. The splitter angle is usually never smaller than  $20^\circ$  to avoid rapid destruction. The water leaving in rearward direction, towards the root, should not impinge on the runner flange. [7]

## 2.2 Optimal rotational speed

Euler's turbine equation shows the theoretical ratio between the energy available in the flow and the energy transferred to the turbine [1], and is shown in Equation 2.1. The subscription 1 denotes inlet, subscription 2 denotes outlet and  $u$  denotes the peripheral velocity component.

$$\eta_h = \frac{c_{u1} \cdot u_1 - c_{u2} \cdot u_2}{g \cdot H_e} [-] \quad (2.1)$$

With this equation it is possible to find the optimal rotational speed of a Pelton turbine. With the assumption that all the energy is transferred to the turbine, the absolute velocity of the water leaving the turbine bucket,  $c_{u2}$ , is zero at the best point of operation. However, when exiting the bucket,

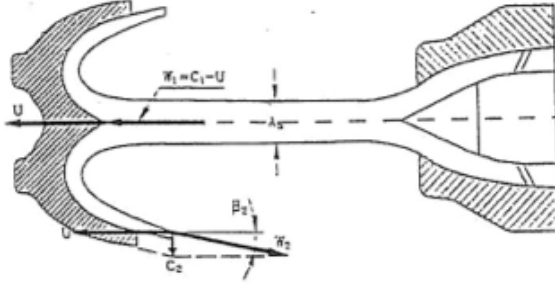


Figure 2.5: Velocity diagram for a Pelton turbine [1]

the water leaving the bucket may hit the oncoming bucket. This results in what we call back wash. The simplification, shown in Equation 2.2, is still assumed to be a good approximation when determining the optimal peripheral speed,  $u$ . [10]

$$\eta_h = \frac{c_{u1} \cdot u_1}{g \cdot H_e} [-] \quad (2.2)$$

The velocity diagrams for the flow entering and leaving the runner of a Pelton turbine is shown in Figure 2.5.  $c$  denotes the absolute velocity,  $w$  denotes the relative velocity and  $u$  denotes the peripheral velocity of the runner. The flow exiting the nozzle has only a component in the peripheral direction,  $c_{u1} = c_1$ . The velocity out of the nozzle, including a loss coefficient  $\sigma$ , can be expressed as in Equation 2.3.

$$c_1 = \sigma \sqrt{2 \cdot g \cdot H_e} [m/s] \quad (2.3)$$

By solving Equation 2.2 for  $u_1$  with  $c_1$  from Equation 2.3 an expression for the optimal peripheral speed can be obtained as in Equation 2.4 [10].

$$u_1 = \frac{\eta_h \cdot h \cdot H_e}{c_1} = \frac{\eta_h \cdot g \cdot H_e \cdot c_1}{\sigma^2 \cdot 2 \cdot g \cdot H_e} = \frac{\eta_h \cdot c_1}{2 \cdot \sigma^2} [m/s] \quad (2.4)$$

The rotational speed of the turbine is defined as  $\omega = 2u/D$ . The expression for the optimal rotational speed becomes as in the equation below.

$$\omega = \frac{2 \cdot \eta_h \cdot c_1}{2 \cdot D \cdot \sigma^2} [1/s] \quad (2.5)$$



## 2.2.1 Outlet velocity diagrams

Figure 2.6 shows the velocity diagram to the water at the outlet of the bucket. Different ratios between the rotational speed and the jet velocity,  $u/c_1$  is shown. The water leaves the bucket with the relative velocity  $\omega_2$  with an angle  $\beta$  to the original direction of the flow. The absolute velocity,  $c_1$ , for the jet at the inlet is equal for the different cases of outlet flow. When  $\beta$  is small,  $\omega_{2u}$  is bigger than when  $\beta$  is large and  $u/c_1$  is kept constant. If  $\omega_{2u}$  is too large compared to  $u$ , *i.e.*  $\beta$  becomes too small and  $u/c_1$  becomes too big, will back wash occur, as illustrated in Figure 2.7. This means that when the water leaves one bucket it subsequently carshes into the next, creating torque in the negative direction. [12]

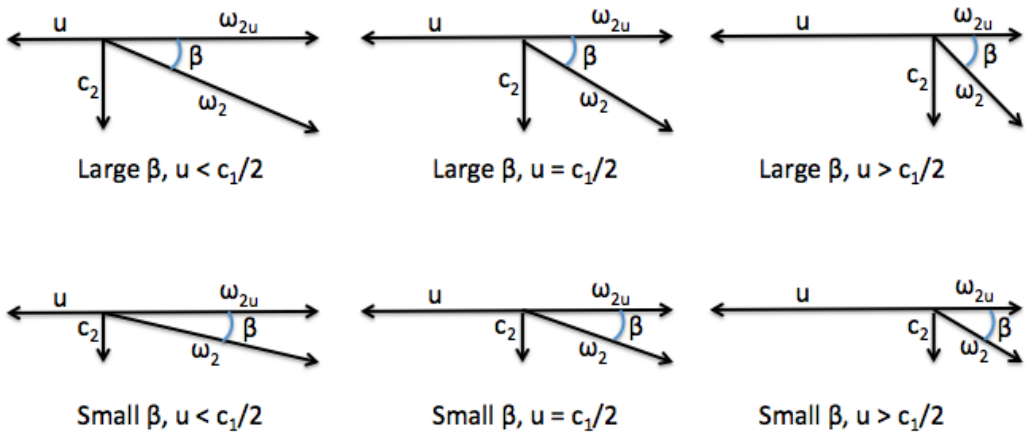


Figure 2.6: Velocity diagram for the outlet of a Pelton bucket

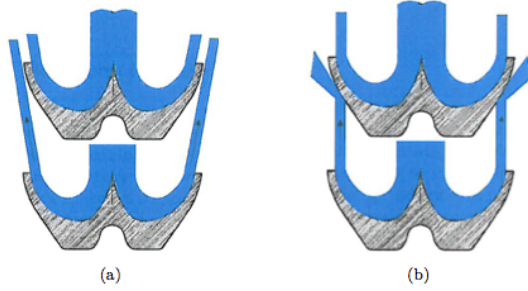


Figure 2.7: Sketch of Pelton turbine buckets without and with backwash, respectively [12]

## 2.3 Reduced Values

As described in the authors project thesis [13], the use of reduced values makes scaling the results easier. The dimensionless parameters for the discharge factor,  $Q_{ED}$ , and for the speed factor,  $n_{ED}$ , are shown in Equation (2.6) and (2.7), and the modified parameters,  $Q_{11}$  and  $n_{11}$ , are shown in Equation (2.8) and (2.9) respectively.

$$Q_{ED} = \frac{Q}{D^2 \sqrt{g \cdot H_e}} [-] \quad (2.6)$$

$$n_{ED} = \frac{n \cdot D}{\sqrt{g \cdot H_e}} [-] \quad (2.7)$$

$$Q_{11} = \frac{Q}{D^2 \sqrt{H_e}} [l/sm^{5/2}] \quad (2.8)$$

$$n_{11} = \frac{n \cdot D}{\sqrt{H_e}} [rpm\sqrt{m}] \quad (2.9)$$

Both the parameters  $n_{ED}$  and  $Q_{ED}$  and the modified parameters  $n_{11}$  and

$Q_{11}$  are commonly used. The modified parameters,  $Q_{11}$  and  $n_{11}$ , have been used throughout this report.

## 2.4 Testing Turbine Models

Model tests are often conducted before a prototype is produced. A model test is a good tool when predicting the operation and performance of the actual turbine. This is beneficial because of the smaller production cost of a model due to the smaller size. According to the international standard IEC 60193 [4] the following conditions must be fulfilled for a model test to be viable.

*The geometric similarity* (homology) between model and prototype is related to the shape of the turbine. This is done by making an exact replica of the planned prototype, but geometrically scaled down. [10]

*The hydraulic similarity* is related to the forces acting on the model compared to the prototype. For Pelton turbines the hydraulic similarity is defined as when the reduced quantities are the same for both the prototype as for the model, as defined in Equation 2.10 and 2.11. [10]

$$(n_{11})_{Prototype} = (n_{11})_{Model} = \left(\frac{n \cdot D}{\sqrt{H_e}}\right)_{Model} \quad (2.10)$$

$$(Q_{11})_{Prototype} = (Q_{11})_{Model} = \left(\frac{Q}{D^2 \sqrt{H_e}}\right)_{Model} \quad (2.11)$$

## 2.5 Hydraulic efficiency

The hydraulic efficiency,  $\eta$ , is defined by the IEC standard [4] as:

$$\eta_h = \frac{P_m}{P_h} = \frac{P + P_{Lm}}{E \cdot Q \cdot \bar{\rho}} = \frac{P + P_{Lm}}{\bar{\rho} \cdot g \cdot Q \cdot H_e} [-] \quad (2.12)$$

This equation is used when testing model turbines.  $P$  is the power delivered by the turbine shaft and is equal to the product of the torque and the rotational speed,  $P = T * \omega$ .  $P_{Lm}$  is the power dissipated in the bearings and shaft seals.  $Q$  is the volumetric flow and  $\bar{\rho}$  is the density of the water.

$H_e$  is the effective head, and is defined in Equation 2.13. The effective head is the total pressure measured in *meter water column* and consists of the static head,  $H_{stat}$ , and the dynamic head,  $H_{dyn}$ .  $E$  is the specific hydraulic energy and is defined in Equation 2.14. The specific hydraulic energy is the energy available in the water between the high and low pressure side of the machine.

$$H_e = \underbrace{\frac{\Delta p}{\rho \cdot g} + Z}_{\text{Statischehead}(H_{stat})} + \underbrace{\frac{v^2}{2 \cdot g}}_{\text{Dynamichead}(H_{dyn})} \quad [m] \quad (2.13)$$

$$E = \frac{p_{M_1} - p_{amb}}{\bar{\rho}} + g \cdot \Delta h + \frac{c_1^2}{2} = \frac{\Delta p}{\bar{\rho}} + g \cdot \Delta h + \frac{c_1^2}{2} [J] \quad (2.14)$$

$\bar{\rho}$  is the mean density of the water between the high and low pressure side of the machine.  $p_{M_1}$  is the absolute pressure at the turbine inlet and  $p_{amb}$  is the atmospheric pressure.  $\Delta h$  is the height difference between the pressure transducer and the center of the turbine inlet.

### 2.5.1 Influence of head and speed variations

The turbine efficiency will primarily be a function of the specific speed,  $n_{11}$ . The basic concept of the *turbine specific speed* is to identify the optimum operating conditions for a given turbine design [13]. The speed coefficient of the runner and the relative paths of the water changes as a result of variations in speed or head. Overspeed or head decrease away from the best efficiency point results in that the relative paths become shorter and a portion of the water would slip off the runner. Underspeed or head increase would result in that the relative paths become longer and the water particles would encounter the buckets too early. Increasing the relative speed increases the losses, and increased head would increase discharge and the buckets may be flooded. [7]

## 2.6 Flow observations

When designing and improving the Pelton turbine bucket, visual observations of the flow using high-speed camera may be of interest. The informa-

tion obtained can be used to detect errors, and estimate service time and cracking caused by fatigue or corrosion [12]. The Pelton turbines combine four types of flow: (i) confined, steady-state flow in the piping systems and injector, (ii) free water jets, (iii) 3D unsteady free surface flows in the buckets, and (iv) dispersed 2-phase flows in the casing [7]. The flow in Pelton turbines has not been analyzed with much detail so far, and the understanding of the physics of key phenomena, *i.e* the initial jet/bucket interaction or the jet cut process, is weak. Some machines also present erosion damages that have not been sufficiently described before [6]. The optimal angle for the jet to bucket interface is  $90^\circ$  on the ridge in the bucket. What is often not counted for in the theory is the path up to this point and after this point until the next bucket takes over the jet. This ought to be investigated further in order to better understand the behavior of the Pelton turbine runner. The flow in a Pelton turbine is defined as non-stationary. This makes it difficult to establish thoroughly theoretical analyses. In addition, the complex rotating geometry, the interaction between the runner and the casing and the free surface makes it challenging to simulate the flow over the buckets. H. Christie (1918) [3] reconstructed the path of a particle moving with the water in the bucket from the relative acceleration equations. This analysis is based upon the following facts:

- The acceleration on a particle on the jet surface is zero before entering the buckets and the acceleration on the particle is zero after the outlet of the buckets.
- The acceleration on a particle must always be normal to the water surface.
- The water volume on a bucket included the outlet water behind the buckets is equal to the water volume cut out of the jet.

Based on these paragraphs it is possible to carry out a graphical analysis for determination of the particle trace over the buckets on the water surface [2]. According to Perrig [7], who conducted filming with high-speed camera using an onboard endoscope, is the bucket duty cycle divided in to the six following steps:

- Approach of the tip to the jet ( $\theta < -40^\circ$ )

- Initial feeding process ( $\theta = -40^\circ - -10^\circ$ )
- Entire separation of the jet ( $\theta = -10^\circ - 0^\circ$ )
- Last stage of inflow ( $\theta = 0^\circ - 15^\circ$ )
- Last stage of outflow ( $\theta = 15^\circ - 50^\circ$ )
- Series of droplets ( $\theta = 50^\circ - \infty$ )

$\theta$  is the angle between the water jet and the bucket, as illustrated in Figure 2.8. The bucket duty cycle is the path between A and B.

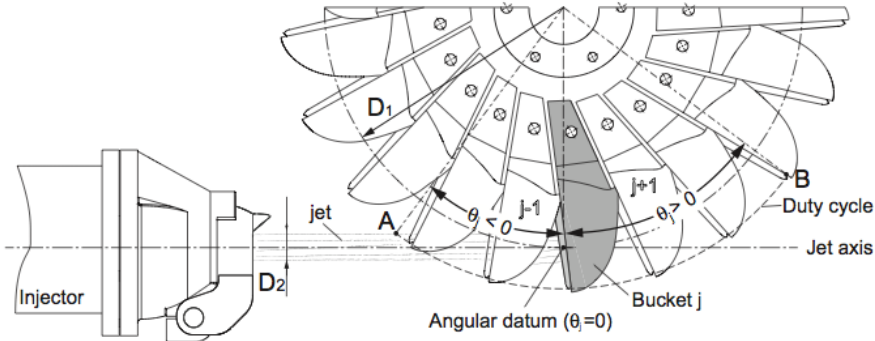


Figure 2.8: Bucket angle definition [7]

### 2.6.1 Requirements

Perrig [7] chose a number of requirements for filming with high speed camera, defined by S. Kvicinsky. There were 6 requirements:

1. The optical dimensions are to be compact enough so as to not disturb the flow around the runner. The water sheets leaving the runner should under no circumstances be deviated back against the runner.
2. It should permit a close observation of the subject.
3. The field of view must offer a large depth without need for focusing, enabling to follow the evolution of flow structures likely to be convected by the main stream.

4. The image distortions are to be kept to the minimum to avoid heavy post-processing of the images. Very short focal lengths like fish-eye lenses are not considered as a solution for this reason.
5. The luminosity must remain acceptable for performing high-speed photography.
6. The system has to be waterproof, and equipped with a lens wiping system to prevent the droplets present in the atmosphere surrounding the turbine to stick on it and reduce the visibility.

The optical requirements presented here match those of medical imagery. A large depth of sight is of primary importance. A range of endoscopes of different lengths and diameters, rigid or flexible are available on the market. Endoscopes meet more and more the requirements for industrial applications for complex structures inspections without need for dismantling. Perrig chose a  $3.8\text{mm}$  diameter rigid borescope for the onboard flow visualizations in the Pelton turbine. Location and assembly of the endoscope is illustrated in Figure 2.9 [7]. The field of observation will, according to Perrig, be as illustrated in Figure 2.10.

## 2.7 Onboard pressure measurement

Onboard pressure measurements in the Pelton turbine buckets can be beneficial in order to investigate the behaviour of the flow, and thus the energy transfer.

### 2.7.1 Piezo-resistive pressure transducers

In order to investigate the pressure distribution in the Pelton turbine bucket, pressure sensors need to be installed. Piezo-resistive sensors are designed for dynamic and static pressure measurements. The pressure sensitive elements are piezo-resistive chips made of micro-machined silicon, mounted in a wheatstone bridge. A schematic illustration can be seen in Figure 2.11 [7]. The pressure sensors have an active face of high stiffness waterproof membrane that will deform when subjected to a force due to pressure. On the periphery of the membrane the piezo-resistive gauges are placed in traction

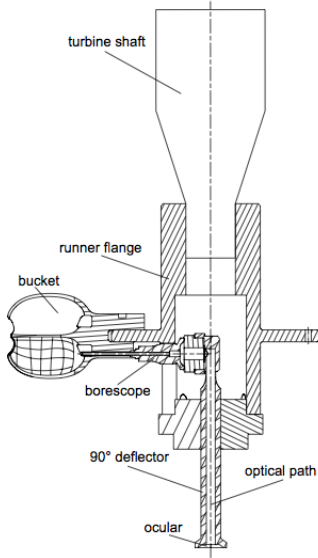


Figure 2.9: Onboard endoscope location and assembly [7]

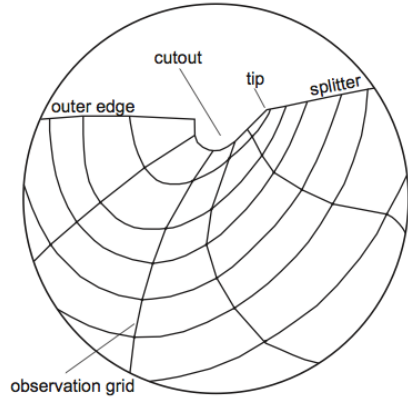


Figure 2.10: Field of observation [7]

and compression zones. When a pressure is applied on the membrane, the deformation is transmitted to the gauges. The deformation leads to change in the resistance or a piezo-resistive element. The membranes are attached to a resistor, or strain gauges, in a so called wheatstone bridge that interprets the deformation in the sensor. The change in the resistance in the wheatstone bridge creates a variation in the output voltage of the sensors and is proportional to the impinging pressure. [7] [5]

A simpler version of the wheatstone bridge is illustrated in Figure 2.12 [5]. The resistors works two and two together. While one of the sensors stretches and the resistance increases, another sensor is compressed and the resistance decreases. Resistor 1 and 2 works together, while resistors 3 and 4 sends the output voltage signal.



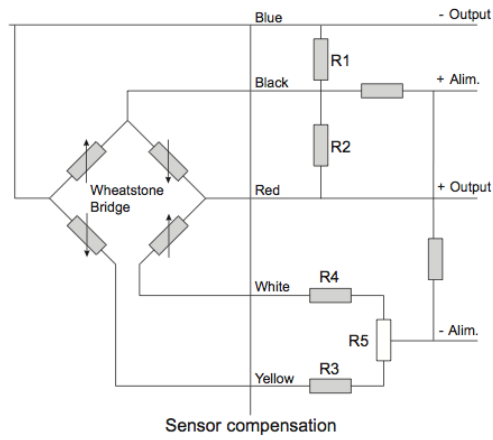


Figure 2.11: Wheatstone bridge of a piezo-resistive sensor [7]

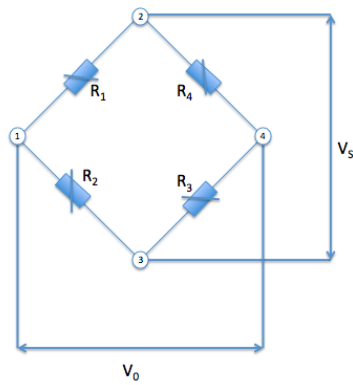


Figure 2.12: Wheatstone bridge

The deformation in the bridge is defined as  $\frac{V_0}{V_S}$  as in Equation 2.15.

$$\frac{V_0}{V_S} = \frac{R_1}{(R_1 + R_2)} - \frac{R_4}{(R_3 + R_4)} [-] \quad (2.15)$$

# Chapter 3

## Equipment and Method

The horizontal shaft single-injector Pelton turbine model is shown in Figure 3.1. Figure 3.2 illustrates the Pelton turbine test rig [8].

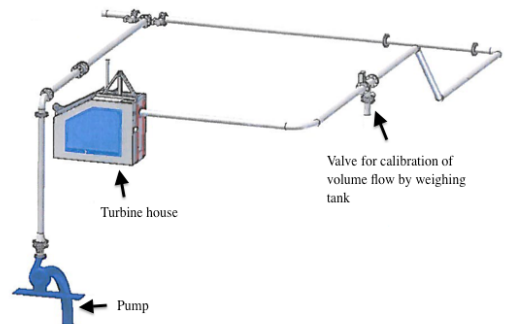
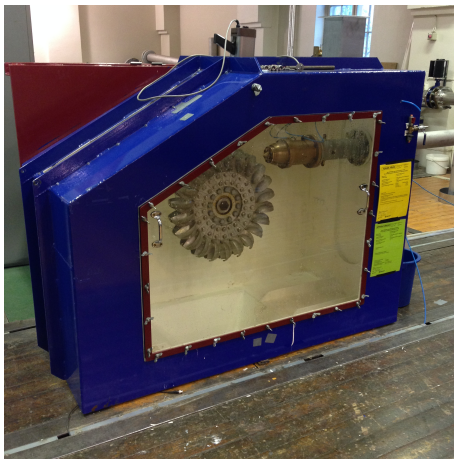


Figure 3.1: The Pelton turbine model      Figure 3.2: The Pelton turbine test rig [8]

In order to conduct a model test of a Pelton turbine some quantities must be measured. The measuring devices and the preparation of these instruments are presented.

<i>Instrument</i>	<i>Model</i>	<i>Producer</i>	<i>Range</i>
Pressure	3276.076.001	Tecsis	0-16 bar
Volume Flow	Optiflux F	Krohne	-
Torque	HBM T10/FS	Hottinger B. Messtechnik	0-500 Nm
Friction Torque	HBM Z6	Hottinger B. Messtechnik	0-14 Nm
Water Temperature	PT 100	-	-

Table 3.1: Instruments

### 3.1 Instrumentation

The turbines that have been tested were connected to a 55 kW DC generator. The test rig included a differential pressure transmitter, a volume flow meter, a torque and friction torque flange, a thermometer and a rotational speed indicator. All the instruments were connected through a National Instruments logging card to a computer with a specialized LabView logging program. The outputs of the instruments included current, voltage and frequency signals. To ease the data logging, the current and frequency signals were converted to voltage signals. The rotational speed measurement output is sent and received as a frequency signal. The instruments used in the model tests is shown in Table 3.1. The volume flow is measured with an electromagnetic flow sensor and the measurement of the torque from the turbine is done with a rotating shaft torque meter. The friction torque is measured with a force cell that has a nominal load of 0-6kg and a lever arm of 0.25m, which gives a measurement range of 0-14Nm. Figure 3.3 shows a schematic overview of the placement of the instruments.

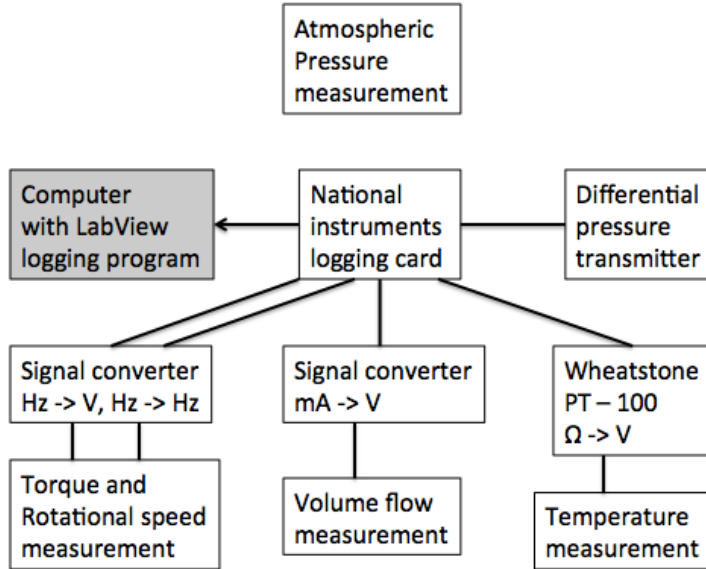


Figure 3.3: Schematic overview of instrument setup

## 3.2 Calibration

When calibrating an instrument a number of measurement points are used. Each measurement point contains a number of individual measurements and is measured at a known physical input. A linear approximation is constructed with the physical input data and the mean value of the measurements in each measurement point. The linear approximation will have the form shown in Equation (3.1)

$$\hat{Y} = C_1x + C_0 \quad (3.1)$$

The procedure of calibrating the instruments in question was conducted as described in the authors project thesis *Laboratory test of a Pelton Turbine* from fall 2013 [13]. All the calibration data can be found in Appendix A.

### 3.2.1 Volume flow meter

The volume flow is a critical property in the calculation of the efficiency of the turbine. The volume flow meter is calibrated using the weighing method, which is recommended as a primary calibration method in the IEC standard [4]. The volume flow meter is calibrated by using the weighing tank, hence the weight sensors in the weighing tank needs to be calibrated before the calibration of the volume flow meter. This was conducted in Fall 2013 in relation to the authors project thesis and is assumed to be viable. The calibration data and the calibration curve can be found in Appendix A. The calibration of the volume flow meter is conducted by running a constant flow rate through the volume flow meter and into a weighing tank while the output signal from the flow meter was recorded for 12 different flow rates in the range of  $0 - 65 \frac{l}{s}$ . Excel was used to process the output data and to calculate the mean values for the volume flow at the different measuring points. This was subsequently compared with the calculated measurements from the weighing tank. The calibration data for the volume flow meter is presented in Appendix A and the calibration curve is shown in Figure 3.4. The weighing tank and the volume flow meter is calibrated as described by Trefall [12].

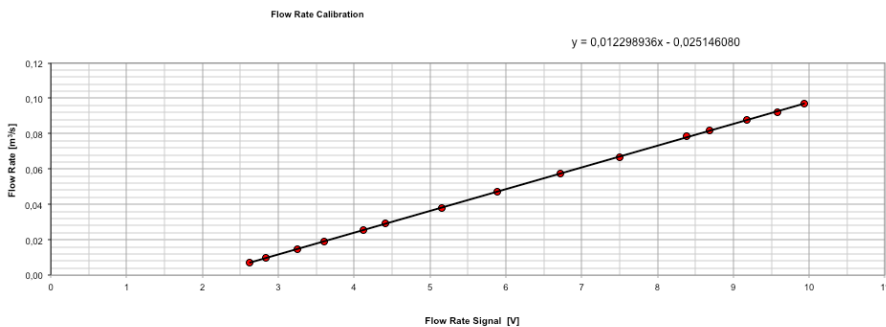


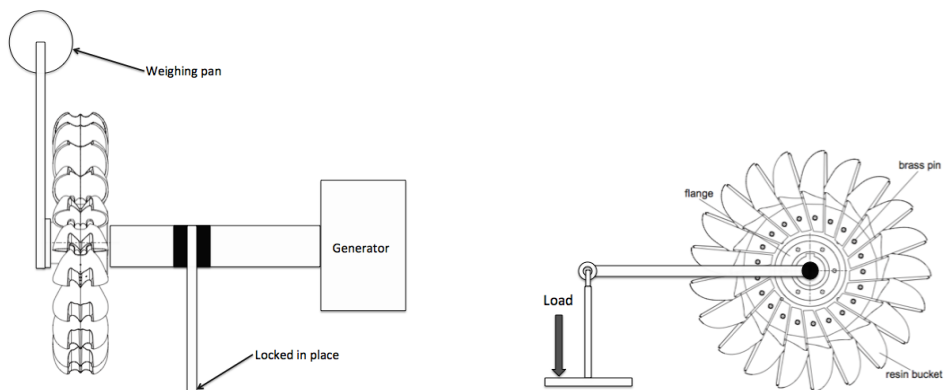
Figure 3.4: Calibration curve for the volume flow meter

### 3.2.2 Torque transducer

The torque transducer was calibrated using the primary method by applying torque to the turbine side of the transducer using calibrated weights. The

shaft from the generator side of the torque flange was locked in place while the shaft from the turbine was exposed to a given torque by loading a metal bar mounted on the turbine shaft, as illustrated in Figure 3.5. A set of precalibrated weights produced the torque. The metal bar was measured from the center of the shaft to the connection point of the weighing pan to obtain the arm the force was acting on. The arm was balanced and did not contribute to the torque. The force,  $F = mg$ , is the gravitational force on the weights, the vertical section of the wire and the weight bed. Equation 3.2 was used to calculate the torque induced. The transducer was calibrated in the range 0-500 Nm. The weights and the weight bed used in the calibration was measured with a Kern FTB 15K0.5 scale in the laboratory.

$$\tau = F * arm = m * g * arm [Nm] \quad (3.2)$$



(a) Fastening the turbine shaft, viewed from above

(b) Loading the turbine shaft

Figure 3.5: Calibrating the torque transducer

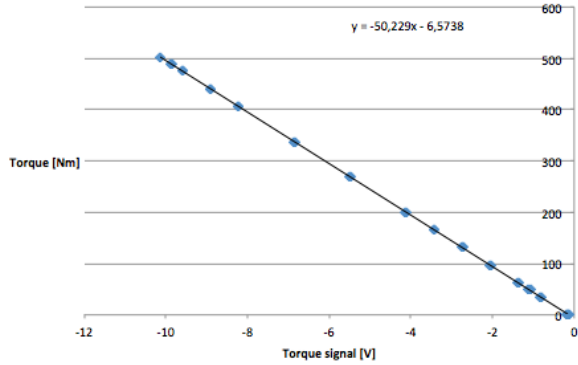


Figure 3.6: Calibration curve for the torque transducer

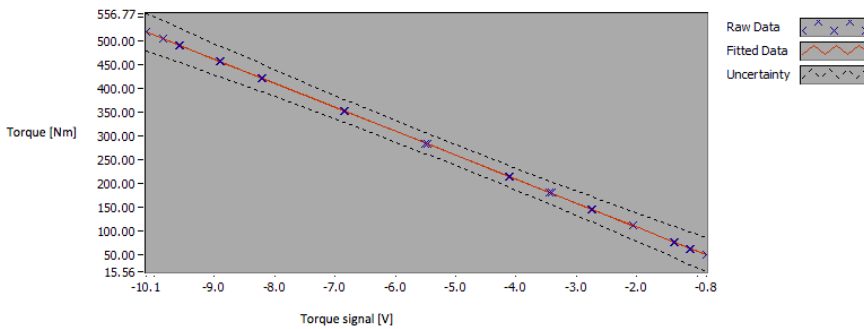


Figure 3.7: Uncertainty band for the torque transducer calibration

During the first calibration of the torque transducer it was evident that something was not right. The calibration was repeated in order to minimize the probability for human error. The error turned out to be incorrect input variables in LabView. This was calculated and corrected for in order to obtain the correct calibration curve. The calibration curve obtained for the torque transducer is shown in Figure 3.6. The first calibration curve obtained, shown in Figure 3.7, shows the first calibration curve obtained, including the uncertainty band which is still assumed to be valid. The torque transducer was calibrated during both on- and off-load in order to



avoid error due to hysteresis, which is a common error found in torque and strain transducers. Error due to hysteresis is therefore assumed negligible.

### 3.2.3 Friction torque transducer

The main shaft was connected to an inner cylinder by two roller bearings and to the generator shaft by a torque flange. In order to calibrate the friction torque transducer the HBM torque transducer is disconnected from the flange connected to the generator flange. It was made sure that there was no contact between the torque transducer and the flange. The inner cylinder was connected to a beam in order to exert a force on the force cell, which had a load capacity of 5kg. On the opposite side of the shaft another beam was placed with a length of 0.25m. The setup for the friction torque calibration is illustrated in Figure 3.8 and the calibration curve for the friction torque transducer is shown in Figure 3.9. The friction torque transducer was calibrated as described by Reinertsen [8].

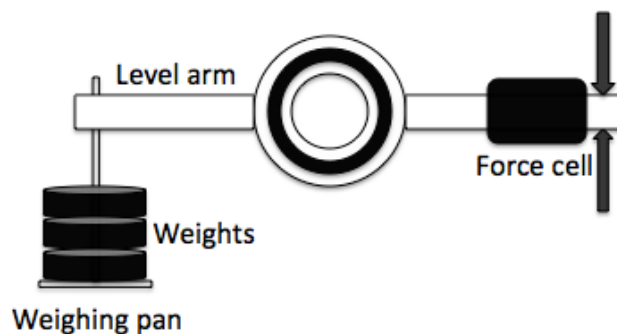


Figure 3.8: Setup for the friction torque calibration

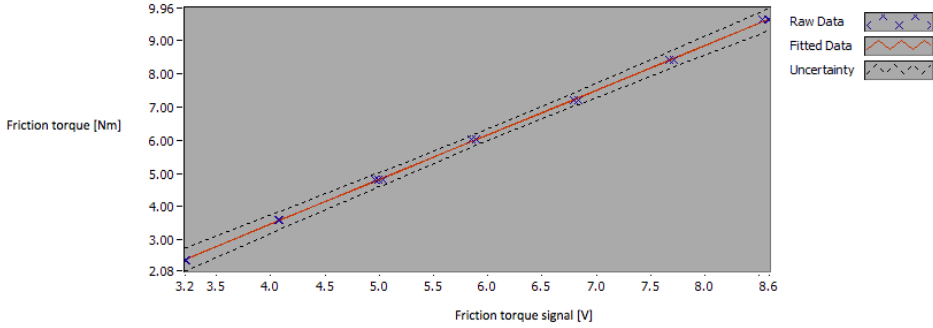


Figure 3.9: Calibration curve for the friction torque transducer

### 3.2.4 Differential pressure transmitter

The differential pressure transmitter was calibrated using a GE Druck 3200 series P3223-1 dead weight manometer produced by GE Sensing. This method is defined by IEC [4] as a primary calibration method for pressure measurements. The pressure transmitter was calibrated for 0-16 bar and was located  $\Delta h_{cal} = 0.075m$  above the zero point of the manometer. The height difference was found with a ruler. Equation 3.3 was used to calculate the total pressure on the transmitter.

$$P_{total} = P_{manometer} + \rho g \Delta h_{cal} [N/m^2] \quad (3.3)$$

The dead weight manometer consists of a piston cylinder with a known area, a pump, an adjustment bolt and a connection point for the pressure transmitter, all adjacent to a chamber filled with fluid. Loads with known values are placed on the piston cylinder. The mass and gravitational force produces force acting on the area of the piston cylinder. The resulting pressure acting on the fluid in the pressure chamber equals the pressure acting on the pressure transmitter, according to Equation 3.4.

$$p_{manometer} = \frac{mg}{A_{piston}} [N/m^2] \quad (3.4)$$

The values obtained from the pressure transducer is found in a program made in LabView. The procedure is repeated until the calibration covers

the desired area of application. The resulting calibration data is found in Appendix A and the obtained calibration curve is shown in Figure 3.10.

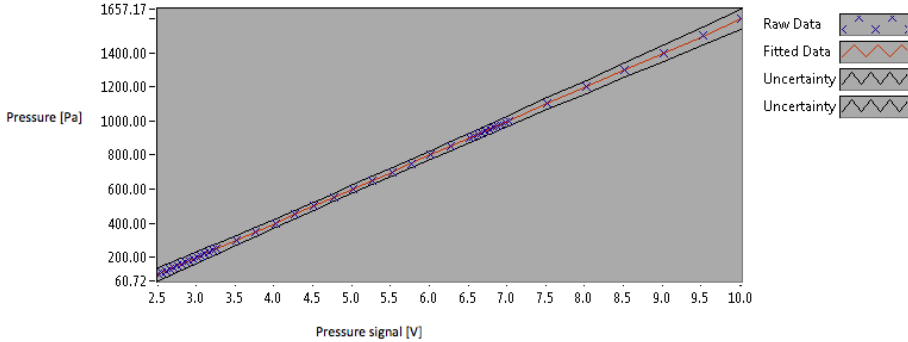


Figure 3.10: Calibration curve for the differential pressure transmitter

### 3.2.5 Temperature measurement

The temperature is measured with a *PT 100 Digital thermometer* which came pre-calibrated from the manufacturer with a specialized LabView program to convert the signal from the thermometer to  $^{\circ}\text{C}$ .

## 3.3 The Test Matrix

The test procedure for model testing of the Pelton turbine test rig in the Water Power Laboratory at NTNU is described in english in Appendix B and in norwegian in Appendix C. The first two sets of buckets is designed by engineers from Dynavec. The two designs will be compared by flow visualization while the first design will be tested with 21 and 22 buckets. The operating points investigated for the first design is defined by DynaVec AS and are shown in Figure 3.13. The difference in the first and second design is shown in Figure 3.11, where the blue color and the red lines represent the first design and the green color represent the second. A third set of buckets, designed by PhD Candidate Bjørn Winther Solemslie, will be tested for 23 buckets and the flow in the buckets will be analyzed with high-speed camera. This bucket design is shown in Figure 3.12. The operating points

investigated for this design is chosen from the estimated BEP and a more thorough investigation around this location and is illustrated in Figure 3.14. An overview of the different turbines and bucket designs investigated in this thesis are presented in Table 3.2.

### 3.4 Analysis procedure for experimental data

From the experiments, the static pressure, volume flow, temperature, torque, friction torque and the rotational speed in the locations shown in the test matrices were obtained. The data were imported to MatLab and a Hill-diagram was created. The MatLab scripts can be found in Appendix G and in the zip-file enclosed with the report. The random errors and the corresponding uncertainty for the measurements is calculated as described Chapter 5.

<i>Referenced name</i>	<i>Designer</i>	<i>Method of investigation</i>
First design, 21 buckets	DynaVec AS	Flow observations, Model test
First design, 22 buckets	DynaVec AS	Flow observations, Model test
Second design	DynaVec AS	Flow observations
Third design	Bjørn W. Solemslie	Flow observations, Model test

Table 3.2: The different turbines investigated

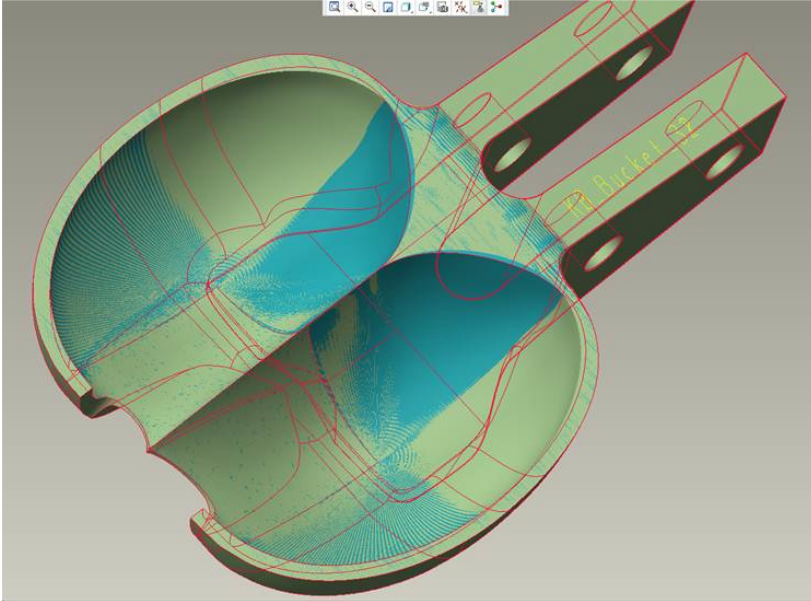


Figure 3.11: The difference between the first and the second design, ref Dynavec AS

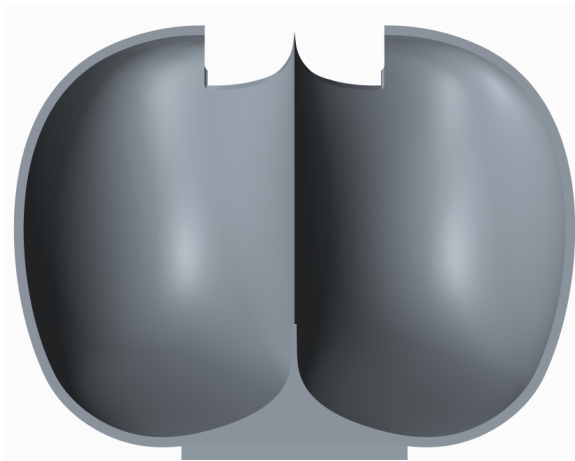


Figure 3.12: The third bucket design, ref Bjørn Winther Solemslie

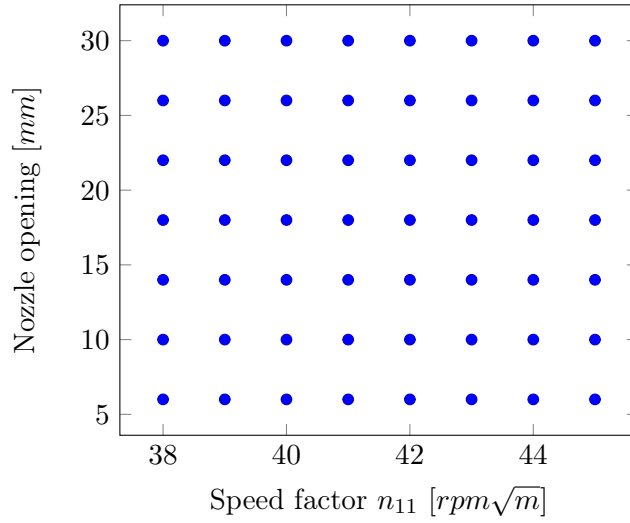


Figure 3.13: Operating points investigated for the first bucket design

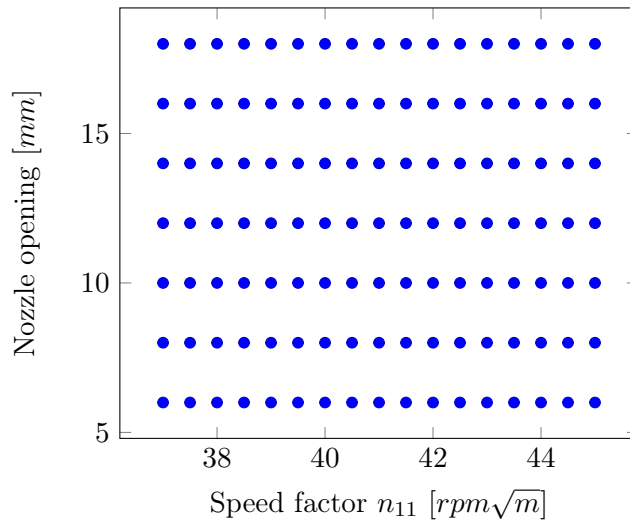


Figure 3.14: Operating points investigated for the third bucket design

## Chapter 4

# Filming With High-Speed Camera

In order to overcome the difficulties with regard to the observation of the flow in the buckets, some requirements are to be followed. Optics, photographic equipment and the lighting system need the correct settings and placement to achieve clear and undistorted images of the flow.

### 4.1 Camera settings and properties

The high-speed camera used is a *Photron Fastcam SA5*. The high-speed imaging system provides recording at frame rates up to 7,000 frames per second with full resolution and up to 775,000 frames per second with reduced resolution. The lens used was a *Tamron 100mm Macro*. The light used was a *Dedolight D* with an output of 400W and a *X0121PDS HMI Fresnell* with an output of 1200W.

When recording and taking the pictures, the camera had the following settings:

Frame rate: 7500 frames per second

Shutter speed:  $1/17,000sec$

Resolution:  $1024 \times 1000$  pixels

The best results were achieved when the camera was placed above the model

turbine house, filming in a downward direction through a square hole above the nozzle. The 1200W light source was placed on the side, by the window, parallel to the turbine axis. The second light source of 400W was placed on the top of the turbine house providing light from above. The placement of the light source and the stand for the video camera can be seen in Figure 4.1.

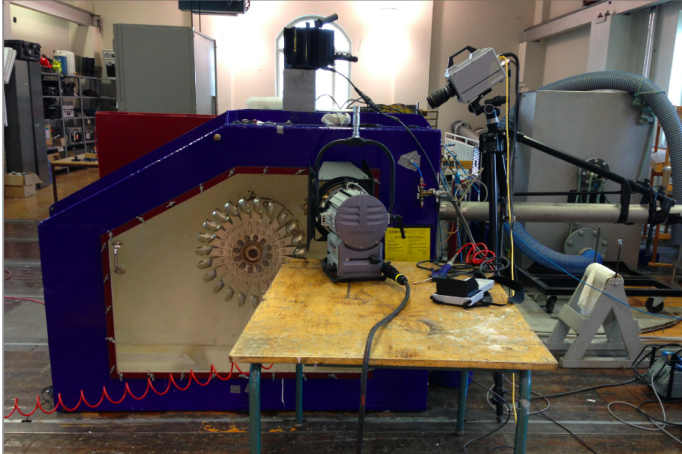


Figure 4.1: Placement of camera and light source

## 4.2 Rig improvements

Some improvements on the rig and devices can be beneficial in order to better enable filming with high-speed camera.

### 4.2.1 Trigger

When conducting the model test and filming of the final installed turbine, *i.e* the third bucket design, a device set to trigger the camera was installed. A signal is sent via an adjustable delay line unit set to fire the camera at the desired angular position of one bucket. The trigger signal is released upon manual activation of the delay line unit. LabView was used as activation of the signal. By using the installed trigger one can more easily obtain a



series of pictures or videos where the buckets are in the same position at different operating points. This enables a faster and easier way to compare the behavior of the flow at different operating points and different stages in the flow development throughout the bucket duty cycle.

When using the trigger, the following settings were used:

Trigger mode: Random reset

Shutter speed:  $1/\text{framesec}$

Resolution:  $576 \times 896$  pixels

Input: rpm of turbine, number of frames, desired angle of bucket/area.

Frame rate: When using the trigger, the frame rate is dependent on the rotational speed of the turbine at a given operating point,  $\omega$ , as shown in the equations below. After the desired number of pictures that should cover a certain angular range is defined, the frame rate is calculated.

$$\theta = 110^\circ$$

$$\frac{110}{\omega} = \text{time}$$

$$\frac{\text{number of pictures}}{\text{time}} = \text{frame rate}$$



## Chapter 5

# Uncertainty Analysis

Statistical methods and uncertainty analysis are tools that can be used to plan and interpret experiments. Measurements during experiments include some level of errors. These errors have their origin in random variations in the measured value and inaccuracy within the instrument, among others. The error in a measurement is defined by the difference between the measured value and the actual physical property. This error can be estimated by the use of statistical methods from where one can find a confidence interval where the error will be located with a certain probability. According to IEC 60193 [4], this probability, or confidence level, should be 95%. Three types of errors is considered.

- Spurious errors
- Systematic errors
- Random errors

*Spurious errors* are caused by failure in the instrument or human error. These errors should usually be recognized when measurements are analyzed. These errors could only occur in some of the measurements as out of line with the rest of the measurement series.

*Systematic errors* are consistent and repeatable. They are calculated and minimized by calibration of equipment. The systematic error,  $e_s$ , is the

difference between the measured value,  $Y_m$ , and the known value that the instruments is calibrated up against,  $Y_{known}$ . The expression for systematic error is shown in Equation (5.1).

$$e_s = Y_m - Y_{known} \quad (5.1)$$

*Random errors* are not repeatable. They occur because of non-controllable factors such as temperature variations. The random error,  $e_r$ , is the difference between the measured value,  $Y_m$ , and the mean of the measured values,  $\bar{Y}_m$ . The expression for the systematic error is shown in Equation (5.2).

$$e_r = Y_m - \bar{Y}_m \quad (5.2)$$

The expression for the mean value from  $n$  measurements is shown in Equation (5.3). The expression for the standard deviation is shown in Equation (5.4).

$$\bar{Y} = \frac{\sum_{r=1}^n y_i}{n} \quad (5.3)$$

$$S_Y = \sqrt{\frac{\sum_{r=1}^n (Y_r - \bar{Y})^2}{n - 1}} \quad (5.4)$$

At a 95% -confidence level, the real mean value for a sequence of measurements will with a 95% probability be in the area  $\bar{Y} \pm t * \frac{S_Y}{\sqrt{n}}$ .  $t$  is the student-t value for a desired confidence level and number of measurements, and is given in Table L.2 in IEC 60193 [4]. For every operating point investigated in this thesis, 60 000 measurements were obtained. At 95% confidence level and more than 120 measurements,  $t = 1.96$ . In this report only the systematic and random error have been accounted for in the calculations.

<i>Error</i>	<i>Description</i>
$f_{X_a}$	Systematic error of the primary calibration method
$f_{X_b}$	Random error of the primary calibration method
$f_{X_c}$	Systematic error (repeatability) of the secondary instrument
$f_{X_d}$	Random error of the secondary instrument
$f_{X_e}$	Physical phenomena and external influences
$f_{X_f}$	Error in physical properties

Table 5.1: Component errors in the calibration of an instrument

## 5.1 Uncertainty in Calibration

During the calibration of an instrument, different sources of errors contribute to the uncertainty. The different errors are defined by IEC [4] and are shown in Table 5.1.

The relative uncertainty in the calibration curve for an instrument is found with the root-sum-square-method, shown in Equation 5.5

$$f_{cal} = \pm \sqrt{(f_a)^2 + (f_b)^2 + (f_c)^2 + (f_d)^2 + (f_e)^2 + (f_f)^2} \quad (5.5)$$

### 5.1.1 Uncertainty in the calibration of the differential pressure transmitter

$f_{p_a}$  and  $f_{p_b}$  consist of the total error in the calibration method. According to the documentation for the dead weigh manometer, the total error in the instrument does not exceed  $\pm 0.0008\%$ . This is found by combining  $f_{p_a}$  and  $f_{p_b}$  with the RSS method.

$f_{p_c}$  is the systematic error in the instrument. By calibrating the signal given by the instrument against a physical quantity, one minimizes this uncertainty. This relative uncertainty has been denoted  $f_{p_{regression}}$  and is found to be  $0.031\%$  for operation around the highest point of efficiency in the calibration report in Appendix A. Figure 3.10 shows the uncertainty band with 95% confidence level multiplied by 100.

$f_{p_d}$  is the random error in the instrument due to the scatter of the signal while logging over time. This uncertainty is included in  $f_{p_{regression}}$ .

$f_{p_e}$  is the error due to physical phenomena and external influences. As

this may originate from changes in temperature within the instrument, and the pressure transducer has been installed in the rig for several months, it was assumed that the instrument had reached thermal equilibrium with the surroundings.  $f_{pe}$  was therefore neglected. [10]

$f_{pf}$  is the error in physical properties obtained by either calculation or in relation to the use of international standard data. This uncertainty includes the uncertainty of the measurement of the height difference between the dead weight manometer and the measuring point of the pressure transmitter,  $Z_{cal}$ . This distance was measured with a ruler. The uncertainty is therefore set to half of the resolution of the ruler,  $\pm 0.0005m$ . The height difference was found to be  $0.075m$ , thus the uncertainty,  $f_{pf} = 0.00667\%$ .

Combining the above mentioned uncertainties with RSS-method, the total relative uncertainty for the calibration of the differential pressure transmitter becomes as shown in Equation 5.6. [10]

$$f_{p_{cal}} = \pm \sqrt{(f_{p_{ab}})^2 + (f_{p_{regression}})^2 + (f_{pf})^2} = 0.032\% \quad (5.6)$$

### 5.1.2 Uncertainty in the calibration of the volume flow meter

The errors contributing to the uncertainty in the calibration of the volume flow meter are the systematic error in the weighing tank system,  $f_{Q_a}$ , the random error in the weighing tank system,  $f_{Q_b}$ , and the systematic and random error in the instrument,  $f_{Q_{regression}}$ , where the latter is specific for the calibration related to the range of operation for these model tests.

- $f_{Q_a} = 0.0889\%$  [11]
- $f_{Q_b} = 0.0503\%$  [11]
- $f_{Q_{regression}} = 0.005482$

Combining the above mentioned uncertainties with the RSS-method, the maximum total relative uncertainty for the calibration of the volume flow meter is found to be as shown in Equation 5.7.

$$f_{Q_{cal}} = \pm \sqrt{(f_{Q_a})^2 + (f_{Q_b})^2 + (f_{Q_{regression}})^2} = \pm 0.10229\% \quad (5.7)$$

### 5.1.3 Uncertainty in the calibration of the torque transducer

The errors contributing to the uncertainty for the calibration of the torque transducer is the systematic error in the weights and the weights bed,  $f_{\tau_W}$ , the systematic error in the length of the arm,  $f_{\tau_{arm}}$ , and the systematic and random error in the instrument for operation around the highest point of efficiency,  $f_{\tau_{regression}}$ . Figure 3.7 shows the uncertainty band with 95% confidence level multiplied by 100.

- $f_{\tau_W} = 0.00154\%$
- $f_{\tau_{arm}} = 0.08536\%$
- $f_{\tau_{regression}} = 0.073\%$

Combining these errors with the RSS-method the maximum total relative uncertainty for the calibration of the torque transducer is found to be as shown in Equation 5.8.

$$f_{\tau_{cal}} = \pm \sqrt{(f_{\tau_{regression}})^2 + (f_{\tau_{arm}})^2 + (f_{\tau_W})^2} = \pm 0.1123\% \quad (5.8)$$

### 5.1.4 Uncertainty in the calibration of the friction torque transducer

The errors contributing to the uncertainty of the friction torque transducer is the uncertainties related to the force cell. The different errors are the systematic error in the weights,  $f_{\tau_W}$ , the systematic error in the length of the arm,  $f_{\tau_{arm}}$ , and the systematic and random error in the instrument for operation around the highest point of efficiency,  $f_{\tau_{regression}}$ . Figure 3.9 shows the uncertainty band with 95% confidence level multiplied by 10.

- $f_{\tau_W} = 0.11\%$
- $f_{\tau_{arm}} = 0.15\%$
- $f_{\tau_{regression}} = 0.305\%$

<i>Error</i>	<i>Description</i>
$f_{cal}$	Systematic error in calibration
$f_h$	Additional systematic error in the instruments
$f_j$	Error in physical properties
$f_{k_s}$	Systematic errors due to physical phenomena and external influences
$f_{k_r}$	Random errors due to physical phenomena and external influences
$f_l$	Random error in repeatability of secondary instrument

Table 5.2: Component errors in the test

Combining these errors with the RSS-method the maximum total relative uncertainty for the calibration of the friction torque transducer is found to be as shown in Equation 5.9.

$$f_{\tau_{cal}} = \pm \sqrt{(f_{\tau_{regression}})^2 + (f_{\tau_{arm}})^2 + (f_{\tau_W})^2} = \pm 0.357\% \quad (5.9)$$

A more detailed description on how to find the different uncertainties mentioned above can be found in the master thesis *Optimalisering av ringledning for Pelton turbin*, Appendix D by Bjørn Winther Solemslie, 2010 [10]. The different values and an explanation of them can also be found in Appendix F.

## 5.2 Uncertainty of the tests

All measurements during an experiment include some level of uncertainties. The uncertainties in the measurements include factors such as inaccuracy within the instruments used to measure the physical quantities and random variations of the measured value. The different errors are defined by IEC 60193 [4] and are shown in Table 5.2.

The systematic, random and total uncertainty for an instrument is found with the root-sum-square-method.

The relative systematic uncertainty:

$$f_s = \pm \sqrt{(f_{cal})^2 + (f_h)^2 + (f_j)^2 + (f_{k_s})^2} \quad (5.10)$$



The relative random uncertainty:

$$f_r = \pm \sqrt{(f_{kr})^2 + (f_l)^2} \quad (5.11)$$

The relative total uncertainty:

$$f_{tot} = \pm \sqrt{(f_s)^2 + (f_t)^2} \quad (5.12)$$

After the model tests were completed the total uncertainty is found. The total uncertainty is a combination of the calibration uncertainty and other errors from the test itself. The calculation of the uncertainties is done on the basis of IEC 60193 [4] and from the project thesis *Laboratory test of a Pelton turbine* written in 2013 [13]. The Calculation of the uncertainty of the test is described in Appendix F

### 5.2.1 Total uncertainty of the hydraulic efficiency

In order to find the total systematic uncertainty at the highest point of efficiency for each test, the following equations are used:

$$\text{Torque: } f_\tau = \pm \sqrt{(f_{\tau_{cal}})^2 + (f_{T_l})^2}$$

$$\text{Friction torque: } f_{\tau_{Lm}} = \pm \sqrt{(f_{\tau_{Lm_{cal}}})^2 + (f_{\tau_{Lm_l}})^2}$$

$$\text{Total torque: } f_{\tau_m} = \frac{\sqrt{(e_{\tau_{Lm}})^2 + (e_\tau)^2}}{\tau_{tot}}$$

$$\text{Volume flow: } f_Q = \pm \sqrt{(f_{Q_{cal}})^2 + (f_{Q_l})^2}$$

$$\text{Power: } f_P = \pm \sqrt{(f_{\tau_m})^2 + (f_\omega)^2}$$

$$\text{Energy: } f_E = \pm \frac{e_E}{E} = \pm \frac{\sqrt{(f_P * \Delta P)^2 + (g * e_{Z_{dif}})^2 + (\frac{v_1^2 * f_{v1}^2}{2})^2}}{E}$$

$$\text{Hydraulic efficiency: } f_{\eta_h} = \pm \frac{e_{\eta_h}}{\eta_h} = \pm \sqrt{(f_Q)^2 + (f_E)^2 + (f_P)^2}$$

$$\text{Rotational speed: } f_\omega = 0.025\% [8].$$

**First design - 21 buckets**

Uncertainty at the highest point of efficiency:  $f_{\eta_h} = \pm 0.10959\%$ .

**First design - 22 buckets**

Uncertainty at the highest point of efficiency:  $f_{\eta_h} = \pm 0.10962\%$

**Third design - 23 buckets**

Uncertainty at the highest point of efficiency:  $f_{\eta_h} = \pm 0.10965\%$

**5.2.2 Uncertainty in the efficiency**

After the model tests are conducted, the uncertainty in the efficiency,  $e_{\eta_h}$ , is found according to the following Equation.

$$f_{\eta_h} = \frac{e_{\eta_h}}{\eta_h} \quad (5.13)$$

# Chapter 6

## Results

### 6.1 Model tests

Model tests were conducted for the first bucket design with both 21 and 22 buckets and for the third design with 23 buckets. All the model tests are conducted with a 70m head.

#### 6.1.1 First design - 21 buckets

The hill-diagram for the first bucket design and with 21 buckets is shown in Figure 6.1. The design point was at  $n_{11} = 40,2$  and  $Q_{11} = 0,022$ , which corresponds to a nozzle opening of 22mm. The efficiency at this operating point was 90.227%. The point of highest efficiency for this turbine was, according to the model test, located at  $n_{11} = 41$  and  $Q_{11} = 0.020$ . The efficiency at this point was 90.32%.

#### 6.1.2 First design - 22 buckets

A hill-diagram was also found for the same bucket design, but with 22 buckets. This is shown in Figure 6.2. The point of highest efficiency for this turbine is located at  $n_{11} = 40$  and  $Q_{11} = 0.0175$ . The efficiency at this point was 90.62%.

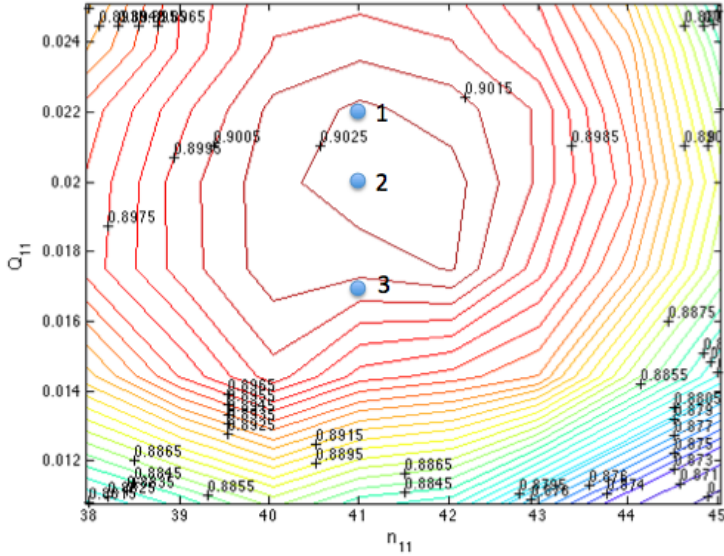


Figure 6.1: Hill-diagram, first design, 21 buckets

### 6.1.3 Third design - 23 buckets

A third model test was conducted for Pelton turbine buckets designed by PhD Candidate Bjørn Winther Solemslie. The turbine consisted of 23 buckets.

#### The first test series

The location of the highest point of efficiency was calculated for  $Q_{11}$  and  $n_{11}$  and for a jet diameter of 35mm. This is calculated in order to find out approximately in which operating region the model test should be conducted, shown in Table 6.1. The first test series was conducted with the nozzle placed too high with regards to the runner. This led to many areas of evident loss and the model test showed a highest efficiency of 78.9%. The hill-diagram for this model test is shown in Figure 6.3.

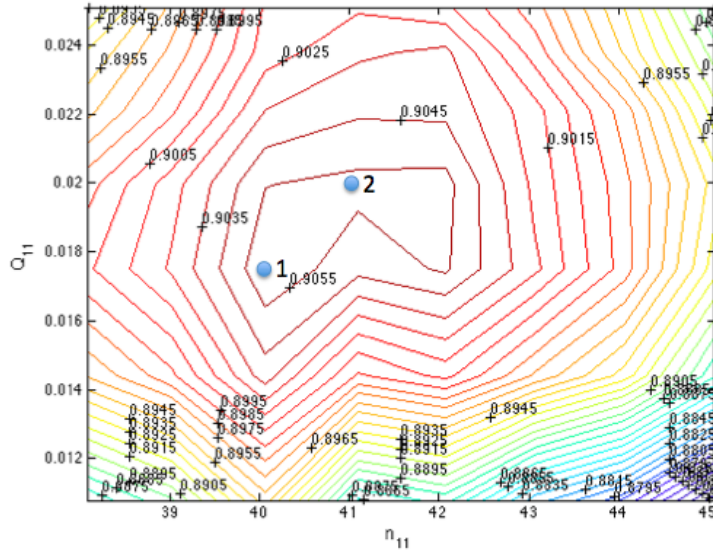


Figure 6.2: Hill-diagram, first design, 22 buckets

### The second test series

The buckets in this turbine was shorter than the previous buckets used in this rig, hence, the water jet did not impact the bucket in the middle, but on the upper part, nearer to the bucket lip. The result of this was that most of the water went straight through the bucket lip, not contributing much to the energy transfer. It was evident that the nozzle needed to be lowered in order to achieve a more accurate hill-diagram for this turbine. The nozzle was lowered 10mm. The water jet was then split at the middle of the bucket ridge when in a 90 degree angle. This lead to a decresed pitch diameter. The location of the highest point of efficiency was again calculated for the new pitch diameter  $D$ , also shown in Table 6.1. The hill-diagram obtained from the second model test is shown in Figure 6.4. The highest point of efficiency for this turbine was 83.42% and was located at  $n_{11} = 44$  and  $Q_{11} = 0.012$ . Another point of high efficiency was at  $n_{11} = 38.5$  and  $Q_{11} = 0.012$ . The efficiency at this location was 83.25%

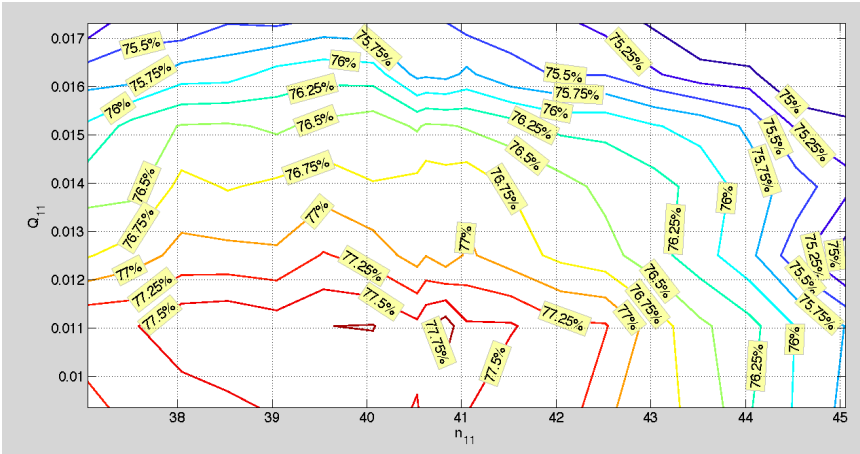


Figure 6.3: Hill-diagram, first model test

## 6.2 Filming with high speed camera

The flow observations evidence the unsteadiness of the successive steps of the jet-bucket interaction, free surface flow development and the evolution throughout the bucket duty cycle. Two bucket designs were first compared, both with a turbine consisting of 21 buckets. Three buckets of the second design was replaced with three buckets of the first in order to compare the two designs with a high-speed camera. The first design was then run for 21 and 22 buckets. A third turbine consisting of 23 buckets, designed by PhD candidate Bjørn Winther Solemslie, referenced as the third design, was later investigated. The different elements discovered and investigated with the high-speed camera are listed below, and will later be discussed. Pictures from every operating point investigated by flow observations are found in Appendix E. The pictures as well as videos recorded are available in the zip-file enclosed with this report.

- **Back wash**

Back wash was to some extent discovered for every turbine investigated. When the water leaves one bucket it stays in the air until it crashes into the oncoming bucket, contributing negatively to the runner torque.

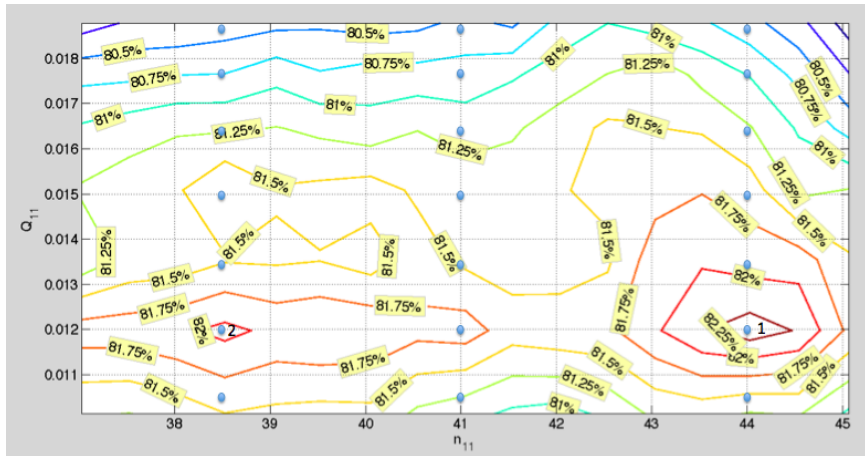


Figure 6.4: Hill-diagram, second model test

- **Loss through bucket cut-out**

This was especially found for the third bucket design. The bucket should have a sufficient positive gradient towards the lip in order to lead the water in an outward direction, towards the outlet edge. A lot of water was instead led in a forward direction and out of the bucket lip.

- **Jet-bucket interaction**

The behavior of the flow is dependent on the placement of the water jet with regard to the runner. As mentioned earlier should the ridge, or splitter, in the middle of the bucket be perpendicular to the jet axis when the center of gravity of the jet reaches the bucket. The jet should be split in the middle. This is sometimes difficult to achieve precisely and affects the behavior of the flow in the bucket and thus the energy transfer.

- **Steadiness of the water film in the buckets**

This is largely dependent on the jet-bucket interaction.

- **Development of the water jet**

This may effect the steadyness of the water film in the buckets and occurs as the water develops before impact with the bucket.

<i>Test series</i>	<i>I</i>	<i>II</i>
$H$	70m	70m
$d_s$	0.035m	0.035m
$D_1$	0.51372m	0.49372m
$c = \sqrt{2 \cdot g \cdot H}$	37.06m/s	37.06
$Q = c \cdot \pi \cdot r_s^2$		
$Q_{11} = \frac{Q}{D^2 \sqrt{H}}$	0.016 l/sm <sup>5/2</sup>	0.0086 l/sm <sup>5/2</sup>
$n = \frac{\omega}{2 \cdot \pi} \cdot 60$		
$u = \omega \cdot R_1$		
$\underline{u} = \frac{\omega \cdot R_1}{\sqrt{2 \cdot g \cdot H}}$		
$\omega$	69.29 $\frac{1}{s}$	72.06 $\frac{1}{s}$
$n$	661.69 rpm	688.12 rpm
$n_{11} = \frac{n \cdot D}{\sqrt{H}}$	40.62 rpm $\sqrt{m}$	40.62 rpm $\sqrt{m}$

Table 6.1: Calculation of the location of BEP

- **Behavior of the flow when leaving the bucket**

Different forces acting on the flow affects the behavior of the water leaving the bucket. Forces such as the Coriolis, that acts to change the direction of a rotating fluid, or the Coanda effect, that may create low pressure on the backside of the bucket [7], may affect the flow and the turbine runner. The different forces acting on the fluid and the result of these will be further discussed in Chapter 7.7.2.



### 6.2.1 First design - 21 buckets

The operating points investigated with high-speed camera for the first design are marked with blue dots in the Hill-diagram in Figure 6.1. Pictures obtained are shown in Figure 6.5 for (a)  $Q_{11} = 0.0175$  and (b)  $Q_{11} = 0.022$ . These are marked with the number 3 and 1 in the hill-diagram. Figure 6.6 shows the operating point of  $Q_{11} = 0.020$  and is marked with the number 2 in the hill-diagram. All of these are from running with  $n_{11} = 41$ . The point of highest efficiency was found for  $n_{11} = 41$  and  $Q_{11} = 0.020$ . At the point of highest efficiency, some degree of back wash can be seen, as marked with a red circle in Figure 6.6. From the videos recorded, a higher degree of back wash was observed for  $Q_{11} = 0.022$  and higher.



(a)  $Q_{11} = 0.0175$



(b)  $Q_{11} = 0.022$

Figure 6.5: First design, 21 buckets, 70m head,  $n_{11} = 41$



Figure 6.6: First design, 21 buckets, 70m head,  $Q_{11} = 0.020$ ,  $n_{11} = 41$

### 6.2.2 First design - 22 buckets

The first design was tested for both 21 and 22 buckets. The highest point of efficiency for the runner consisting of 22 buckets was found at an operating point of  $n_{11} = 40$  and  $Q_{11} = 0.0175$ , marked with a blue dot and the number 1 in the Hill-diagram in Figure 6.2. The objective with the comparison was to observe the effect of an additional bucket. Highest efficiency for 21 buckets was found at an operating point of  $n_{11} = 41$  and  $Q_{11} = 0.020$ . In order to compare the two with regard to back wash, the operating point was filmed for 22 buckets. Operating with 22 buckets can be seen in Figure 6.7 for  $n_{11} = 41$  and  $Q_{11} = 0.020$ . Back wash can be seen at the lower left side in this picture as a splash at the lower part of the bucket, marked with a red circle. Water loss through the bucket lip is marked with a yellow circle. The operating point investigated with high-speed camera is marked with a blue dot and the number 2 in the Hill-diagram for this runner.

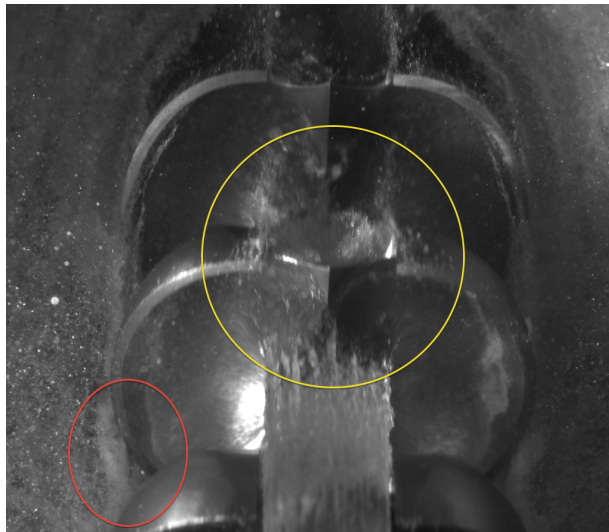


Figure 6.7: First design, 22 buckets, 70m head,  $Q_{11} = 0.020$ ,  $n_{11} = 41$

### 6.2.3 Second design

This turbine consisted of 21 buckets, 18 of the first design and 3 of the second. The second design was identical to the first design except for a slightly smaller width at the bottom rim near the root, as illustrated in Figure 7.3. This will be further discussed in Chapter 7.5. The slight difference in the design resulted in a higher degree of back wash. This can be seen in Figure 6.8 and 6.9. The back wash is marked with red circles. Figure 6.9 shows the design operating point and Figure 6.8 shows the operating point where the highest efficiency was achieved for the first design and 21 buckets. When filming the three buckets installed, the rim of the bucket was painted white in order to distinguish them from the other buckets.

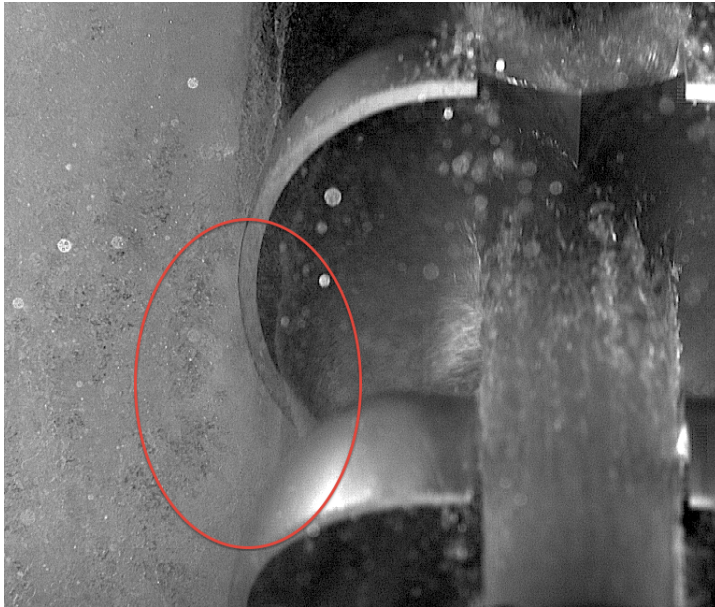


Figure 6.8:  $Q_{11} = 0.020$ ,  $n_{11} = 41$



Figure 6.9:  $Q_{11} = 0.022$ ,  $n_{11} = 41$

### 6.2.4 Third design

Flow observations was conducted for the buckets designed by Bjørn Winther Solemslie after the nozzle was lowered. The operating points investigated with high-speed camera are marked with blue dots in the hill-diagram in Figure 6.4. Highest efficiency for this turbine was found for  $n_{11} = 38,5$  and  $n_{11} = 44$ . Figure 6.12 and Figure 6.10 show a snapshot from an operating point of  $n_{11} = 44$ ,  $Q_{11} = 0.012$  and respectively, 70m and 25m head. This operating point is marked with a blue dot and the number 1 in the hill-diagram. Figure 6.11 show an operating point of  $n_{11} = 38,5$ ,  $Q_{11} = 0.012$  and with 25m head. This operating point is marked with a blue dot and the number 2 in the hill-diagram. The figures show the turbine in the exact same position at different operating points. In these figures unsteadyness of the water film in the bucket is evident, and the behavior of the flow is different for the left and right side of the bucket. Water loss through the bucket lip is marked with a yellow circle and an arrow in Figure 6.10. Back wash is marked with a red circle in the same picture. Signs that may be of the coriolis effect is marked with a blue circle and back wash with a red in Figure 6.11. This will be discussed later in the report. When filming this turbine with a head of 70m it was difficult to obtain undistorted images, as seen in Figure 6.12. Due to a lot of water splashing in the direction of the camera, filming the operating point  $n_{11} = 38,5$  with a head of 70m was not carried out. A second series of filming was therefore conducted for 25m head. The effect of this will also be discussed later in the report.

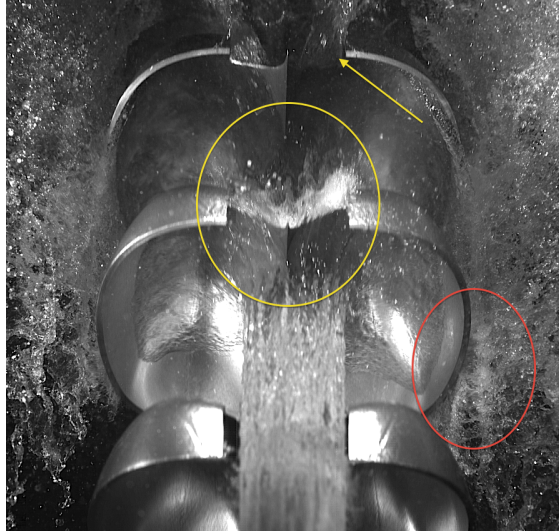


Figure 6.10: Third design, 25m head,  $Q_{11} = 0.012$ ,  $n_{11} = 44$

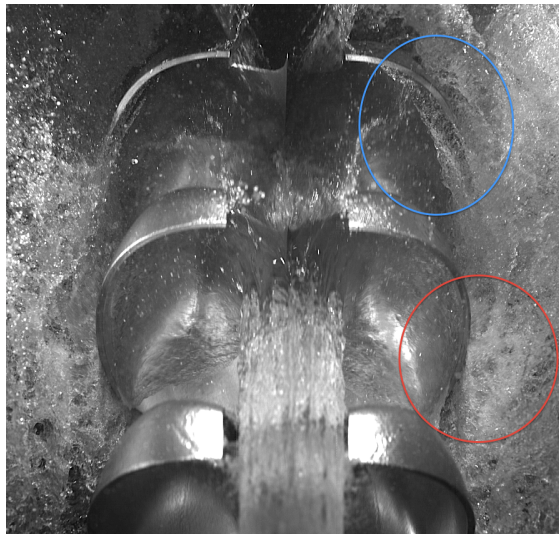


Figure 6.11: Third design, 25m head,  $Q_{11} = 0.012$ ,  $n_{11} = 38.5$

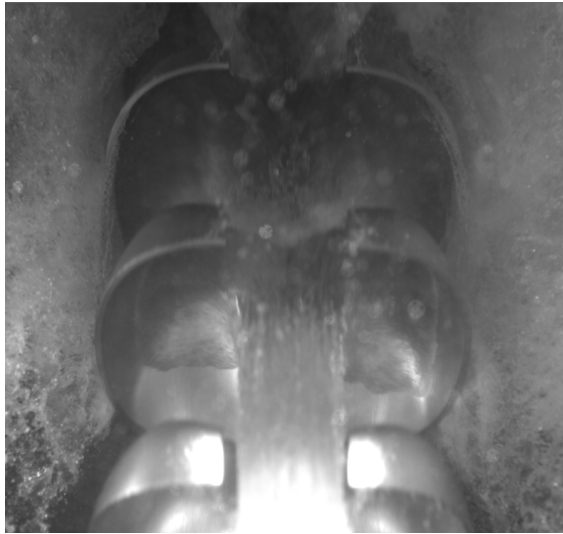


Figure 6.12: Third design, 70m head,  $Q_{11} = 0.012$ ,  $n_{11} = 44$



## Chapter 7

# Discussion

### 7.1 Misplaced nozzle

As evident from the project thesis, written in fall 2013 [13], the nozzle was slightly misplaced with regard to the runner. This resulted in the water jet crashing on one side of the bucket lip. This had to be adjusted in order to obtain more accurate model tests. Figure 7.1 shows the misplaced nozzle and Figure 7.2 shows the adjusted nozzle.



Figure 7.1: Misplaced nozzle

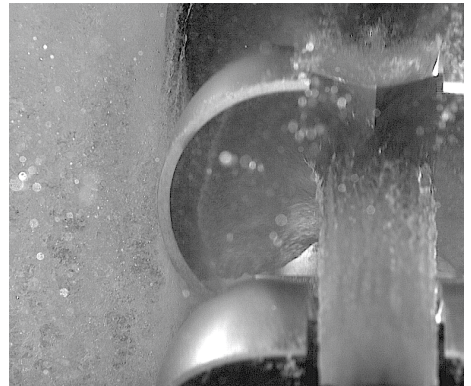


Figure 7.2: Adjusted nozzle

## 7.2 Problems encountered during the experiments

During the first model test conducted in this experiment the nozzle didn't react by signal to open between a nozzle opening of 6 and 8mm, 10 and 12mm, 14 and 18mm and so on. The nozzle is made out of several pistons where the different pistons stretch in different lengths, respectively 2mm, 4mm, 8mm and 16mm. When running on full load, *i.e* 30mm nozzle opening, none of the pistons are filled with water. The nozzle openings that didn't react to signal from the control room were the ones involving the 2mm piston. The error turned out to be a dysfunctional valve connecting the 2mm piston to the water upstream the turbine. The problem was fixed by lubricating the magnet valve.

## 7.3 First design - 21 buckets

Some degree of back wash is seen for this design. The back wash increases for  $Q_{11} = 0.022$  and higher. Point of highest efficiency was found for  $Q_{11} = 0.020$ . This complies with the flow observations. The point of highest efficiency was not located at the same operating point as the design point, according to the model test.

## 7.4 First design - 22 buckets

A model test for 22 buckets was conducted where the highest point of efficiency was found for the operating point  $n_{11} = 41$  and  $Q_{11} = 0.0175$ . 22 buckets compared to 21 buckets can lead to less back wash due to a smaller amount of water in each bucket. At the same time the buckets are closer to each other, which in turn can lead to a greater back wash effect. The two cases can be seen in Figure 6.7 for 22 buckets, and in Figure 6.1 for 21 buckets. Both of these pictures are taken for an operating point of  $n_{11} = 41$  and  $Q_{11} = 0.020$ . When comparing the results for 22 buckets with 21 buckets, it was found that the turbine with 22 buckets had 0,3% higher efficiency. This is a significant improvement and can imply that back wash occurs to a smaller extent with the use of one more bucket. Less water in each bucket would for this design lead to less water lingering in the air and impact the oncoming bucket. This assumption was reinforced by studying the videos

recorded. Visual observations also showed less water loss through the lip of the bucket during the stage of outflow.

## 7.5 Second design

After 21 buckets of the first design were installed, three of these were replaced with three buckets of a second design, in order to film the difference in the flow pattern. In the front of the bucket the two designs are identical, but there is a small difference in the back. For the second design, the rearmost point is moved approximately 5% inwards to the middle, as illustrated in Figure 7.3. This Figure is provided from Dynavec AS. As mentioned earlier, the blue color and the red lines represent the first design and the green color represent the second. That the buckets lower rim width is decreased for the second design may lead to more water crashing into the next bucket. Where the water flows faster in a downward and out direction for the first design, changes to a more sideways and out for the second design. The goal of comparing the two by flow visualization was to see how the small change in the design affects the behavior of the flow. This may be the cause of the increased back wash and is shown in Figure 6.8 and by the circle in Figure 6.9. This picture is obtained from an operating point of 70m head,  $n_{11} = 41$  and  $Q_{11} = 0.020$ . After studying the videos and pictures obtained, a slight increase in back wash was evident.

## 7.6 Third design - 23 buckets

When filming with a 70m head for this bucket design, the water from the bucket outlet was in such a way that it limited the accessibility for the light required in order to obtain a clear, undistorted image of the bucket flow. Filming was therefore carried out for both 70m head and 25m head to find out if there was a significant visual difference in the flow in the bucket. If the visual difference was negligible, one can use videos recorded at 25m head and more easily see the behavior of the flow and assume a similar behavior at 70m head. Figure 7.5a and Figure 7.5b shows 70m head and 25m head, respectively, at the same operating point. Another operating point is shown in Figure 7.6a and Figure 7.6b.

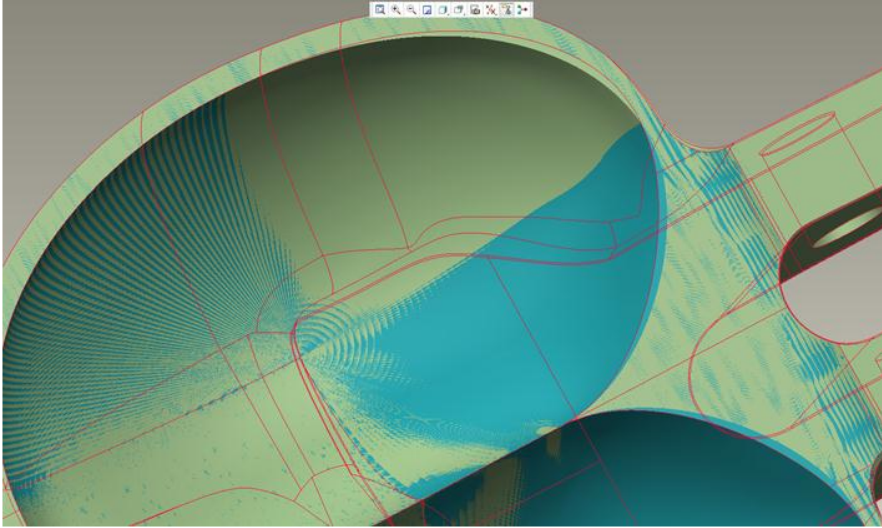


Figure 7.3: The difference between the first and the second design, ref Dynavec AS

### 7.6.1 Loss

The videos obtained for the third bucket design also showed that a lot of water is lost through the bucket lip. This may imply that the bucket does not have a positive elevation gradient, towards the bucket lip, large enough to lead the water away from the lip. More water is therefore being led right through the cut-out, as illustrated in Figure 7.7 with red arrows, instead of out on each side of the bucket, towards the outlet edge, as illustrated with blue arrows in the same figure. The water lost here contributes little to the energy transfer.

### 7.6.2 Misplaced nozzle

The videos recorded after the nozzle was lowered and adjusted for the last time reveals that the nozzle was again slightly misplaced with regards to the bucket. A higher efficiency might have been possible if the turbine was placed a couple of millimeters further in. Energy loss occurs when the right side of the jet starts crashing on the right side of the bucket at a lower

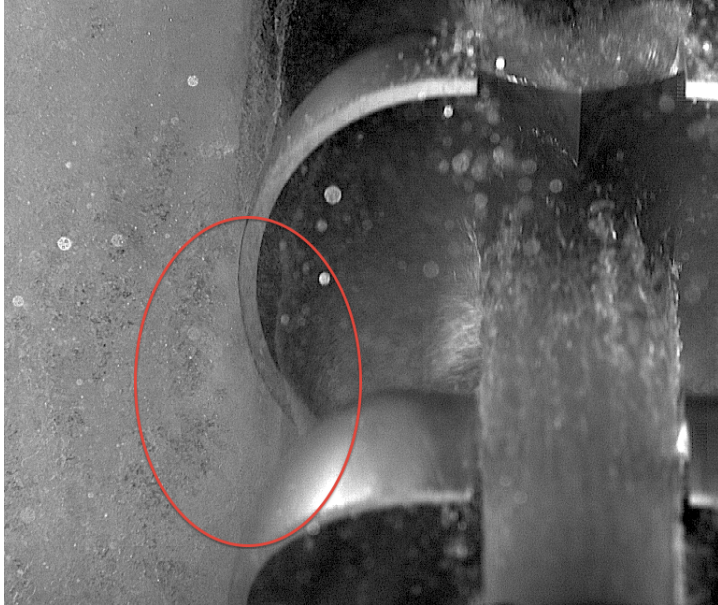
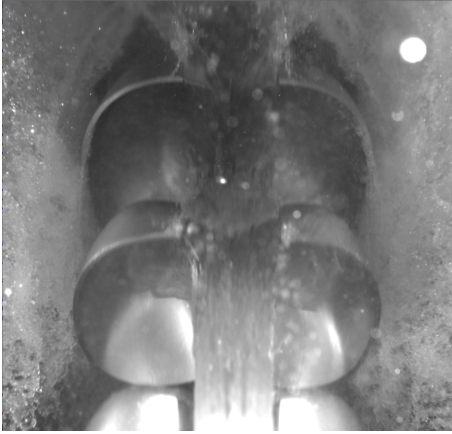


Figure 7.4: Second design

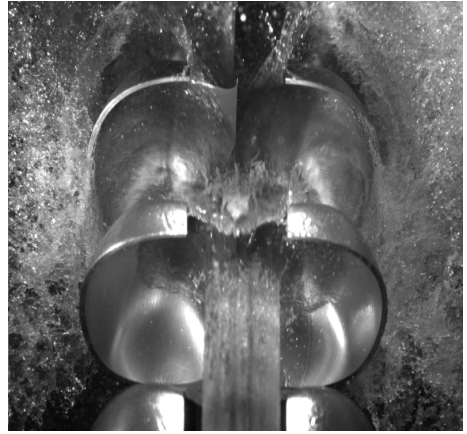
nozzle opening than it would if the turbine was correctly placed. There was no time to adjust the placement of the turbine for one last time as the last model test had to be carried out in time.

### 7.6.3 Multiple efficiency peaks

The fact that the model test for this turbine showed two efficiency peaks at two different operating points was peculiar and needed to be investigated further with the high-speed camera. As mentioned before are the two peaks located at  $n_{11} = 38, 5$  and at  $n_{11} = 44$  with a nozzle opening of 8mm, where the latter resulted in a slightly higher efficiency. When finding the optimal operating point for a Pelton turbine one may observe as the water leaves the bucket in an almost flat water film, preferable with as low velocity as possible. In the case of this turbine, the outflow stage of the water was quite unsteady, which implies a disturbed flow. The reason for the two efficiency peaks should be investigated further in order to improve the design of the bucket and to obtain a more steady flow. However, a plausible theory might



(a) 70m head



(b) 25m head

Figure 7.5: Third design,  $n_{11} = 41$ ,  $Q_{11} = 0.0101$

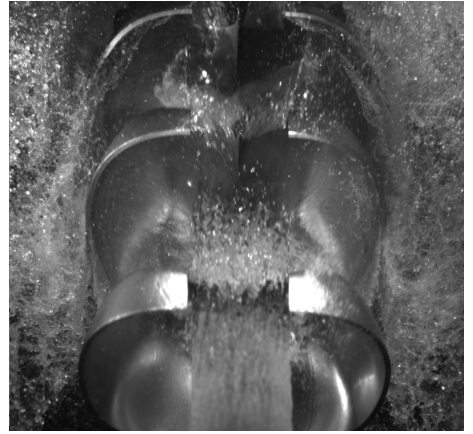
lie in the behavior of the flow near the bucket lip. A higher degree of water lost through the lip was observed for  $n_{11} = 41$ , which is an operating point located right between the two efficiency peaks and, oddly enough, the calculated design point. For  $n_{11} = 38.5$  compared to  $n_{11} = 41$  the water has a higher velocity relative to the runner. Because of inertia in the water it may react by moving faster out to the sides towards the bucket outer edge. For  $n_{11} = 44$  the runner moves faster which implies less water in each bucket. This would subsequently lead to less water lost through the bucket lip compared to  $n_{11} = 41$ . The reason for this behavior may be that the bucket angle of setting is too large, *i.e* the angle between the jet and the upper part of the bucket is too big. Hence, the splitter in the bucket is not perpendicular to the jet axis the moment the jet reaches the bucket.

#### 7.6.4 Effect of lowered effective head

By looking at the pictures obtained it is evident that undistorted images are more easily obtained with 25m head due to a smaller water wave blocking the light source. This can be seen in Figure 7.5 and Figure 7.6. To which extent the effect of a lowered head would affect the flow visually must be taken into consideration. Seim [9] found that the effect of a lower specific



(a) 70m head



(b) 25m head

Figure 7.6: Third design,  $n_{11} = 44$ ,  $Q_{11} = 0.0176$

head was not significant on the hydraulic efficiency at heads higher than 30m. This study was also done on a distributor with only one nozzle and indicates that the effect may be small, but significant. As the static head is reduced, the velocity of the water exiting through the nozzle is reduced. This is shown in Equation 2.3. The velocity in the pipes will be reduced as well as the dynamic head and the Reynolds number. This would result in a higher friction factor but the total friction head loss will be reduced due to dominance of the velocity. The magnitude of this effect is difficult to quantify, but is assumed to be small. The main bucket flow is independent on the test head according to Perrig [7]. It may have a significant effect on the hydraulic efficiency, but by comparing the pictures one can see that the behavior of the flow is visually very similar for both 70m head and 25m head. This implies that one can use pictures and videos recorded at a lower head to analyse the flow in order to detect areas of energy loss.

## 7.7 General observations

The following elements discussed are general observations of the flow, not specific for one turbine design. The observations are unfavorable elements observed for all the buckets investigated.

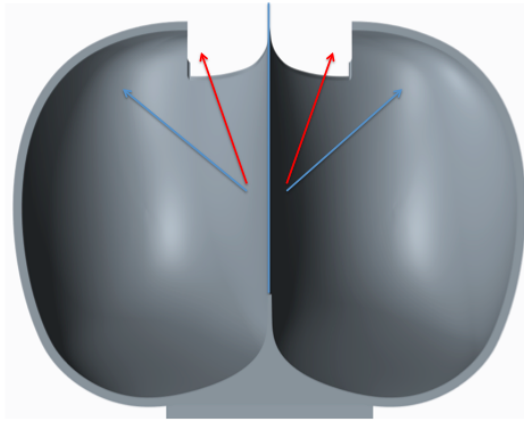


Figure 7.7: Water loss through bucket lip

### 7.7.1 Irregular water film

When filming with high-speed camera one could observe the behaviour of the flow throughout the bucket duty cycle. It was often evident that the edge of the water film was rough and irregular. This can imply that the water jet has developed as illustrated in Figure 7.8 just before impact with the bucket inner surface. This could be the probable occurrence of compressible effects generating an outburst of the jet, resulting in an additional "mini-jet" in the middle of the jet from the nozzle. In the figure the blue lines represent the velocity profile of the flow and the red line emphasizes the direction of the outburst of the jet. According to Perrig [7] there is a high-pressure pulse caused by compressible effects during the initial jet/bucket interaction. If the nozzle was placed closer to the turbine, this effect might be smaller, resulting in a more steady flow through the bucket. This can be further investigated by conducting onboard pressure measurements in the bucket.

### 7.7.2 Forces acting on the water flow

The coriolis force does not work on the fluid, but acts to change the direction of the fluid [7]. The moment the water leaves the bucket, the velocity changes to the direction of the acceleration of the runner and may linger in



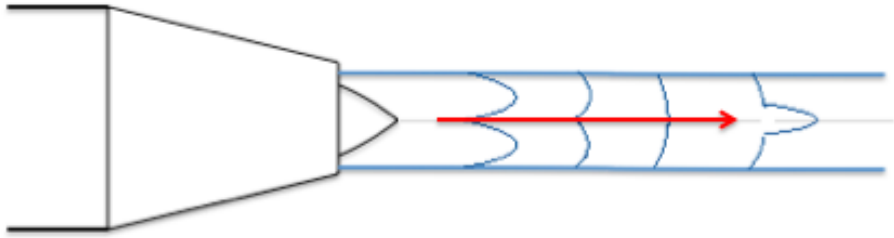


Figure 7.8: Development of water jet

the space between two buckets. The effect of this is uncertain, but some of this water may stay in the air until it crashes into the oncoming bucket. Signs of significant amount of water splashing from the upper backside of the buckets were evident in several of the pictures obtained, for example in Figure 6.11 for the third design. Due to the direction of the filming it made it difficult to quantify the extent of this effect, and whether or not this is a sign of the coriolis acceleration could be investigated further.

In experiments conducted by Perrig [7] it was found that the jet appeared to remain attached to the backside of the buckets far in the duty cycle. The bucket backside acted as the suction side of a hydrofoil undergoing the Coanda effect, generating low pressure, and in turn a lift force contributing positively to the bucket and runner torques. This low pressure can nevertheless lead to cavitation, causing erosion. Yet again, the direction of the filming made it difficult to get a view of the backside of the bucket. However this may be an effect worthy of further investigation.

Different forces acting on the flow are evident. Even if the inertia forces, i.e. the deviation, coriolis and centrifugal forces, globally dominate, the viscous and surface-tension forces outweigh the formers at the end of the evacuation process and in the jet separation process, according to Perrig [7]. Obtaining significant improvements of the forces of Pelton turbines requires to adequately take into account the secondary forces, such as surface tension

and viscosity, for the bucket flow and to improve the design of the backside in order to maximize the torque and at the same time promoting a neat separation of the water jet.

## **7.8 Onboard pressure measurements**

Onboard pressure measurements is beneficial in order to obtain a better understanding and possible assurance of the different elements of loss discussed in this chapter. Previous experiments with onboard pressure sensors are presented.

### **7.8.1 Location and distribution of sensors**

Anna Louise Martinsen [5] conducted an experiment with onboard pressure measurements in the Pelton turbine. This was, as mentioned earlier, conducted with five pressure sensors in one half of the bucket, and one sensor in the other half. In this case, some of the sensors failed to work. An experiment like this should be repeated in order to obtain viable results. Installing additional sensors would provide a more extensive basis for analysis, as illustrated by Perrig [7] and as mentioned in Chapter 7.7.1. In combination with onboard endoscope, providing a close-up view of the flow in the Pelton turbine bucket, this could be beneficial in order to further investigate the flow.

### **7.8.2 Instrumented shaft**

A. Martinsen obtained the signal from the pressure sensors via an extension of the shaft from the turbine. The output signal from the pressure sensors can be received via an extension of the shaft, a sender or by retrieving information from memory storage, if equipment is available. Due to time limitations this was not carried out in this report.

## Chapter 8

# Conclusion

The highest efficiency obtained for the first bucket design and 21 buckets was 90.32% and was achieved for the operating point  $n_{11} = 41$  and  $Q_{11} = 0.020$ .

The highest efficiency obtained for the first bucket design and 22 buckets was 90.62%, and was achieved for the operating point  $n_{11} = 40$  and  $Q_{11} = 0.0175$ . The efficiency at this point was 0.3% higher compared to the BEP for 21 buckets for the same bucket design. Visual observations also revealed a lower degree of back wash as well as less water lost through the bucket lip.

Visual observations from the second design revealed a slightly higher degree of back wash compared to the first design.

The highest efficiency obtained for the third design was 83.42%. This was achieved at the operating point  $n_{11} = 44$  and  $Q_{11} = 0.012$ . The visual observations of the flow in the turbine buckets revealed that the water jet hit skewed on the bucket. The nozzle should be adjusted in order to obtain a more accurate model test of the turbine. Two efficiency peaks were obtained for this turbine. This is peculiar and may be a result of unsteady flow in the bucket as well as several areas of evident loss. This should be further investigated.

Different signs of loss were revealed for the different turbines by the use of

high-speed camera. Signs of back wash was discovered to some extent for every turbine investigated as well as signs that indicated that the runner was placed too far from the nozzle. Loss through the bucket lip was especially evident for the third design. The various losses may be the reason why the design points does not coincide with the location of the highest points of efficiency.

From the uncertainty analysis the following results were obtained for the highest point of efficiency:

*First design - 21 buckets:*  $\eta_h = 90.32 \pm e_{\eta_h} \% = 90.32 \pm 0.0989\%$

*First design - 22 buckets:*  $\eta_h = 90.62 \pm e_{\eta_h} \% = 90.62 \pm 0.0993\%$

*Third design - 23 buckets:*  $\eta_h = 83.42 \pm e_{\eta_h} \% = 83.42 \pm 0.0915\%$

The uncertainty in the discharge had the greatest impact in the uncertainties for the tests conducted in this thesis.

Due to time limitation was pressure measurements in the buckets and the implementation of this in the Water Power Laboratory not carried out.

# Chapter 9

## Further Work

### 9.1 Pressure measurement in the buckets

Due to time limitations, the pressure measurements in the buckets were not carried out. These measurements also require equipment not available in the laboratory at the moment. This would have been beneficial in order to further investigate the flow in the turbine buckets as well as providing understanding of the behavior of the flow.

### 9.2 Onboard borescope

During the project thesis of fall 2013, an attempt was made to film with a borescope that was available in the lab. However, the videos obtained were distorted and it was found that a different setup was needed in order to obtain images of the desired quality. An onboard endoscope could provide a close-up view of the flow in the bucket, but the onboard endoscopes assembly and location must be investigated further according to the illustration in Figure 2.9. This would provide a closer view of the total bucket duty cycle.

### 9.3 Future work

- Conduct more tests to achieve a better resolution around the indicated best point of operation in the complete Hill diagram

- Obtain close-up videos or pictures from filming with onboard borescope
- Conduct experiments with pressure measurements in the Pelton turbine buckets
- Reason for two efficiency peaks obtained for the third design should be investigated further.

# Bibliography

- [1] Hermod Brekke. *Grunnkurs i hydrauliske strømningsmaskiner*. 2000.
- [2] Hermod Brekke. *Pumper og Turbiner*. Vannkraftlaboratoriet NTNU, 2003.
- [3] H. Christie. *Teoretisk undersøkelse av vandstraalens bevægelse over en peltonturbinskovl*. NTNU, 1918.
- [4] International Electrotechnical Commission. *Hydraulic turbines, storage pumps and pump-turbines - Model acceptance tests*. International Electrotechnical Commission, 1999.
- [5] Anna Louise Martinsen. *CFD-analyse av strømmingen i en peltonskovl*. Vannkraftlaboratoriet NTNU, 2000.
- [6] A. Perrig. *Flow in a Pelton Turbine Bucket: Numerical and Experimental Investigations*. 2006.
- [7] Alexandre Perrig. *Hydrodynamics of the Free Surface Flow in Pelton Turbine Buckets*. 2007.
- [8] Kyrre Reinertsen. *Testrigg for Pelton-turbinmodeller ved Vannkraftlaboratoriet*. Vannkraftlaboratoriet NTNU, 2012.
- [9] Bjarte Grytil Seim. *Flow condition in a pelton runner*. NTNU, 2008.
- [10] Bjørn Winther Solemslie. *Pelton Turbine*. NTNU, 2009.
- [11] Bjørn Winther Solemslie. *Optimalisering av ringledning for Pelton-turbin*. 2010.

- [12] Stine Trefall. *Modelltester av Pelton turbiner ved Vannkraftlaboratoriet*. 2011.
- [13] Martine C S Wessel. *Laboratory test of a Pelton turbine*. Vannkraftlaboratoriet NTNU, 2013.



# Appendix



# Appendix A

## Calibration data

In this chapter all the calibration data is found and is put in the following order:

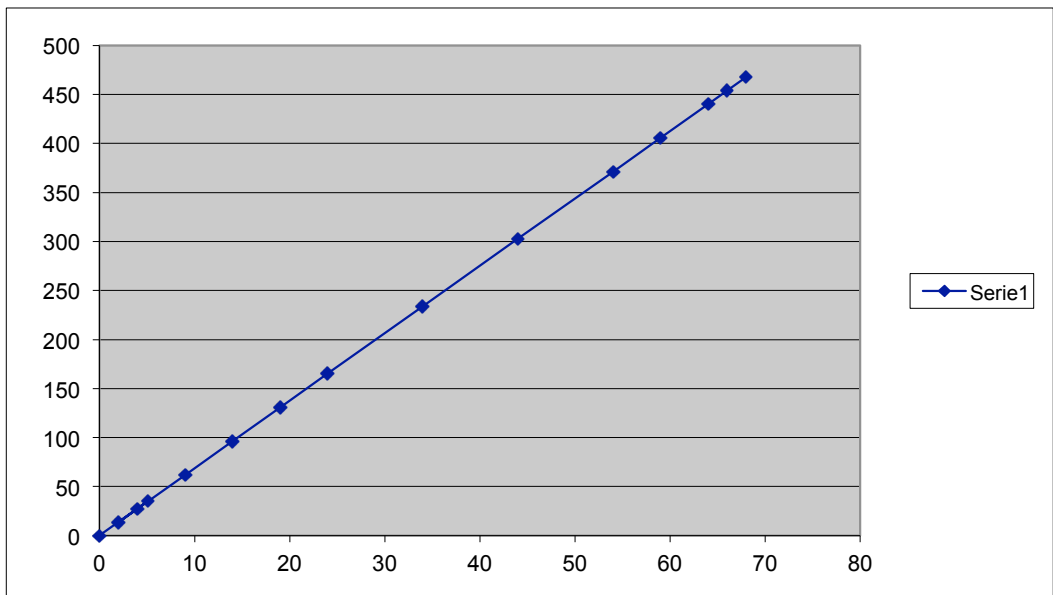
1. Shaft torque
  - Calibrated weights
  - First calibration - Uncertainty band
  - Adjusted calibration of the shaft torque
2. Friction torque
3. Pressure sensor
4. Weighing tank load cells
5. Flow meter

# THE CALIBRATED WEIGHTS

Arm: 0.69994 m

Gravitation: 9.821465

ID	Vekt [kg]	Moment [Nm]	Vekter	legg på	Ta av
0	0	0		0	
1	5,1275	35,24867168		5,1275	
2	1,999164	13,7431254	21	1,9991641	<b>21</b>
3	3,998942	27,49047169	21 22	3,998942	<b>22</b>
4	8,999272	61,86492132	21 22 1	8,999272	<b>1</b>
5	13,999672	96,23985215	21 22 1 2	13,999672	<b>2</b>
6	18,999962	130,6140268	21 22 1 2 3	18,999962	<b>3</b>
7	23,999652	164,9840768	21 22 1 2 3 4	23,999652	<b>4</b>
8	34,000722	233,7357946	21 22 1 2 3 4 5 6	34,000722	<b>5&amp;6</b>
9	44,002102	302,4896434	21 22 1 2 3 4 5 6 7 8	44,002102	<b>7&amp;8</b>
10	54,003232	371,2417736	21 22 1 2 3 4 5 6 7 8 9 10	54,003232	<b>9&amp;10</b>
11	59,003632	405,6167045	21 22 1 2 3 4 5 6 7 8 9 10 11	59,003632	<b>11</b>
12	64,003732	439,989573	21 22 1 2 3 4 5 6 7 8 9 10 11 12	64,003732	12 <b>23</b>
13	66,003511	453,7369261	21 22 1 2 3 4 5 6 7 8 9 10 11 12 23	66,003511	23 <b>24</b>
14	68,001023	467,468695	21 22 1 2 3 4 5 6 7 8 9 10 11 12 23 24	68,001023	24



# CALIBRATION REPORT

---

## CALIBRATION PROPERTIES

Calibrated by: Martine Wessel  
Type/Producer: HBM T12  
SN: 0  
Range: 0-500Nm  
Unit: Nm

## CALIBRATION SOURCE PROPERTIES

Type/Producer: Torque Transducer HBM  
SN: 66256  
Uncertainty [%]: 0,01

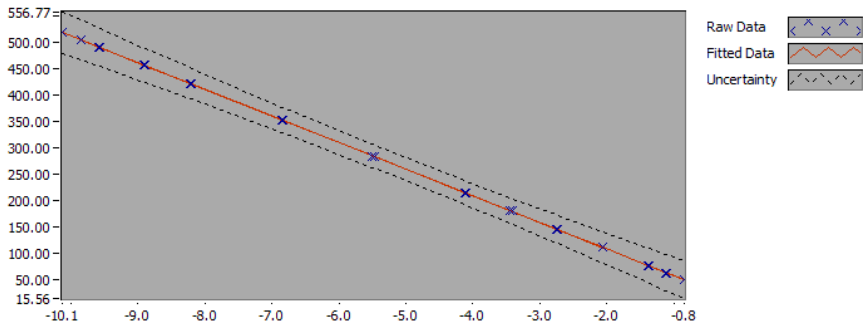
## POLY FIT EQUATION:

$$Y = + 8.17901108E+0X^0 - 50.35720637E+0X^1$$

## CALIBRATION SUMMARY:

Max Uncertainty : 0.700083 [%]  
Max Uncertainty : 0.387333 [Nm]  
RSQ : 0.999989  
Calibration points : 27

Figure 1 : Calibration chart (The uncertainty band is multiplied by 100 )



---

Martine Wessel

---

**CALIBRATION VALUES**

Value [Nm]	Voltage [V]	Best Poly Fit [Nm]	Deviation [Nm]	Uncertainty [%]	Uncertainty [Nm]
112,224483	-2,055314	111,678872	0,545611	0,262793	0,294918
146,599414	-2,731145	145,711839	0,887575	0,181767	0,26647
180,973589	-3,408451	179,819063	1,154526	0,134374	0,243181
215,343639	-4,096429	214,463715	0,879924	0,104917	0,225932
284,095356	-5,459195	283,088818	1,006539	0,076059	0,21608
352,849205	-6,830034	352,120445	0,72876	0,068299	0,240993
421,601335	-8,205507	421,385439	0,215897	0,069305	0,29219
455,976266	-8,887927	455,750195	0,226071	0,071005	0,323768
490,349135	-9,56855	490,024483	0,324652	0,072994	0,357924
504,096488	-9,848667	504,130366	-0,033878	0,073912	0,372586
517,828257	-10,124822	518,036783	-0,208526	0,074799	0,387333
504,096488	-9,852317	504,314166	-0,217678	0,073953	0,372792
490,349135	-9,58201	490,702253	-0,353118	0,073135	0,358618
455,976266	-8,902558	456,486968	-0,510702	0,07116	0,324471
421,601335	-8,215493	421,888284	-0,286949	0,069409	0,292631
352,849205	-6,847997	353,025034	-0,175829	0,068449	0,241521
284,095356	-5,49727	285,006158	-0,910802	0,076146	0,216328
215,343639	-4,126107	215,958252	-0,614614	0,104619	0,22529
180,973589	-3,442746	181,546073	-0,572485	0,133804	0,24215
146,599414	-2,756079	146,96745	-0,368036	0,181116	0,265516
112,224483	-2,069859	112,411303	-0,18682	0,26177	0,29377
77,850033	-1,387938	78,07171	-0,221676	0,418092	0,325485
64,102688	-1,122022	64,680913	-0,578225	0,528194	0,338587
50,359562	-0,847047	50,833924	-0,474362	0,700037	0,352536
50,359562	-0,846611	50,811974	-0,452412	0,700083	0,352559
64,102688	-1,112156	64,184074	-0,081386	0,528979	0,33909
77,850033	-1,378017	77,57209	0,277944	0,418708	0,325964

**COMMENTS:**

Arm: 0.69994 m

Sk\_lvekt: 5.1275 kg

The values are invalid due to incorrect use of load arm, but the uncertainty band is correct.

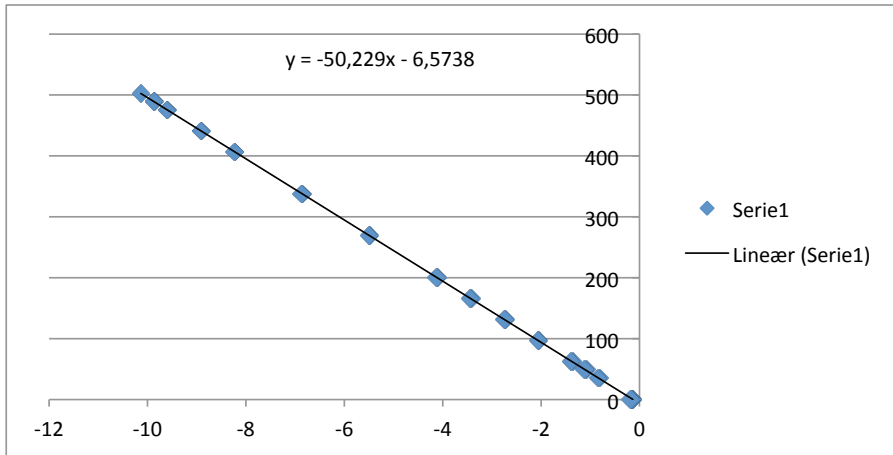
---

The uncertainty is calculated with 95% confidence. The uncertainty includes the randomness in the calibrated instrument during the calibration, systematic uncertainty in the instrument or property which the instrument under calibration is compared with (dead weight manometer, calibrated weights etc.), and due to regression analysis to fit the calibration points to a linear calibration equation. The calculated uncertainty can be used as the total systematic uncertainty of the calibrated instrument with the given calibration equation.

Value [Nm]	Voltage [V]	Best Poly Fit [Nm]	Deviation [Nm]	Uncertainty [%]	Uncertainty [Nm]	Uncertainty [Nm]
0	-0,14693	10,996236	-10,996236	Inf	NaN	0
0	-0,13502	10,39009	-10,39009	Inf	NaN	0
0	-0,149	11,101425	-11,101425	Inf	NaN	0
35,24867189	-0,80415	44,454997	5,904565	5,220948	2,629246	50,359562
48,99179789	-1,07927	58,461165	5,641523	3,945039	2,528876	64,102688
62,73914289	-1,35476	72,486097	5,363936	3,124557	2,432468	77,850033
97,11359289	-2,03908	107,324758	4,899725	1,972832	2,214001	112,224483
131,4885239	-2,72778	142,386339	4,213075	1,386147	2,032083	146,599414
165,8626989	-3,41764	177,506827	3,466761	1,049298	1,898952	180,973589
200,2327489	-4,10429	212,463848	2,879791	0,847926	1,825954	215,343639
268,9844659	-5,4735	282,169253	1,926103	0,661661	1,879749	284,095356
337,7383149	-6,84928	352,209985	0,63922	0,616277	2,17453	352,849205
406,4904449	-8,22356	422,173967	-0,572631	0,623858	2,630195	421,601335
440,8653759	-8,90322	456,774762	-0,798495	0,634423	2,892817	455,976266
475,2382449	-9,59162	491,821144	-1,47201	0,647659	3,17579	490,349135
488,9855979	-9,86165	505,568046	-1,471558	0,652752	3,290499	504,096488
502,7173669	-10,1363	519,549697	-1,72144	0,658324	3,40899	517,828257
488,9855979	-9,86473	505,72482	-1,628332	0,653013	3,291817	504,096488
475,2382449	-9,60146	492,322064	-1,972929	0,648504	3,179935	490,349135
440,8653759	-8,91674	457,463314	-1,487048	0,635609	2,898226	455,976266
406,4904449	-8,23098	422,551585	-0,95025	0,624512	2,632952	421,601335
337,7383149	-6,86948	353,238295	-0,389089	0,617901	2,180258	352,849205
268,9844659	-5,50336	283,689636	0,40572	0,663096	1,883824	284,095356
200,2327489	-4,13064	213,80497	1,538668	0,847225	1,824446	215,343639
165,8626989	-3,44279	178,787073	2,186515	1,047205	1,895165	180,973589
131,4885239	-2,74709	143,369042	3,230372	1,383096	2,027611	146,599414
97,11359289	-2,06398	108,592186	3,632297	1,966322	2,206695	112,224483
62,73914289	-1,38631	74,092292	3,757742	3,110732	2,421706	77,850033
48,99179789	-1,11412	60,235274	3,867414	3,925645	2,516444	64,102688
35,24867189	-0,83962	46,260937	4,098625	5,194769	2,616063	50,359562
0	-0,18041	12,700517	-12,700517	Inf	NaN	0

Calibration constants,  
20.02.2014

$C_0$	-6,573847
$C_1$	-50,22896





# CALIBRATION REPORT

## CALIBRATION PROPERTIES

Calibrated by: Martine Wessel  
 Type/Producer: Druck PTX 1830  
 SN: 0  
 Range: 0-10 Nm  
 Unit: Nm

## CALIBRATION SOURCE PROPERTIES

Type/Producer: Load Beam Force Cell Z6 HBM  
 SN:  
 Uncertainty [%]: 0,01

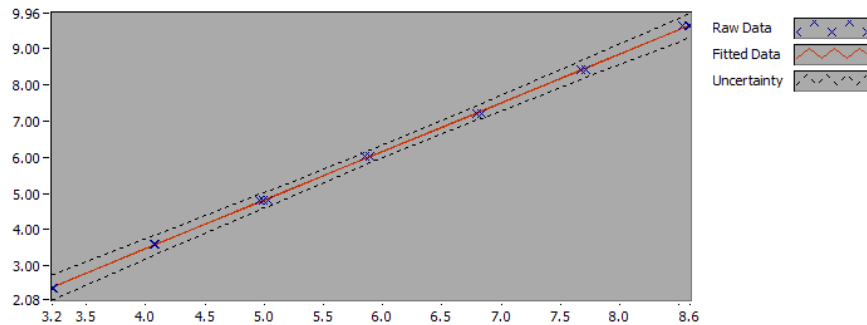
## POLY FIT EQUATION:

$$Y = -1.89877295E+0X^0 + 1.34231177E+0X^1$$

## CALIBRATION SUMMARY:

Max Uncertainty : 1.406244 [%]  
 Max Uncertainty : 0.033762 [Nm]  
 RSQ : 0.999767  
 Calibration points : 17

Figure 1 : Calibration chart (The uncertainty band is multiplied by 10)



Martine Wessel

## CALIBRATION VALUES

Value [Nm]	Voltage [V]	Best Poly Fit [Nm]	Deviation [Nm]	Uncertainty [%]	Uncertainty [Nm]
2,400857	3,213598	2,414877	-0,01402	1,406244	0,033762
3,595393	4,074794	3,570872	0,024521	0,743377	0,026727
4,811536	4,960868	4,760258	0,051277	0,437474	0,021049
6,006071	5,852146	5,956631	0,04944	0,307272	0,018455
7,211656	6,787273	7,211863	-0,000207	0,283082	0,020415
8,406192	7,666421	8,391955	0,014237	0,305603	0,02569
9,615951	8,524625	9,543931	0,07202	0,338215	0,032523
8,406192	7,709197	8,449373	-0,043181	0,309302	0,026001
7,211656	6,83587	7,277096	-0,06544	0,286156	0,020637
6,006071	5,896454	6,016106	-0,010035	0,306985	0,018438
4,811536	5,035286	4,86015	-0,048614	0,429957	0,020688
3,595393	4,083899	3,583093	0,0123	0,741478	0,026659
2,400857	3,223411	2,42805	-0,027193	1,402694	0,033677
4,794839	4,962671	4,762678	0,032161	0,43881	0,02104
4,794839	4,996512	4,808104	-0,013264	0,435327	0,020873
9,605638	8,58335	9,622759	-0,01712	0,343821	0,033026
9,615951	8,590855	9,632833	-0,016882	0,344124	0,033091

## COMMENTS:

# CALIBRATION REPORT

---

## CALIBRATION PROPERTIES

Calibrated by: Martine Wessel  
Type/Producer: Tecsis  
SN: 3276.076.001  
Range: 0-16 bar  
Unit: Pa

## CALIBRATION SOURCE PROPERTIES

Type/Producer: Pressurements deadweight tester P3223-1  
SN: 66256  
Uncertainty [%]: 0,008

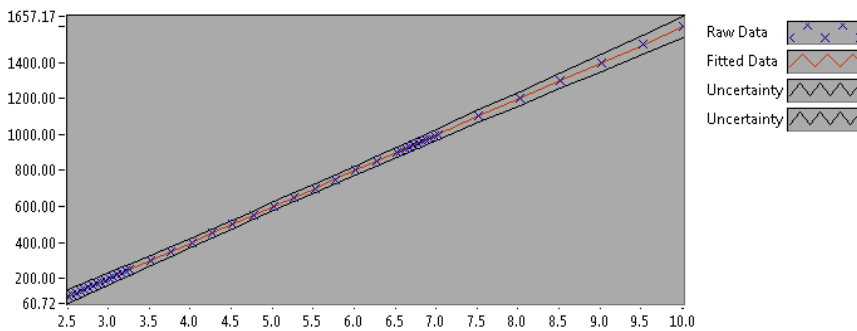
## POLY FIT EQUATION:

$$Y = -401.83525906E+0X^0 + 199.71381920E+0X^1$$

## CALIBRATION SUMMARY:

Max Uncertainty : 0.380832 [%]  
Max Uncertainty : 0.581445 [Pa]  
RSQ : 0.999997  
Calibration points : 46

Figure 1 : Calibration chart (The uncertainty band is multiplied by 100 )



Martine Wessel

---

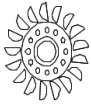
**CALIBRATION VALUES**

Value [Pa]	Voltage [V]	Best Poly Fit [Pa]	Deviation [Pa]	Uncertainty [%]	Uncertainty [Pa]
99,415864	2,505652	98,577978	0,837886	0,380832	0,378607
109,430971	2,555868	108,606842	0,824129	0,342023	0,374279
119,446078	2,606222	118,663337	0,782741	0,30974	0,369972
129,461185	2,656647	128,733828	0,727357	0,282473	0,365692
139,476293	2,707136	138,817223	0,65907	0,259142	0,361442
149,4914	2,75762	148,899483	0,591917	0,238963	0,357229
159,506507	2,808097	158,980528	0,525979	0,221341	0,353053
169,521614	2,858384	169,023605	0,498009	0,205834	0,348933
179,536721	2,908857	179,103772	0,432949	0,19207	0,344836
189,551828	2,959229	189,163705	0,388123	0,179787	0,34079
199,566935	3,009594	199,222349	0,344586	0,168759	0,336788
209,582042	3,059978	209,284566	0,297477	0,158806	0,332828
219,597149	3,110451	219,364754	0,232395	0,149778	0,328908
229,612256	3,160757	229,411686	0,200571	0,141564	0,325049
239,627363	3,211043	239,454479	0,172885	0,134059	0,321241
249,642471	3,261373	249,505912	0,136558	0,127174	0,317481
299,718006	3,513312	299,821731	-0,103725	0,099926	0,299497
349,793541	3,764368	349,961092	-0,167551	0,08095	0,283157
399,869077	4,015922	400,199924	-0,330847	0,067187	0,268659
449,944612	4,267467	450,436942	-0,49233	0,056974	0,256353
500,020148	4,518897	500,650876	-0,630728	0,049312	0,246572
550,095683	4,770027	550,804951	-0,709268	0,043561	0,239626
600,171219	5,020893	600,906467	-0,735248	0,039281	0,235752
650,246754	5,271995	651,054984	-0,80823	0,036155	0,235096
700,32229	5,523024	701,188969	-0,866679	0,033939	0,237686
750,397825	5,773602	751,232849	-0,835024	0,032437	0,243406
800,473361	6,024218	801,284364	-0,811003	0,031487	0,252044
850,548896	6,274798	851,328587	-0,779691	0,030958	0,263314
900,624432	6,525456	901,38841	-0,763978	0,030745	0,276899
950,699967	6,775832	951,39205	-0,692083	0,030762	0,292458
1000,775503	7,026177	1001,389292	-0,61379	0,030946	0,309699
1000,775503	7,023608	1000,876292	-0,100789	0,030927	0,309514
910,639539	6,575441	911,371135	-0,731596	0,030732	0,279858
920,654646	6,625663	921,401245	-0,746599	0,030729	0,282905
930,669753	6,675799	931,414058	-0,744305	0,030733	0,286023
940,68486	6,725998	941,439545	-0,754685	0,030745	0,289217
960,715074	6,825895	961,390303	-0,675229	0,030787	0,295778
970,730181	6,876327	971,462282	-0,732101	0,030821	0,299189
980,745288	6,926278	981,438236	-0,692947	0,030857	0,302632
990,760395	6,976137	991,395711	-0,635316	0,030898	0,306128
1100,926573	7,523867	1100,785006	0,141567	0,031607	0,347966
1201,077644	8,023592	1200,586988	0,490656	0,032504	0,390404
1301,228715	8,52311	1300,34761	0,881105	0,033482	0,435675
1401,379786	9,022154	1400,013525	1,366261	0,034462	0,482944
1501,530857	9,520629	1499,56591	1,964947	0,035408	0,531656
1601,681928	10,018639	1599,025354	2,656574	0,036302	0,581445

**COMMENTS:**

---

The uncertainty is calculated with 95% confidence. The uncertainty includes the randomness in the calibrated instrument during the calibration, systematic uncertainty in the instrument or property which the instrument under calibration is compared with (dead weight manometer, calibrated weights etc.), and due to regression analysis to fit the calibration points to a linear calibration equation. The calculated uncertainty can be used as the total systematic uncertainty of the calibrated instrument with the given calibration equation.



NTNU

# WATERPOWER LABORATORY

Date:

30.09.2013

Operator:

Inger Johanne Rasmussen

## Calibration Sheet

Calibration of weighing tank load cells

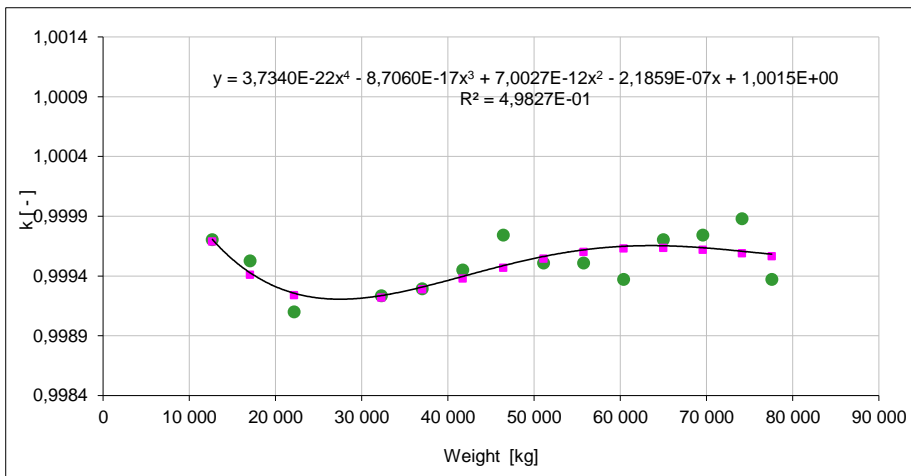
Unit: Weighing tank load cells, reg. nr. 4331-5/6/7

$W_L$  5126,075 [kg]

Comments:

The flow controlled via the loft storage tanks. Indicated Q= ca.200 l/s ->time of filling->30s  
"Valve 1" 200% open

Manual Observation	Manual Observation	Displayed load increase	$k = \frac{W_L}{\Delta W}$	Weight midpoint	Estimated correction factor	Difference in real k and estimated k	
Weights off	Weights on	$\Delta W$	k	Weight	k	$\Delta k$	$\Delta k$
[kg]	[kg]	[kg]	[-]	[kg]	[-]	[-]	[%]
10096	15223,6	5127,6	0,9997	12659,8	0,99969	-0,00001	0,001
14489,8	19618,3	5128,5	0,9995	17054,1	0,99941	-0,00012	0,012
19589,2	24719,9	5130,7	0,9991	22154,6	0,99924	0,00014	0,014
29710,4	34840,4	5130	0,9992	32275,4	0,99922	-0,00002	0,002
34446,6	39576,3	5129,7	0,9993	37011,5	0,99929	0,00000	0,000
39164,7	44293,6	5128,9	0,9994	41729,2	0,99938	-0,00007	0,007
43860	48987,4	5127,4	0,9997	46423,7	0,99947	-0,00027	0,027
48532,1	53660,7	5128,6	0,9995	51096,4	0,99954	0,00004	0,004
53182,2	58310,8	5128,6	0,9995	55746,5	0,99960	0,00009	0,009
57805,7	62935	5129,3	0,9994	60370,4	0,99963	0,00026	0,026
62412	67539,6	5127,6	0,9997	64975,8	0,99963	-0,00007	0,007
66999,6	72127	5127,4	0,9997	69563,3	0,99962	-0,00012	0,012
71560,3	76687	5126,7	0,9999	74123,7	0,99959	-0,00029	0,029
74996,2	80125,5	5129,3	0,9994	77560,9	0,99956	0,00019	0,019



Calibration constants	
$a_1$	3,73400E-22
$a_2$	-8,70600E-17
$a_3$	7,00270E-12
$a_4$	-2,18590E-07
$a_5$	1,00150E+00



# WATERPOWER LABORATORY

## Calibration Sheet

Calibration of flow meter

Date: 20.02.14  
 Operator: Martine Wessel

Calibrator: Weighing tank system Unit: Flowmeter, reg nr. 4624-7 (A03 36133)

Calibration constants for weighing tank correction	
a <sub>1</sub>	3.73E-22
a <sub>2</sub>	-8.71E-17
a <sub>3</sub>	7.00E-12
a <sub>4</sub>	-2.19E-07
a <sub>5</sub>	1.02E-020

Corrected weight is calculated from formula where parameters a, b, c, d and e is achieved through substitution calibration.

$$W = a \frac{mW^5}{5} + b \frac{mW^4}{4} + c \frac{mW^3}{3} + d \frac{mW^2}{2} + e \cdot mW$$

Density of water is calculated from formula

$$\rho_w = \frac{1000}{(1 - 4.669 \cdot 10^{-6} \cdot (p_w - 1) + 6 \cdot 10^{-8} \cdot (p_w - 1)^2 - 9 \cdot 4 + 2.131891 \cdot 10^{-6} \cdot (p_w - 1)^3 - 6 \cdot 10^{-8} \cdot (p_w - 1 + 2.131891 \cdot 10^{-6} \cdot (p_w - 1)^2))}$$

Density of air is calculated from formula

$$\rho_a = \frac{(p_a - 3.4837 \cdot 10^{-3})}{(273.15 + \theta)}$$

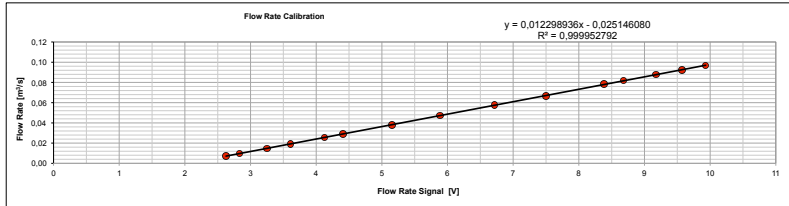
Discharge is found from formula

$$Q = \frac{W_1 - W_2}{\rho_w \cdot t} \cdot \left(1 - \frac{\rho_a}{\rho_w}\right)$$

Comments:  
 The flow rate changes during calibration. The inlet conditions to the pumps will change due to leak water in the reservoir

Date	Manual Observation before Weight [kg]	Manual Observation after Weight [kg]	Manual Observation Voltage [V]	Time [s]	Ambient pressure [kPa]	Water temp [°C]	Air temp [°C]	Calculated value before Weight [kg]	Calculated value after Weight [kg]	Differential weight [kg]	Density of water [kg/m³]	Density of air [kg/m³]	Differential volume [m³]	Calculated Flow Rate [m³/s]	Estimate [m³/s]	Deviation [%]
20.02.14	2265,1	2466,0	2.826470	280,096	99,920	12,41	17,96	2265,8	2466,2	2010,3	995,5136	1,1966	2,01371	0,0071893	0,00716	-0,45599
20.02.14	2466,0	2658,2	2.829460	200,099	99,910	12,20	17,84	2466,2	2658,8	1920,6	995,5390	1,1969	1,92384	0,0096144	0,00965	0,40223
20.02.14	2658,2	2865,9	3.251250	140,099	99,900	12,14	17,64	2658,8	2865,0	2066,0	995,5461	1,1976	2,06344	0,0137713	0,01404	0,46879
20.02.14	2827,4	2618,0	3.605520	100,102	99,880	12,13	17,67	24271,9	26185,5	1914,1	995,5473	1,1973	1,91722	0,0151527	0,01520	0,23585
20.02.14	2618,0	2823,3	4.124060	80,101	99,870	12,15	17,59	26185,9	28234,6	2048,6	995,5449	1,1975	2,05203	0,0256180	0,02558	-0,16626
20.02.14	2823,3	3027,6	4.410960	70,100	99,870	12,15	17,55	28234,6	30269,2	2034,7	995,5449	1,1977	2,03802	0,0290731	0,02909	0,06828
20.02.14	3027,6	3218,4	5.151340	50,102	99,870	12,17	17,50	30269,2	32180,5	1911,3	995,5425	1,1978	1,91445	0,0382111	0,03821	0,00317
20.02.14	3218,4	3408,2	5.887920	40,102	99,860	12,16	17,51	32180,5	34073,0	1892,5	995,5437	1,1977	1,89567	0,0472713	0,04727	-0,00476
20.02.14	3408,2	3638,9	6.714740	40,102	99,850	12,14	17,48	34073,0	36374,8	2301,8	995,5461	1,1977	2,30560	0,0574934	0,05744	-0,09638
20.02.14	3638,9	3906,7	7.489690	40,101	99,850	12,20	17,41	36374,8	39047,8	2672,8	995,5390	1,1980	2,67727	0,0667633	0,06706	0,43536
20.02.14	3906,7	4202,8	8.382420	40,099	99,790	12,41	17,36	39047,6	42187,9	3140,3	995,5136	1,1975	3,14558	0,0784451	0,07795	-0,63666
20.02.14	4202,8	4548,9	8.682740	40,101	99,780	12,45	17,30	42188,2	45472,5	3284,4	995,5087	1,1976	3,28995	0,0820416	0,08164	-0,48895
20.02.14	4548,9	49001,8	9.172580	40,101	99,770	12,43	17,30	45472,4	48983,1	3510,7	995,5111	1,1975	3,51661	0,0876939	0,08767	-0,03079
20.02.14	49001,8	52699,7	9.575500	40,102	99,760	12,46	17,33	48983,2	52679,3	3696,0	995,5074	1,1973	3,70226	0,0923210	0,09262	0,32255
20.02.14	52699,7	56573,2	9.932450	40,100	99,760	13,50	17,30	52679,1	56551,2	3872,1	995,5024	1,1970	3,87868	0,0967251	0,09701	0,28619

Calibration constants, 20.02.2014	
C <sub>0</sub>	-0,025146080
C <sub>1</sub>	0,012298936





# Appendix B

## Test Procedure

This chapter includes the routine for running the Pelton turbine test rig at the Water Power Laboratory at NTNU. The water is directed from the reservoir, through the pump and from there through the turbine to the draft tube and back to the reservoir. The Pelton turbine test rig is illustrated in Figure 3.2 [8].

### A Start Up

1. **Start the programs**

The pump, the generator, valves and water levels are controlled from the control room. Start the program *Pelton logging program* for monitoring the different operational values.

2. **Control the loop**

Make sure that the valves joining the loop and the valves adjacent to the loop is in the correct position. It may be necessary to walk around in the lab and manually adjust the valves.

3. **Make sure the pump is submerged**

The pump will not start unless it is submerged in water. The pump is submerged by manually opening the valve above the pump and thus increasing the water level in the pipe. The water level in the pipe should be at least 2-3 meters. If the pump is already initiated it will start running when necessary water level is reached.

4. **Start the generator at 100 rpm**
5. **Start the pump at 100 rpm**
6. **Increase the rotational speed of the pump**  
Increase the rotational speed of the pump up to 500 rpm and wait for the water to reach the nozzle.
7. **There may be a lot of air in the pipes**  
Run the turbine at current operating point and wait for the air to pass through the nozzle until the rotational speed of both the pump and the generator can be increased further.
8. **Vent out the tubes by the pressure sensor**  
Open the valves shown in Figure C.3 by the the tubes leading to the pressure sensor until the air bubbles are gone. Close the valves.

## **B Taking Measurements for a Hill Diagram**

1. **Prepare a running sequence**  
You should record a measurement sequence for one nozzle opening at the time. Before you start, make sure the nozzle opening is changing by instructions from the computer in the control room. The nozzle opening is changed by the help of water from upstream of the turbine, but if the pressure here is not high enough it may be necessary to use the water from the tap. Adjust the valves accordingly. The valves in question are shown in Figure C.1 and Figure C.2. The position of the valves shown in these pictures are applicable for low head, as the water used for adjusting the nozzle is from the tap.
2. **Set recording time and directory**  
Set the recording time to 60 seconds, and specify the name of your recording file and the directory you want to save in.
3. **Adjust head**  
Set the head for the measurements by adjusting the rotational speed of the pump. This may need to be adjusted slightly throughout the measurements. Make sure the value for  $n_{11}$  stays between 30 and



50. Increasing the rotational speed for the generator will make  $n_{11}$  increase. Increasing the rotational speed for the pump will make  $n_{11}$  decrease.

4. **Set nozzle opening**

Adjust the nozzle opening according to the flow rate of your first measurements series.

5. **Set generator speed**

Adjust the speed according to the value of  $n_{11}$  for your first measurement point.

6. **Record measurement point**

Clear the graph and hit the record button. Check your file to make sure that the recording was saved.

7. **Set generator speed**

Adjust the speed according to the value of  $n_{11}$  for your next measurement point.

8. **Complete first measurement series**

Repeat the three latter steps until you have completed the measurement series for the first nozzle opening.

9. **Set new nozzle opening**

10. **Set generator speed**

Adjust the generator speed according to the same value for  $n_{11}$  as for the previous measurement series.

11. **Record measurement point**

12. **Complete measurement series**

Repeat the two latter steps until you have completed the measurement series for the current nozzle opening.

13. **Carry out remaining measurement series**

Repeat until you have completed the measurement sequence for the different nozzle openings.

## C Shut Down

1. **Run down**

Decrease the rotational speed for the pump and the generator step by step and make sure the value for  $n_{11}$  stays between 30 and 50.

2. **Stop the pump** When the rotational speed of both the pump and the generator is at 100 rpm, stop the pump.

3. **Stop the generator**

# Appendix C

## Prosedyre for modelltest - Norwegian

Dette kapittelet inneholder rutine for igangsetting, testkjøring og nedkjøring av Pelton-sløyfen ved Vannkraftlaboratoriet ved NTNU

### A Igangsetting av Pelton-sløyfen

#### 1. Start programmene

Justering av turtall til pumpe og generator, vannivå i rørene og åpning og lukking av ventilene gjøres fra kontrollrommet. Start programmet *Pelton logging program* for overvåking av de forskjellige driftsverdiene.

#### 2. Kontroller sløyfen

Sjekk at alle ventiler som grenser til sløyfen eller som er inne i sløyfen er i riktig posisjon. Ta en runde i langs sløyfen i laboratoriet for å være sikker på posisjonen og eventuelt åpne og lukke ventiler manuelt.

#### 3. Pass på at pumpen er dykket i vann

Pumpen vil ikke starte dersom den ikke er dykket. Pumpen dykkes ved at vannivået økes i røret. Dette gjøres ved å åpne ventilen over pumpen til vannivået i røret er minst 2-3 meter. Dersom pumpen allerede er startet vil den begynne å gå når nødvendig vannivå er nådd.

#### 4. Start generatoren på 100 rpm

5. **Start pumpen på 100 rpm**

6. **Øk turtallet til pumpen**

Øk turtallet til pumpen til 500 rpm og vent på vann fra dysen.

7. **Det kan være en del luft i rørene**

La dysen hoste seg ferdig før turtallet til pumpen og generatoren økes ytterligere.

8. **Luft ut rørene ved trykksensoren**

Dette gjøres ved å åpne ventilene, vist i Figur C.3, til rørene som leder til trykksensoren. Ha ventilene åpne til luftboblene har forsvunnet. Lukk ventilene.

## B Gjennomføring av tester

1. **Forbered en testsekvens**

Det bør gjøres tester for en dyseåpning av gangen. Før start, pass på at dyseåpningen endres ved instruksjon fra kontrollrommet. Dyseåpningen endres ved hjelp av vann oppstrøms turbinen, men dersom dette trykket ikke er høyt nok kan det være nødvendig å bruke vann fra springen. Juster ventilene tilsvarende. Ventilene det er snakk om her er vist i Figur C.1 og Figur C.2. Ved ventilenes posisjon i disse bildene tas vannet fra springen. Dette må brukes dersom man kjører på lav head.

2. **Still inn loggetid og lagringssted for filene**

Still inn loggetid til 60 sekunder og spesifiser lagringssted og filnavn for datafilene.

3. **Still inn riktig vannhøyde**

Juster vannhøyde for målingene ved å justere turtallet til pumpen. Det kan være nødvendig å finjustere denne, så godt det lar seg gjøre, underveis i testen. Sørg for at verdien for  $n_{11}$  holder seg mellom 30 og 50. Når turtallet for generatoren øker vil verdien for  $n_{11}$  øke. Når turtallet for pumpen øker vil verdien for  $n_{11}$  minke.

4. **Still inn dyseåpningen**

Juster dyseåpningen tilsvarende volumstrømmen for første målepunkt.

5. **Juster turtall for generator**  
Juster turtallet tilsvarende verdien for  $n_{11}$  for første målepunkt.
6. **Logg målepunkt**  
Trykk *clear graph* og deretter *logg*. Sjekk filen for å passe på at måledataene ble lagret.
7. **Juster turtall for generatoren**  
Juster turtall for generatoren tilsvarende verdien for  $n_{11}$  for neste målepunkt.
8. **Fullfør første måleserie**  
Repetér de tre siste stegene til måleserien for første dyseåpning er fullført.
9. **Juster dyseåpningen for neste måleserie**
10. **Juster turtall for generatoren**  
Juster turtallet til generatoren tilsvarende for den samme verdien for  $n_{11}$  som for forrige måleserie.
11. **Logg målepunkt**
12. **Fullfør måleseriene**  
Repetér de to siste stegene til måleserien for nåværende dyseåpning.
13. **Fullfør resterende måleserier**  
Repetér til målesekvensene for alle dyseåpningene er fullført

## C Nedkjøring av Pelton-sløyfen

1. **Kjør ned**  
Mink turtallet til pumpen og generatoren steg for steg og sørg for at verdien for  $n_{11}$  holder seg mellom 30 og 50.
2. **Stopp pumpen**  
Når turtallet til pumpe og generator begge er på 100 rpm kan pumpen stoppes.
3. **Stopp generatoren**

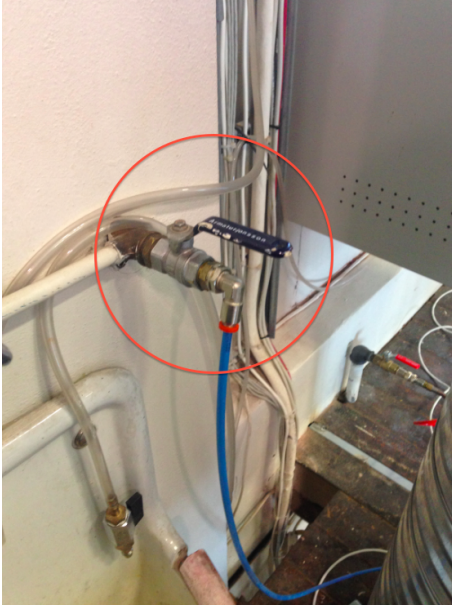


Figure C.1: Valve number 1 for controlling the water adjusting the nozzle

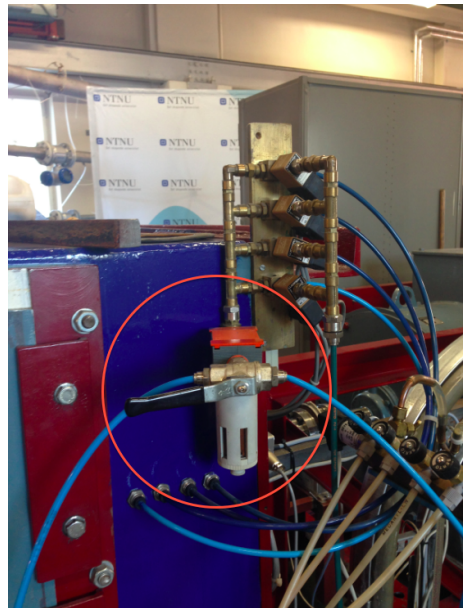


Figure C.2: Valve number 2 for controlling the water adjusting the nozzle

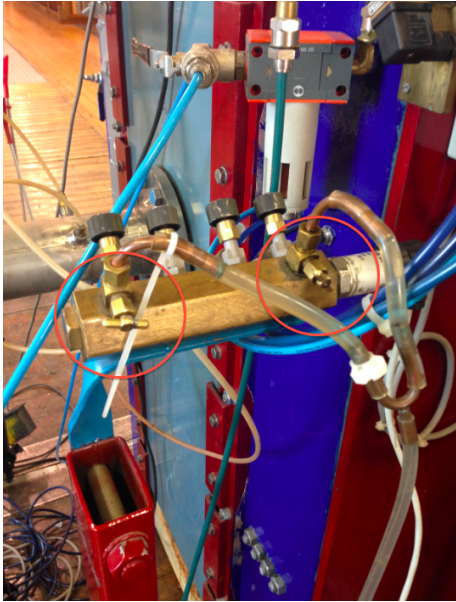


Figure C.3: Valves for venting out air ahead of pressure sensor





# Appendix D

## Results

The following tables show the mean values obtained from the model test. The values presented are those used in order to create the Hill-diagrams.

Mean values obtained from the model test for the third bucket design

n_11	Nozzle opening						
	6mm	8mm	10mm	12mm	14mm	16mm	18mm
37	0.833284	0.827133	0.827108	0.819554	0.81663	0.812540	0.806819
37,5	0.831933	0.827366	0.828847	0.820721	0.817588	0.812897	0.808281
38	0.832181	0.828174	0.827863	0.821637	0.818461	0.813508	0.808356
38,5	0.832543	0.829472	0.828668	0.824610	0.818528	0.813702	0.809099
39	0.831747	0.828163	0.828359	0.822539	0.819033	0.815388	0.809713
39,5	0.831139	0.828858	0.827975	0.823048	0.818393	0.813956	0.809994
40	0.831141	0.828664	0.826622	0.823638	0.817498	0.815040	0.809477
40,5	0.828531	0.827565	0.828272	0.822324	0.819027	0.814966	0.809916
41	0.827134	0.828256	0.826429	0.821914	0.817996	0.815230	0.811288
41,5	0.825723	0.825863	0.825812	0.821907	0.819027	0.817272	0.810213
42	0.825175	0.826738	0.825140	0.823221	0.820655	0.819111	0.814244
42,5	0.825250	0.827109	0.826240	0.824124	0.822584	0.821050	0.815783
43	0.827690	0.829937	0.830404	0.825077	0.82199	0.824108	0.814439
43,5	0.827659	0.832708	0.830932	0.826094	0.821736	0.817690	0.813519
44	0.826535	0.834263	0.829977	0.825211	0.819651	0.815940	0.811434
44,5	0.825831	0.833011	0.829937	0.820907	0.816297	0.812868	0.809010
45	0.822604	0.827922	0.826416	0.822065	0.81323	0.808902	0.804483

Mean values obtained from the model test for the first bucket design, 21 buckets

n_11	Nozzle opening						
	6mm	10mm	14mm	18mm	22mm	26mm	30mm
38	0.881352	0.892070	0.896892	0.896622	0.895904	0.893446	0.892179
39	0.883881	0.896685	0.900005	0.900097	0.899214	0.897749	0.897641
40	0.886811	0.900071	0.902090	0.902189	0.901793	0.900588	0.900236
41	0.883845	0.897017	0.901905	0.903168	0.902722	0.901173	0.900289
42	0.882844	0.896011	0.902598	0.902936	0.902022	0.900655	0.899860
43	0.876894	0.894402	0.898910	0.900317	0.900342	0.898474	0.897490
44	0.871557	0.887342	0.894025	0.895967	0.895040	0.894084	0.892338
45	0.866417	0.881102	0.886438	0.888037	0.886475	0.884619	0.882812

Mean values obtained from the model test for the first bucket design, 22 buckets

n_11	Nozzle opening						
	6mm	10mm	14mm	18mm	22mm	26mm	30mm
38	0.886651	0.896629	0.900379	0.899133	0.896196	0.894608	0.892364
39	0.889360	0.899253	0.902667	0.902082	0.899276	0.897809	0.896805
40	0.895956	0.904052	0.906251	0.905461	0.903503	0.902002	0.901639
41	0.886317	0.899325	0.904858	0.905792	0.904325	0.903315	0.902349
42	0.887886	0.900862	0.905658	0.905844	0.904250	0.903744	0.901725
43	0.881966	0.897387	0.902746	0.902213	0.901935	0.900046	0.898943
44	0.878691	0.894043	0.898991	0.898809	0.897942	0.895318	0.894450
45	0.872303	0.887653	0.892963	0.894122	0.891925	0.890050	0.888336



## Appendix E

# Filming with high-speed camera

The videos and pictures shown in this chapter and on the enclosed CD are denoted with the nozzle opening. The correlations between the nozzle opening and  $Q_{11}$  for the first and second bucket design are as follows.

$6mm$	$\rightarrow 0.0108 \text{ l/sm}^{5/2}$
$10mm$	$\rightarrow 0.0144 \text{ l/sm}^{5/2}$
$14mm$	$\rightarrow 0.0175 \text{ l/sm}^{5/2}$
$18mm$	$\rightarrow 0.0200 \text{ l/sm}^{5/2}$
$22mm$	$\rightarrow 0.0221 \text{ l/sm}^{5/2}$
$26mm$	$\rightarrow 0.0238 \text{ l/sm}^{5/2}$
$30mm$	$\rightarrow 0.0251 \text{ l/sm}^{5/2}$

## A First design - 21 buckets



Figure E.1: 70m head, Nozzle opening=14mm,  $n_{11} = 41$



Figure E.2: 70m head, Nozzle opening=18mm,  $n_{11} = 41$



Figure E.3: 70m head, Nozzle open-



Figure E.4: 70m head, Nozzle opening=18mm,  $n_{11} = 41$



Figure E.5: 70m head, Nozzle open-  
ing=22mm,  $n_{11} = 41$



Figure E.6: 70m head, Nozzle open-  
ing=24mm,  $n_{11} = 41$





Figure E.7: 70m head, Nozzle opening=24mm,  $n_{11} = 41$

## B First design - 22 buckets

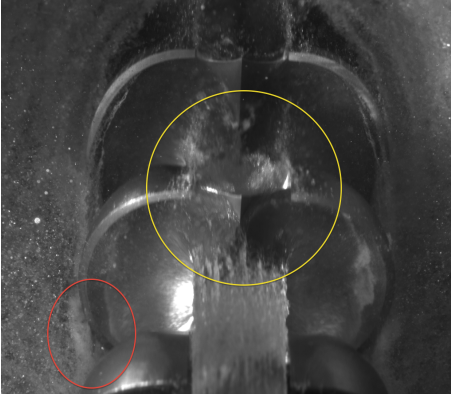


Figure E.8: 70m head, Nozzle opening=18mm,  $n_{11} = 41$

## C Second design



Figure E.9: 70m head, Nozzle opening=14mm,  $n_{11} = 41$

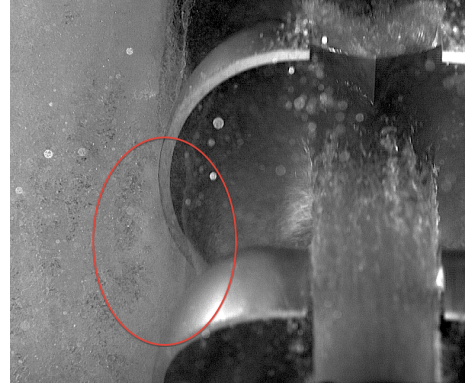


Figure E.10: 70m head, Nozzle opening=18mm,  $n_{11} = 41$



Figure E.11: 70m head, Nozzle open-  
ing=22mm,  $n_{11} = 41$



Figure E.12: 70m head, Nozzle open-  
ing=24mm,  $n_{11} = 41$



Figure E.13: 70m head, Nozzle open-  
ing=24mm,  $n_{11} = 41$

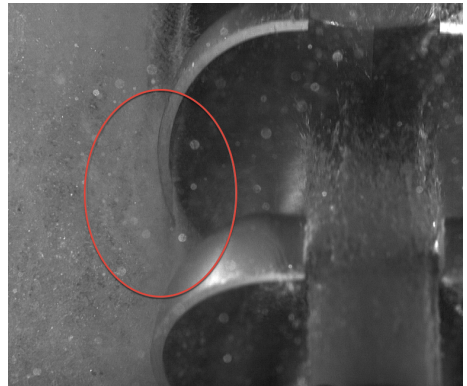


Figure E.14: 70m head,  $Q_{11} = 0,022$ ,  
 $n_{11} = 41$

## D Pelton buckets designed by Bjørn Winther Solemslie

After the nozzle was lowered the following pictures were obtained for the different operating points. The videos and pictures shown in this chapter and on the enclosed CD are denoted with the nozzle opening. The correlations between the nozzle opening and  $Q_{11}$  for the third bucket design are as follows.

$$6mm \Rightarrow 0.0101 \text{ l/sm}^{5/2}$$

$$8mm \Rightarrow 0.0120 \text{ l/sm}^{5/2}$$

$$10mm \Rightarrow 0.0135 \text{ l/sm}^{5/2}$$

$$12mm \Rightarrow 0.0151 \text{ l/sm}^{5/2}$$

$$14mm \Rightarrow 0.0164 \text{ l/sm}^{5/2}$$

$$16mm \Rightarrow 0.0176 \text{ l/sm}^{5/2}$$

$$18mm \Rightarrow 0.0187 \text{ l/sm}^{5/2}$$

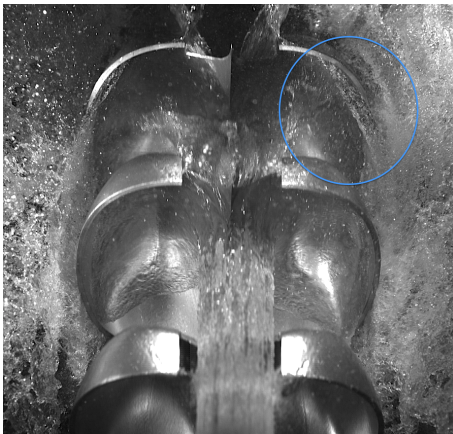


Figure E.15: 25m head, Nozzle opening=6mm,  $n_{11} = 38,5$

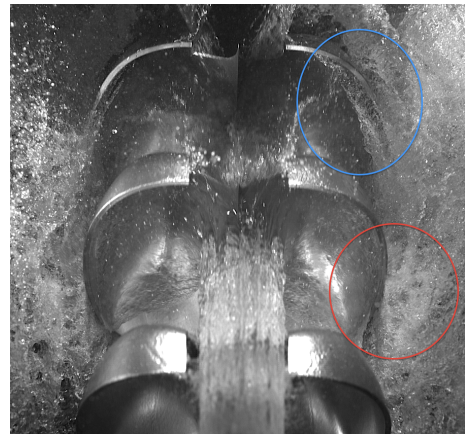


Figure E.16: 25m head, Nozzle opening=8mm,  $n_{11} = 38,5$



Figure E.17: 25m head, Nozzle open-  
ing=10mm,  $n_{11} = 38,5$



Figure E.18: 25m head, Nozzle open-  
ing=12mm,  $n_{11} = 38,5$



Figure E.19: 25m head, Nozzle open-  
ing=14mm,  $n_{11} = 38,5$



Figure E.20: 25m head, Nozzle open-  
ing=16mm,  $n_{11} = 38,5$



Figure E.21: 25m head, Nozzle open-  
ing=18mm,  $n_{11} = 38,5$

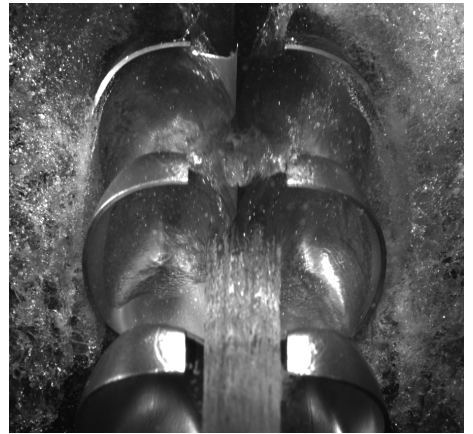


Figure E.22: 25m head, Nozzle open-  
ing=6mm,  $n_{11} = 41$



Figure E.23: 25m head, Nozzle open-  
ing=8mm,  $n_{11} = 41$



Figure E.24: 25m head, Nozzle open-  
ing=10mm,  $n_{11} = 41$



Figure E.25: 25m head, Nozzle open-  
ing=12mm,  $n_{11} = 41$



Figure E.26: 25m head, Nozzle open-  
ing=14mm,  $n_{11} = 41$





Figure E.27: 25m head, Nozzle open-  
ing=16mm,  $n_{11} = 41$



Figure E.28: 25m head, Nozzle open-  
ing=18mm,  $n_{11} = 41$

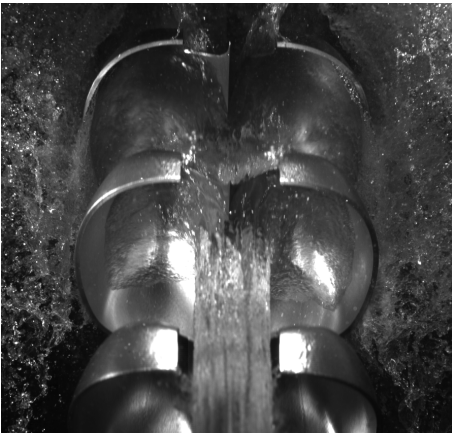


Figure E.29: 25m head, Nozzle open-  
ing=6mm,  $n_{11} = 44$

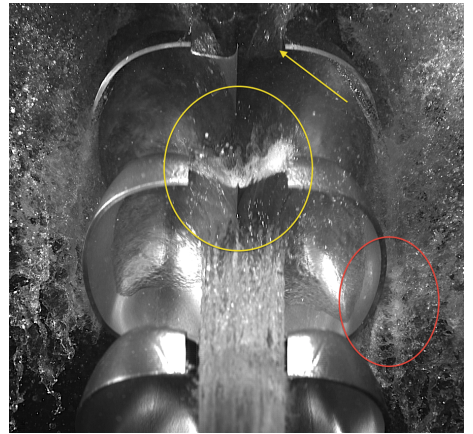


Figure E.30: 25m head, Nozzle open-  
ing=8mm,  $n_{11} = 44$

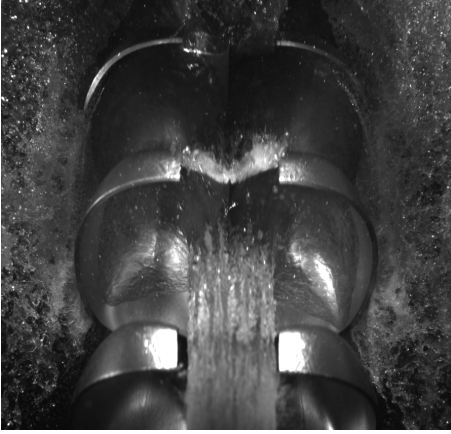


Figure E.31: 25m head, Nozzle open-  
ing=10mm,  $n_{11} = 44$



Figure E.32: 25m head, Nozzle open-  
ing=12mm,  $n_{11} = 44$

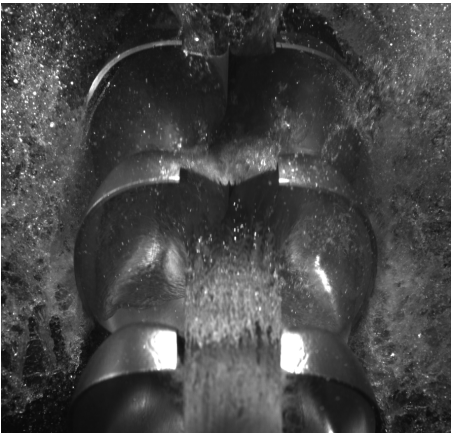


Figure E.33: 25m head, Nozzle open-  
ing=14mm,  $n_{11} = 44$

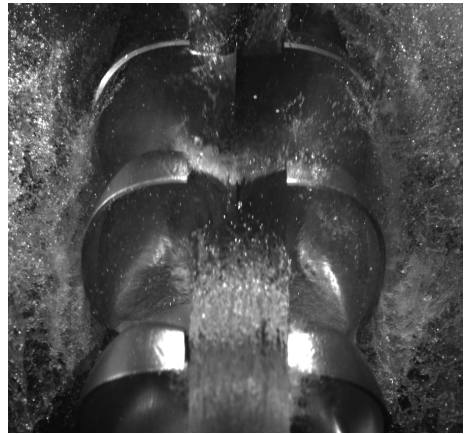


Figure E.34: 25m head, Nozzle open-  
ing=16mm,  $n_{11} = 44$



Figure E.35: 25m head, Nozzle opening=18mm,  $n_{11} = 44$

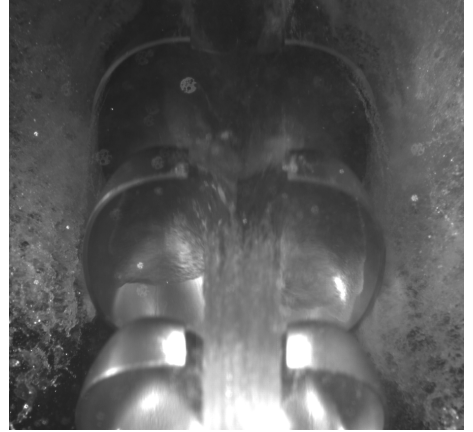


Figure E.36: 70m head, Nozzle opening=6mm,  $n_{11} = 44$



Figure E.37: 70m head, Nozzle opening=8mm,  $n_{11} = 44$



Figure E.38: 70m head, Nozzle opening=10mm,  $n_{11} = 44$



Figure E.39: 70m head, Nozzle opening=12mm,  $n_{11} = 44$



Figure E.40: 70m head, Nozzle opening=14mm,  $n_{11} = 44$



Figure E.41: 70m head, Nozzle opening=16mm,  $n_{11} = 44$

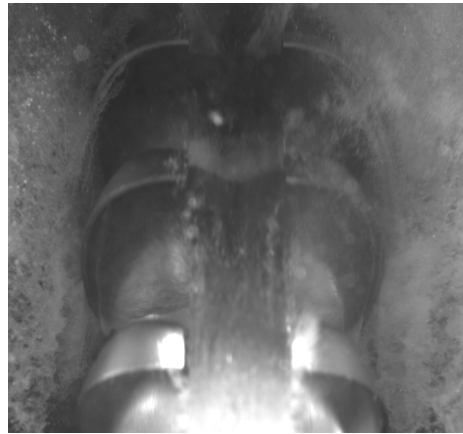


Figure E.42: 70m head, Nozzle opening=18mm,  $n_{11} = 44$



Figure E.43: 70m head, Nozzle open-  
ing=6mm,  $n_{11} = 41$



Figure E.44: 70m head, Nozzle open-  
ing=8mm,  $n_{11} = 41$



Figure E.45: 70m head, Nozzle open-  
ing=10mm,  $n_{11} = 41$

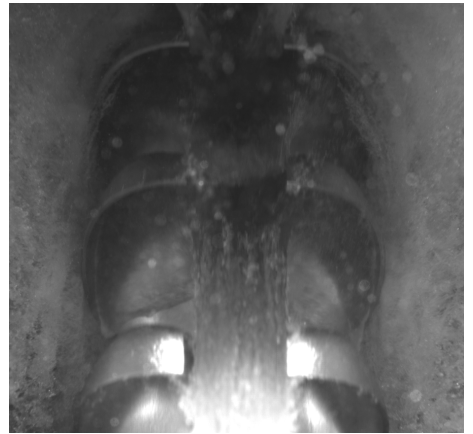


Figure E.46: 70m head, Nozzle open-  
ing=12mm,  $n_{11} = 41$



Figure E.47: 70m head, Nozzle opening=14mm,  $n_{11} = 41$



Figure E.48: 70m head, Nozzle opening=16mm,  $n_{11} = 41$

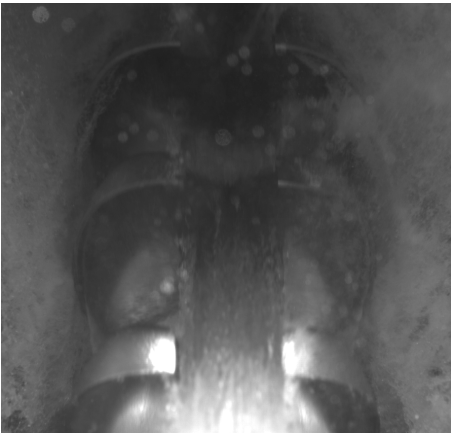


Figure E.49: 70m head, Nozzle opening=18mm,  $n_{11} = 41$

# Appendix F

## Uncertainty Analysis

In this section the uncertainties will be calculated. The uncertainty is calculated for operation around the highest point of efficiency.

### A Uncertainty in the calibration

#### A.1 Uncertainty in the calibration of the differential pressure transmitter

$f_{p_a}$  and  $f_{p_b}$  consist of the total error in the calibration method. According to the documentation for the dead weigh manometer, the total error in the instrument does not exceed  $\pm 0.0008\%$ . This is found by combining  $f_{p_a}$  and  $f_{p_b}$  with the RSS method.

$f_{p_c}$  is the systematic error in the instrument. By calibrating the signal given by the instrument against a physical quantity, one minimizes this uncertainty. This relative uncertainty has been denoted  $f_{p_{regression}}$  and is found to be  $0.031\%$  from the calibration report in Appendix A.

$f_{p_d}$  is the random error in the instrument due to the scatter of the signal while logging over time. This uncertainty is included in  $f_{p_{regression}}$ .

$f_{p_e}$  is the error due to physical phenomena and external influences. As this may originate from changes in temperature within the instrument, and the pressure transducer has been installed in the rig for several months, it was assumed that the instrument had reached thermal equilibrium with the surroundings and  $f_{p_e}$  was neglected. [10]

$f_{p_f}$  is the error in physical properties obtained by either calculation or in relation to the use of international standard data. This uncertainty includes the uncertainty of the measurement of the height difference between the dead weight manometer and the measuring point of the pressure transmitter,  $Z_{cal}$ . This distance was measured with a ruler. The uncertainty is therefor set to half of the resolution of the ruler,  $\pm 0.0005m$ . The height difference was found to be  $0.075m$ , thus the uncertainty,  $f_{p_f} = 0.00667\%$ .

Combining the above mentioned uncertainties with RSS-method, the total relative uncertainty for the calibration of the differential pressure transmitter becomes as shown in Equation F.1. [10]

$$f_{p_{cal}} = \pm \sqrt{(f_{p_{ab}})^2 + (f_{p_{regression}})^2 + (f_{p_f})^2} = 0.032\% \quad (F.1)$$

## A.2 Uncertainty in the calibration of the volume flow meter

The errors contributing to the uncertainty in the calibration of the volume flow meter are the systematic error in the weighing tank system,  $f_{Q_a}$ , the random error in the weighing tank system,  $f_{Q_b}$ , and the systematic and random error in the instrument,  $f_{Q_{regression}}$ , where the latter is specific for the calibration related to these model tests.

$$f_{Q_a} = 0.0889\% [10]$$

$$f_{Q_b} = 0.0503\% [10]$$

$$f_{Q_{regression}} = 0.005482$$

Combining the above mentioned uncertainties with the RSS-method, the maximum total relative uncertainty for the calibration of the volume flow meter is found to be as shown in Equation F.2.

$$f_{Q_{cal}} = \pm \sqrt{(f_{Q_a})^2 + (f_{Q_b})^2 + (f_{Q_{regression}})^2} = \pm 0.10229\% \quad (F.2)$$

## A.3 Uncertainty in the calibration of the torque transducer

The errors contributing to the uncertainty for the calibration of the torque transducer is the systematic error in the weights and the weights bed,  $f_{\tau_W}$ , the systematic error in the length of the arm,  $f_{\tau_{arm}}$ , and the systematic and random error in the instrument,  $f_{\tau_{regression}}$ .

$$f_{\tau_W} = 0.00154\%$$

$$f_{\tau_{arm}} = 0.08536\%$$



$$f_{\tau_{regression}} = 0.073\%$$

Combining these errors with the RSS-method the maximum total relative uncertainty for the calibration of the torque transducer is found to be as shown in Equation F.3.

$$f_{\tau_{cal}} = \pm \sqrt{(f_{\tau_{regression}})^2 + (f_{\tau_{arm}})^2 + (f_{\tau_W})^2} = \pm 0.1123\% \quad (\text{F.3})$$

#### A.4 Uncertainty in the calibration of the friction torque transducer

The errors contributing to the uncertainty of the friction torque transducer is the uncertainties related to the force cell. The different errors are systematic error in the weights,  $f_{\tau_W}$ , the systematic error in the length of the arm,  $f_{\tau_{arm}}$ , and the systematic and random error in the instrument,  $f_{\tau_{regression}}$ .

$$f_{\tau_W} = 0.11\%$$

$$f_{\tau_{arm}} = 0.15\%$$

$$f_{\tau_{regression}} = 0.305\%$$

Combining these errors with the RSS-method the maximum total relative uncertainty for the calibration of the friction torque transducer is found to be as shown in Equation F.4.

$$f_{\tau_{cal}} = \pm \sqrt{(f_{\tau_{regression}})^2 + (f_{\tau_{arm}})^2 + (f_{\tau_W})^2} = \pm 0.357\% \quad (\text{F.4})$$

A more detailed description on how to find the different uncertainties mentioned above can be found in the master thesis *Optimalisering av ringledning for Peltoneturbin*, Appendix D by Bjørn Winther Solemslie, 2010 [10].

## B Uncertainty of the Test

### B.1 Rotational Speed

According to Reinertsen [8] is the constant uncertainty related to the measurement of the rotational speed  $f_{\omega} = 0.025\%$ .

## B.2 Hydraulic energy

The calculation of the uncertainty in the hydraulic energy is as follows.

$$f_E = \pm \frac{e_E}{E} = \pm \frac{\sqrt{\left(\frac{e_p}{\rho}\right)^2 + (g * e_{Zdif})^2 + \left(\frac{e_{v_1}^2}{2}\right)^2}}{\frac{p}{\rho} + g * e_{Zdif} + \frac{e_{v_1}^2}{2}} \quad (\text{F.5})$$

As the experiments are carried out on a Pelton turbine which runs on high pressure and low volume flow some simplifications can be justified. The height difference between the pressure transducer and the inlet is measured to be  $217mm$  with a measurement uncertainty of  $0.5mm$  [8]. During the experiments is the total head held constant at  $70m$ . The relative total uncertainty this error imposes on the total uncertainty in the hydraulic energy is as in Equation (F.6).

$$\frac{e_{Zdif}}{E} = \frac{0.0005m}{70m} = 0.00071\% \quad (\text{F.6})$$

The contribution of the error in the inlet velocity to the total hydraulic efficiency has to be taken into consideration. At the maximum nozzle opening we have a discharge of  $0.0476 \frac{m^3}{s}$ . With a  $100mm$  pipe this results in an inlet velocity  $v_1 = 6.06 \frac{m}{s}$ . The uncertainty related to the discharge varies, but when calculating the uncertainty in the inlet velocity the maximum uncertainty in the discharge is used.

$$f_{v_1} = \sqrt{f_Q^2 + f_A^2} \quad (\text{F.7})$$

$$\frac{e_{v_1}^2}{2} = v_1^2 * f_{v_1} \quad (\text{F.8})$$

$e_{Zdif} = 0.0005m$	Error set to half of the resolution of teh ruler.
$f_{pab} = 0.0008\%$	Found from the documentation of the dead weight manometer.
$f_{preg} = 0.0.031\%$	Found from the calibration file for the range used in the tests.
$f_Q = 0.0926\%$	Highest systematic uncertainty in the discharge during the tests. [8]
$f_{A_i} = 0.01\%$	Found from Reinertsen [8].
$\Delta p = 670kPa$	The static pressure in front of the nozzle.
$v_1 = 6.06 \frac{m}{s}$	The velocity of the water prior to the nozzle.
$E = g * 70m$	The hydraulic energy available before the nozzle.

$$f_E = \pm \frac{\sqrt{\left(\frac{f_p * \Delta p}{\rho}\right)^2 + (g * e_{Zdif})^2 + \left(\frac{v_1^2 * f_{v_1}^2}{2}\right)^2}}{E} \quad (\text{F.9})$$

By using the values presented in Equation (F.9), the total systematic uncertainty in the hydraulic energy is obtained.

In order to find the total systematic uncertainty at the highest point of efficiency for each test, the following equations are used:

**Torque**

$$f_{\tau} = \pm \sqrt{(f_{T_{cal}})^2 + (f_{T_l})^2}$$

**Friction torque**

$$f_{\tau_{Lm}} = \pm \sqrt{(f_{T_{Lm_{cal}}})^2 + (f_{T_{Lm_l}})^2}$$

$$f_{\tau_m} = \frac{\sqrt{(e_{\tau_{Lm}})^2 + (e_{\tau})^2}}{\tau_{tot}} \quad \text{Volume flow}$$

$$f_Q = \pm \sqrt{(f_{Q_{cal}})^2 + (f_{Q_l})^2}$$

**Effect**

$$f_P = \pm \sqrt{(f_{\tau_m})^2 + (f_{\omega})^2}$$

$$\text{where } f_{\tau_m} = \frac{\sqrt{(e_{T_{Lm}})^2 + e_T^2}}{T_{tot}}$$

**Energy**

$$f_E = \pm \sqrt{\frac{(f_P \frac{\Delta p}{\bar{p}})^2 + (g * e_{Z_{dif}})^2 + (\frac{v_1^2 * f_{v1}^2}{2})^2}{E}}$$

**Hydraulic efficiency**

$$f_{\eta_h} = \pm \frac{e_{\eta_h}}{\eta_h} = \pm \sqrt{(f_Q)^2 + (f_E)^2 + (f_P)^2}$$

**First design - 21 buckets**

**Uncertainty for the highest point of efficiency**

For  $n_{11} = 41$  and a nozzle opening of 18mm:

$$f_{Q_l} = \pm 0,002610665\%$$

$$f_{\tau_l} = \pm 0,02951011\%$$

$$f_{\tau_{Lm_l}} = \pm 0,149399998\%$$

$$\tau = 314,0470104Nm \quad \tau_{Lm} = 2,237988099Nm$$

With these numbers, combined with the uncertainty in the calibration, we obtain:

$$f_P = \pm 0,025000051\%$$

$$f_Q = \pm 0,10232331\%$$

$$f_E = \pm 0,03025\%$$

$$\Rightarrow f_{\eta} = \pm 0,10959\%$$

### First design - 22 buckets

#### Uncertainty for the highest point of efficiency

For  $n_{11} = 40$  and a nozzle opening of 18mm:

$$f_{Q_i} = \pm 0,003625515\%$$

$$f_{\tau_i} = \pm 0,024498408\%$$

$$f_{\tau_{Lm_i}} = \pm 0,063282087\%$$

$$\tau = 320,4623758Nm \quad \tau_{Lm} = 4,124736193Nm$$

With these numbers, combined with the uncertainty in the calibration, we obtain:

$$f_P = \pm 0,025000048\%$$

$$f_Q = \pm 0,102354\%$$

$$f_E = \pm 0,03025\%$$

$$\Rightarrow f_{\eta} = \pm 0,109619\%$$

### Third design - 23 buckets

#### Uncertainty for the highest point of efficiency

For  $n_{11} = 44$  and a nozzle opening of 8mm:

$$f_{Q_i} = \pm 0,00448658\%$$

$$f_{\tau_i} = \pm 0,05300718\%$$

$$f_{\tau_{Lm_i}} = \pm 0,154428423\%$$

$$\tau = 176,9072466Nm \quad \tau_{Lm} = 2,25241419Nm$$

With these numbers, combined with the uncertainty in the calibration, we obtain:

$$f_P = \pm 0,025000158\%$$

$$f_Q = \pm 0,10238834\%$$

$$f_E = \pm 0,03025\%$$

$$\Rightarrow f_{\eta} = \pm 0,109651\%$$

# Appendix G

## Matlab source code

The following code was used to obtain the Hill-diagrams. The code is created by Kyrre Reinertsen and Bjørn Winther Solemslie.

### A Import raw data

```
%----- IMPORT PELTON RAW DATA -----  
%  
% This function import rawdata from .txt files of the form:  
  
% -----  
% | A | B | C | D | E |  
% -----  
% | a_1 | b_1 | c_1 | . | . |  
% | a_2 | b_2 | . | . | . |  
% | . | . | . | . | . |  
% | a_n | b_n | c_n | . | . |  
% -----  
% | A | B | C | D | E |  
% -----  
% | a_1 | b_1 | c_1 | . | . |  
% | . | . | . | . | . |  
% | a_n | b_n | c_n | . | . |  
% -----  
%  
% and return a matrix
```

```

function [rawdata] = rawdata_import()

%Open file import dialog
[path] = uigetdir;
listing=dir(path);
c = 0;
for i = 3:length(listing)
    if listing(i).isdir == 1
        c = c + 1;
        folders(c).name = listing(i).name;
        names(c)=sscanf(folders(c).name, '%dmm');
    end
end

[~,order] = sort(names);

c = 0;

for k = order
    files = dir(folders(k).name);
    %files = files(4:end);

    c = c + 1;
    %%
    %Find number of files selected
    fileNum = length(files);

    %Loop through source files
    i=1;
    for j = 1:fileNum
        if ~isempty(regexpi(files(j).name, '.xls', 'once'))
            OS = computer;
            OS = OS(1:3);
            if strcmp(OS, 'MAC')
                filepath = [path, '/', folders(k).name, '/', files(j).name];
            else
                filepath = [path, '\', folders(k).name, '\', files(j).name];
            end
            file = files(j);
            fid = fopen(filepath);

            pos = 1; %Byte number to start import
            %i = 2+(j-1);

```

```

        i=i+1;
        while pos < file.bytes

            [rawdata(i,c),pos] = textscan(fid, '%f %f %f %f %f %f ', 'CollectOutput', 1);
        end

        fclose(fid);
    end

end
rawdata{1,c} = folders(k).name; %Set file info as column header
end

```

## B Calculate mean data from raw data

```

%----- CALCULATE MEAN DATA FROM RAW DATA (meandata_create.m) -----
%
% Creates a new matrix 'meandata' from a source MxN:
%
%           1         .         .         .         N
%   -----
%   1 |   A   |   B   |   C   |   D   |   E   |
%   . | -----
%   | a_1 | b_1 | c_1 | . | . |
%   . | a_2 | b_2 | . | . | . |
%   | . | . | . | . | . |
%   . | . | . | . | . | . |
%   | . | . | . | . | . |
%   M | a_M | b_M | . | . | . |
%   -----
%
% Where A-E indicates different nozzles (headers), and (a,b,c,..)_m is
% measurements at
% different constant rotational speeds.
%
% OUTPUT      meandata      Nx1 struct table
%             meandata_spl  Nx1 struct table
%             nan_map       (M-1)xN table of '0' and '1' where '1' indica
%                          that the source contains NaN values

```

```

% source      rawdata matrix (from rawdata_import.m)

% function [meandata meandata_spl nan_map] = meandata_create(source)
function [meandata nan_map] = meandata_create(source)

%-----

D = 0.5137;           %Diameter of runner [m]
g = 9.82146514;      %Gravity in the NTNU laboratory
p_error = 0.207;     %Pressure transducer correction [m]
t = 1.960;           %Degrees of freedom (random uncertainty)

n11_a = 37;          %Reduced rot. speed (n_11) start
n11_b = 45;          %n_11 end
n11_step = 1;        %n_11 increment

%-----

s = size(source);
nan_map = zeros(s(1),s(2));

%Create 'meandata'

for j = 1:s(2)

    for i = 1:s(1)-1

        if isempty(source{i+1,j})

            p_temp(i,1) = NaN;
            q_temp(i,1) = NaN;
            T_temp(i,1) = NaN;
            M_temp(i,1) = NaN;
            Mlm_temp(i,1) = NaN;
            Mtot_temp(i,1) = NaN;
            n_temp(i,1) = NaN;
            q11_temp(i,1) = NaN;
            qed_temp(i,1) = NaN;
            n11_temp(i,1) = NaN;
            ned_temp(i,1) = NaN;
            Ph_temp(i,1) = NaN;
            Pm_temp(i,1) = NaN;
            rho_temp(i,1) = NaN;

```



```

    etah_temp(i,1) = NaN;
    head_temp(i,1) = NaN;
    Eh_temp(i,1) = NaN;

    nan_map(i,j) = 1;

else

    p = source{i+1,j}(:,1);
    q = source{i+1,j}(:,2);
    T = source{i+1,j}(:,3);      %temperature
    M = source{i+1,j}(:,4);      %torque
    Mlm = source{i+1,j}(:,5);    %torque friction
    n = source{i+1,j}(:,6);

    %Mean values of raw data
    p_temp(i,1) = mean(p);
    q_temp(i,1) = mean(q);
    T_temp(i,1) = mean(T);
    M_temp(i,1) = mean(M);
    Mlm_temp(i,1) = mean(Mlm);
    Mtot_temp(i,1) = mean(M) + mean(Mlm); %total torque
    n_temp(i,1) = mean(n);

    %Calculate error and standard deviation of raw data
    std_p = std(p);
    std_q = std(q);
    std_T = std(T);
    std_M = std(M);
    std_Mlm = std(Mlm);
    std_n = std(n);

    err_p = (t*std_p)/sqrt(length(p));
    err_q = (t*std_q)/sqrt(length(q));
    err_T = (t*std_T)/sqrt(length(T));
    err_M = (t*std_M)/sqrt(length(M));
    err_Mlm = (t*std_Mlm)/sqrt(length(Mlm));
    err_n = (t*std_n)/sqrt(length(n)/1000);

    p_temp(i,2) = err_p;
    q_temp(i,2) = err_q;
    T_temp(i,2) = err_T;
    M_temp(i,2) = err_M;
    Mlm_temp(i,2) = err_Mlm;

```

```

Mtot_temp(i,2) = sqrt(err_M^2 + err_Mlm^2);
n_temp(i,2) = err_n;

p_temp(i,3) = 100*err_p/p_temp(i,1);
q_temp(i,3) = 100*err_q/q_temp(i,1);
T_temp(i,3) = 100*err_T/T_temp(i,1);
M_temp(i,3) = 100*err_M/M_temp(i,1);
Mlm_temp(i,3) = 100*err_Mlm/Mlm_temp(i,1);
Mtot_temp(i,3) = 100*Mtot_temp(i,2)/Mtot_temp(i,1);
n_temp(i,3) = 100*err_n/n_temp(i,1);

%
%      etah_temp(i,2) = sqrt(p_temp(i,3)^2 + q_temp(i,3)^2 + ...
%      T_temp(i,3)^2 + M_temp(i,3)^2 + n_temp(i,3)^2);

egah_temp(i,2) = sqrt(p_temp(i,3)^2 + q_temp(i,3)^2 + ...
T_temp(i,3)^2 + Mtot_temp(i,3)^2 + n_temp(i,3)^2);

%Calc density (dens), E, H, omega, q11_temp, Ph, Pm, eta, head_temp
dens = 1000/ ( (1 - (4.6699e-10)*p_temp(i,1)*1000) + ...
(8e-6)*(T_temp(i,1) - 4 + (2.1318913e-7)*p_temp(i,1)*1000)^2 -
(6e-8)*(T_temp(i,1) - 4 + (2.1318913e-7)*p_temp(i,1)*1000)^3 )

%E = ((Pstat*1000)/rhow) + g*p_error + 0.5*(q_temp(i,1)...
%/(0.25*pi*0.1^2))^2;
E = ((p_temp(i,1)*1000)/dens) + g*p_error + 0.5*(q_temp(i,1)...
/(0.25*pi*0.1^2))^2;

H = E/g;
omega = ((2*pi)/60)*n_temp(i,1);
q11 = q_temp(i,1)/((D^2)*sqrt(H));
n11 = (n_temp(i,1)*D)/sqrt(H);
Ph = dens*q_temp(i,1)*E;
Pm = Mtot_temp(i,1)*omega;

q11_temp(i,1) = q11;
qed_temp(i,1) = q11/sqrt(g);
n11_temp(i,1) = n11;
ned_temp(i,1) = n11/sqrt(g);
Ph_temp(i,1) = Ph;
Pm_temp(i,1) = Pm;
rho_temp(i,1) = dens;
egah_temp(i,1) = Pm/Ph;
head_temp(i,1) = H;
Eh_temp(i,1) = E;

```

```

        end

    end

    %Insert calculated data into new table 'meandata'

    noz = source{1,j};
    b = length(noz)-7;
    %From raw
    meandata{j,1}.nozzle = noz; %noz(1:b)
    meandata{j,1}.p = p_temp;
    meandata{j,1}.q = q_temp;
    meandata{j,1}.temp = T_temp;
    meandata{j,1}.torque = M_temp;
    meandata{j,1}.torque_lm = Mlm_temp;
    meandata{j,1}.torque_tot = Mtot_temp;
    meandata{j,1}.n = n_temp;
    %Calculated
    meandata{j,1}.q11 = q11_temp;
    meandata{j,1}.qed = qed_temp;
    meandata{j,1}.n11 = n11_temp;
    meandata{j,1}.ned = ned_temp;
    meandata{j,1}.power_h = Ph_temp;
    meandata{j,1}.power_m = Pm_temp;
    meandata{j,1}.density = rho_temp;
    meandata{j,1}.etah = etah_temp;
    meandata{j,1}.head = head_temp;
    meandata{j,1}.energy = Eh_temp;

    clear q11_temp qed_temp n11_temp ned_temp Ph_temp Pm_temp rho_temp ..
        etah_temp head_temp Eh_temp p_temp q_temp T_temp n_temp
end
end

```

## C Add systematic uncertainty to mean data matrix

```

%----- ADD SYSTEMATIC UNCERTAINTY TO MEAN DATA MATRIX -----
%
% Computes and adds systematic uncertainty to efficiency
%
% Note: Every parameter must be changed in different tests!

```

```

%
% source = meandata_spl

function [meandata_ok] = meandata_esys(source)

%Systematic uncertainty
esys_n = 0.025;           %Rotational speed
esys_E = 0.0385;        %Energy
esys_M_c = 0.08536;     %Torque - constant
esys_Q_c = 0.08536;     %Volume flow - constant

for i = 1:length(source)

    for ii = 1:length(source{i,1}.etah)

        M = source{i,1}.torque(ii,1);
        Q = source{i,1}.q(ii,1);

        %Volume flow - variable
        esys_Q_v = (0.0000003395*(Q*1000)^2-0.000023697*(Q*1000)...
            +0.0034582)/(Q*1000)*100;

        %Torque - variable
        esys_M_v = -0.9798E-08*M^3 + 1.3044E-05*M^2 - 0.00565863*M +...
            .953585;

        %Constant + variable
        source{i,1}.etah(ii,3) = sqrt(esys_n^2 + esys_M_c^2 +...
            esys_M_v^2+ esys_E^2 + esys_Q_c^2 + esys_Q_v^2);

        %Total uncertainty efficiency
        source{i,1}.etah(ii,4) = sqrt((source{i,1}.etah(ii,2))^2 +...
            (source{i,1}.etah(ii,3))^2);

        %Total uncertainty efficiency - Absolute
        source{i,1}.etah(ii,5) =...
            source{i,1}.etah(ii,4)*source{i,1}.etah(ii,1);

    end

end

end

```

```
meandata_ok = source;
```

```
end
```

## D Efficiency curve fitting

```
%----- EFFICIENCY CURVE FITTING (meandata_fit.m) -----  
%  
% Creates a duplicate "meandata_fitted" of the source where the efficiency  
% substituted with a curvefit of the original efficiency curve. The new  
% efficiency curve consists of "a" times more data points than the source  
% (becomes smoother).  
%  
% source: meandata or meandata_spl
```

```
function [meandata_fitted] = meandata_fit(source,a)
```

```
%----- CHANGE -----  
  
n11_a = 37;           %Reduced rot. speed (n_11) start  
n11_b = 45;           %n_11 end  
n11_step = 0.5;       %n_11 increment  
g = 9.82146514;  
  
%-----  
  
rows = length(source);  
  
n11_ideal = (n11_a:n11_step:n11_b)/sqrt(g);  
n11_len = a*length(n11_ideal);  
n11_step = (n11_b-n11_a)/(n11_len-1);  
n11_new = (n11_a:n11_step:n11_b);  
  
% Set up fitype and options.  
  
%ft = fitype( 'poly2' );  
%opts = fitoptions( ft );  
%opts.Lower = [-Inf -Inf -Inf];  
%opts.Upper = [Inf Inf Inf];
```

```

ft = fittype( 'smoothingspline' );
opts = fitoptions( ft );
opts.SmoothingParam = 0.9910932135110677; %0.975726050374513

meandata_fitted = source;

for i = 1:rows

    q11(i) = mean(source{i,1}.q11(:,1));

    xData = source{i,1}.n11(:,1);
    yData = source{i,1}.etah(:,1);

    %x_sp = source{i,1}.ned(:,1);
    %y_sp = source{i,1}.etah(:,1);

    %[xData, yData] = prepareCurveData(x_sp,y_sp);

    fitresult = fit(xData,yData,ft,opts);

    for ii = 1:n11_len

        meandata_fitted{i,1}.etah(ii,1) = fitresult(n11_new(ii));
        meandata_fitted{i,1}.n11(ii,1) = n11_new(ii);

        eta(ii,i) = fitresult(n11_new(ii));

    end

    clear val

end

end

```

## E Plot efficiency Hill chart

```

%----- PLOT EFFICIENCY HILL CHART (meandata_hillplot.m) -----
function [qed ned eta] = meandata_hillplot(source,varargin)

%----- CHANGE -----

```

```

n11_a = 38;           %Reduced rot. speed (n_11) start
n11_b = 45;           %n_11 end
n11_step = 1;        %n_11 increment
xval = n11_a:n11_step:n11_b;    %Chart x-values (n_ED)

%-----

rows1 = length(source);
rows2 = length(source{1,1}.etah);

g = 9.82146514;
qed = zeros(1,rows1);
if isempty(varargin) || strcmp(varargin{1},'11')
    ned = (n11_a:n11_step:n11_b);
elseif strcmp(varargin{1},'ed')
    ned = (n11_a:n11_step:n11_b)/sqrt(g);
end
eta = zeros(rows2,rows1);

k = 1;
for i = 1:rows1

    if isempty(varargin) || strcmp(varargin{1},'11')
        qed(i) = mean(source{i,1}.q11);
    elseif varargin{1}=='ed'
        qed(i) = mean(source{i,1}.qed);
    end

    for ii = 1:rows2

        eta(ii,i) = source{i,1}.etah(ii,1);
        k = k + 1;
    end

end

%Create Hill chart of (ned,qed,eta) = (x,y,z)
dfig('Hill Chart');

set(gcf,'paperOrientation','landscape','paperUnits','normalized',...
    'paperType','A4')

[c,h] = contour(ned,qed',eta'*100,...
    [75:2:85,85.5:0.5:90,90.1:0.1:91],...

```

```

        'linewidth',1.5);
text_handle = clabel(c,h);
set(text_handle,'BackgroundColor',[1 1 .6],...
    'Edgecolor',[.7 .7 .7],...
    'fontsize',20)
% set(gca,'fontsize',20);
if isempty(varargin) || strcmp(varargin{1},'11')
    xlabel('$n_{11}$','fontsize',20,'interpreter','latex');
    ylabel('$Q_{11}$','fontsize',20,'interpreter','latex');
elseif varargin{1}=='ed'
    xlabel('$n_{ED}$','fontsize',20,'interpreter','latex');
    ylabel('$Q_{ED}$','fontsize',20,'interpreter','latex');
end
set(gca,'fontsize',20);
grid on

for i=1:length(text_handle)
    set(text_handle(i),'string',strcat(get(text_handle(i),'string'),'%'));
end

end

```